Precipitable water in cloudy areas from combined solar, thermal, and microwave radiance measurements

Final Report

Heike Hauschildt, Andreas Macke
IFM–GEOMAR
Leibniz Institut für Meereswissenschaften
Düsternbrooker Weg 20
D–24105 Kiel
and Jörg Schulz
DWD
Satellite Application Facility on Climate Monitoring
Dept. Climate and Environment
P.O. Box 10 04 65
D–63004 Offenbach

Contents

1 Introduction **1**

2 Water Vapour, Clouds, and Climate **4**

3 NAO **11**

4 Ground and Satellite–based Retrieval Techniques **15**

4.1 Ground based Instruments and Techniques 15

4.2 Satellite Instruments and Techniques 16

5 Ground–based analysis **19**

5.1 Cloud to clear TPW differences 19

5.2 TPW under all–sky and clear–sky conditions 27

5.2.1 TPW statistics for Lindenberg 28

5.3 The excess water vapour 38

5.3.1 Distinction of clear and cloudy cases from radiosoundings 38

5.3.2 All–sky vs clear–sky TPW 42

5.3.3 Sensitivity study 46

5.3.4 Excess water vapour for Europe 51

5.4 The vertical distribution of excess water vapour 57

5.4.1 Layered excess water vapour 62

5.5 Concluding Remarks 66

6 Satellite observed low pressure systems **67**

6.1 First case: 28–29 January 2001 67

6.2 Second case: 28 – 30 March 2001 74

6.3 Concluding Remarks 83

7 Spatial TPW as measured from Satellite **84**

7.1 Global TPW Distributions 85

7.2 Excess Water Vapour over the North Atlantic 90

7.3 Concluding remarks 95

8 Summary and conclusions **101**

Bibliography 102

A Cloud — clear statistics from radiosonde measurements **105**

B Spatial TPW as measured from Satellite **114**

B.1 South Atlantic 114

B.2 Pacific 119

B.3 Indic 124

B.4 Antarctic circumpolar ocean 129

Chapter 1

Introduction

Water vapour is an inhomogeneous quantity on all temporal and spatial scales. Its natural variability plays a crucial role in the climate system. Through positive feedback water vapour takes an important part in anthropogenically induced changes in climate resulting from increases in carbon dioxide and other greenhouse gases. Hence, determining its spatial and temporal variability is a challenging task. The vertical integrated water vapour denoted as total precipitable water (TPW) is derived using various techniques. Hauschildt and Macke (2004) summarises previous work on the retrieval of TPW from ground and satellite based measurements. A common problem in remote sensing from satellite of water vapour path is the limitation to clear–sky observations for infrared and solar retrieval techniques.

The question, therefore, arises whether there is a significant difference in mean values between TPW in cloudy– and clear–sky observations? It is important to know at which time scales this bias is most apparent and how it can be corrected. It seems obvious that the atmospheric water vapour in cloudy skies exceeds the TPW in clear skies. Warm front clouds are associated with advection of warm humid air. Furthermore, convective clouds transport moisture from the boundary layer into the free atmosphere. Gaffen and Elliot (1993) found out that the climatological column water vapour content of clear–sky atmospheres derived from north hemispheric radiosoundings is significantly lower than for cloudy–skies. The magnitude of the bias is lower in tropical regions than at midlatitudes where the largest values are found in winter. The variability cannot be explained by variations in surface temperature or by instrument biases. However, quantitative estimates of the variation of TPW with cloud cover are lacking. Crewell et al. (2002) estimate the difference between mean TPW in cloudy to clear skies from ground based microwave radiometer measurements. For the European area they retrieve a mean ratio (TPW (cloud) /TPW (clear)) of 1.2 to 1.3, showing a slight dependency on latitude. However, these values were derived from two month of measurements.

Inside clouds the relative humidity usually remains close to 100 % although considerable departures from these value have been observed. In cumulus clouds the relative humidity ranges from 80 % at the cloud boundary to supersaturation in the centre of the cloud exceeding 107 %. The median of the supersaturation is given with 0.1 %. Outside the cloud the

relative humidity drops to values near 70 % due to turbulent mixing. Flights through clouds over Montana show supersaturation ranging from - 0.5 % to + 0.5 %, but averaged to 0 % (see Pruppacher and Klett (1997), Chapter 2).

Marsden and Valero (2004) show that water vapour in clear–sky situation is lower compared to convective situations. The increase in the resulting greenhouse effect from the clear to the cloudy case can not be explained by the increase in vertical integrated water vapour and larger sea surface temperatures. An explanation is found in the humidity profile: an increase of upper tropospheric water vapour is observed. The absolute amount of water vapour decreases with height by three orders of magnitude from the boundary layer to the upper-troposphere. The contribution of the specific water vapour layer to the effective greenhouse effect increases with height. Hence, it is important to monitor the water vapour profile as well.

To constitute a TPW climatology from ground based measurements (using the advantage of high temporal resolution, measurements under all–sky situations, long time series) would lead to several problems. These observations are limited to land surfaces and the distribution of these stations is inhomogeneous over the continents. A global coverage is only available from satellite measurements. Here the temporal resolution depends on number of overpasses per surface point, satellite type (orbiting or geostationary) and number of satellites used. The majority of TPW satellite based estimates over land is derived using thermal measurements. This limits the observations to clear–sky situations. Over oceans TPW can be retrieved using microwave frequencies; here all–sky observations are possible. For IR–techniques a bias is introduced by systematically omitting cloudy atmospheres with their larger TPW. Climatologies based on orbiting satellites run into a sampling problem. When only clear–sky scenes can be observed the atmosphere does not contain clouds over a certain spot on time of the overpass. Therefore only per accident a moist scene near clouds can be observed. This leads to an overestimation of clear–sky cases in the climatologies and consequently to a dry bias.

In literature several quantities concerning the atmospheric water are discussed. The total precipitable water (TPW) is the vertically integrated absolute humidity, whereas the upper tropospheric humidity (UTH) is the relative humidity of the upper troposphere. Unlike the TPW the relative humidity depends on the atmospheric temperature. For models and weather forecasting relative humidities are used. With early satellite instruments, single channel based humidity retrievals have been performend. Measurements in this channel are related to emissions from the upper troposphere, and are more sensitive to UTH then to TPW. Therefore, TPW is a more complete quantity observing changes in the atmospheric water vapour and will be used henceforth.

The focus of this study is the estimation of the TPW in all–sky situations based on ground based measurements. The examination of the difference in TPW for clear and cloudy situations will lead to a quantification of the climatological excess water vapour (EWV). This in turn may be used to correct TPW climatologies based on clear–sky measurements.

In chapter 2 a short summary of the previous work is given. The physical basis and the retrieval techniques used in this study are described in chapter 4. Radiosonde ascents are used to define the difference in TPW in clear– and all–sky situations. A closer view on the time series of TPW and standard meteorological quantities like surface pressure, temperature, humidity, the height of the 500 hPa level and the cloud cover given in the synoptical observations is performed for one station exemplarily (see chapter 5). It is shown that clear–sky days coincide with high pressure and in summer (winter) with higher (lower) temperatures. The bias is influenced by the atmospheric situations described by the data set.

The concept of climatologies includes large scale coverage. For this purpose satellite microwave observations over the oceans are used. Chapter 6 describes the cross section of the TPW through mid–latitude low pressure systems. The monthly mean TPW fields derived from AMSU measurements of TPW are shown in chapter 7.

Chapter 2

Water Vapour, Clouds, and Climate

Several measuring campaigns, retrieval techniques and model sensitivity studies concerning water vapour and its impact on the climate system are resumed in Hauschildt and Macke (2004). A short overview is given here.

The global mean water vapour path as evaluated by Trenberth et al. (1987) is 26 kg/m^2. The geographical distribution varies from ∼5 kg/m^2 in the polar region to ∼60 kg/m^2 in the tropics. These values were derived using global analysis from the European Centre of Medium Range Weather Forecasts (ECMWF). Monthly mean total precipitable water (TPW) fields derived from AMSU measurements over the oceans are shown in figure 2.1. The humid atmospheres in the inner tropical convergence zone (ITCZ) are clearly visible. From January to July the ITCZ moves north in the Atlantic. In the Indic ocean the monsoon area is pronounced by large TPW values. In the western Pacific the warm pool area appears as a region with large water vapour amount. The TPW varies with latitude and season. Hence, determing its variability is a challenging task. In this study we use microwave instruments. Therefore, observations of TPW under all–sky conditions are possible. Microwave methods work well when the cloud particles are small. Therefore, this investigation is limited to non–precipitating clouds. To avoid contributions from precipitation a threshold in LWP is set for the observed area: LWP larger than 0.5 kg/m^2 are not used for this climatology. The problem with large droplets as occurring in precipitating clouds is that scattering effects reduce the measured emitted radiance at the satellite. Figure 2.2 shows the global distribution of monthly mean LWP for non-precipitating clouds.

Water vapour has a strong greenhouse effect. Due to its ability to absorb the thermal emittance of the surface the atmospheric temperature rises and is able to keep more water vapour. This positive natural feedback mechanism is shown in figure 2.3. Furthermore the anthropogenic greenhouse forcing induced by CO_2 which is also a strong thermal absorber couples to the water vapour feedback. The absorption by CO_2 increases the atmospheric temperature which will lead to more water vapour. A warmer atmosphere has a larger vertical extend. The irradiation from the top of the atmosphere is colder due to the increase of height of this

A: January

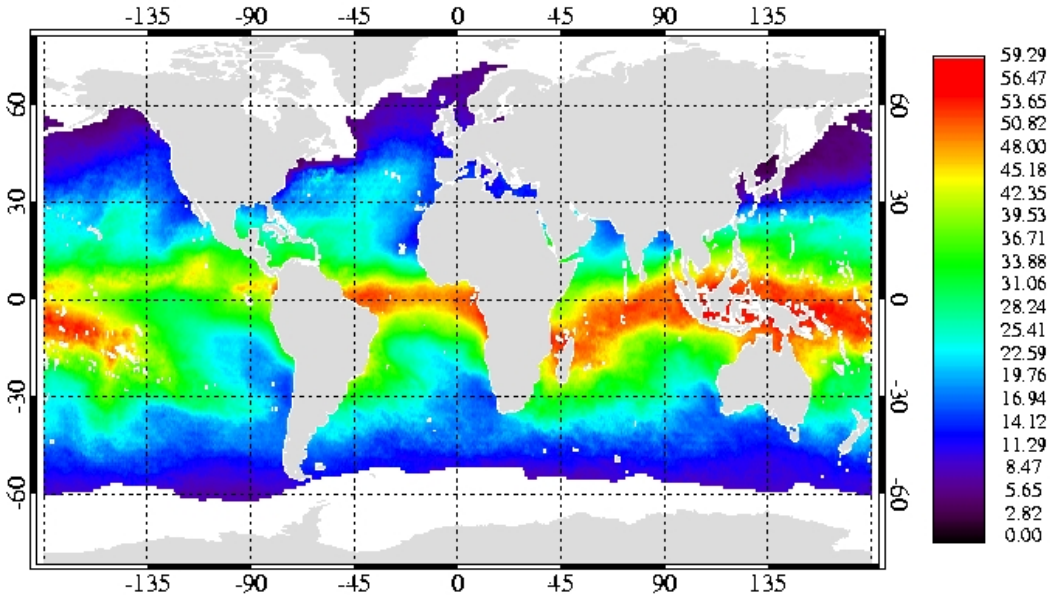

B: July

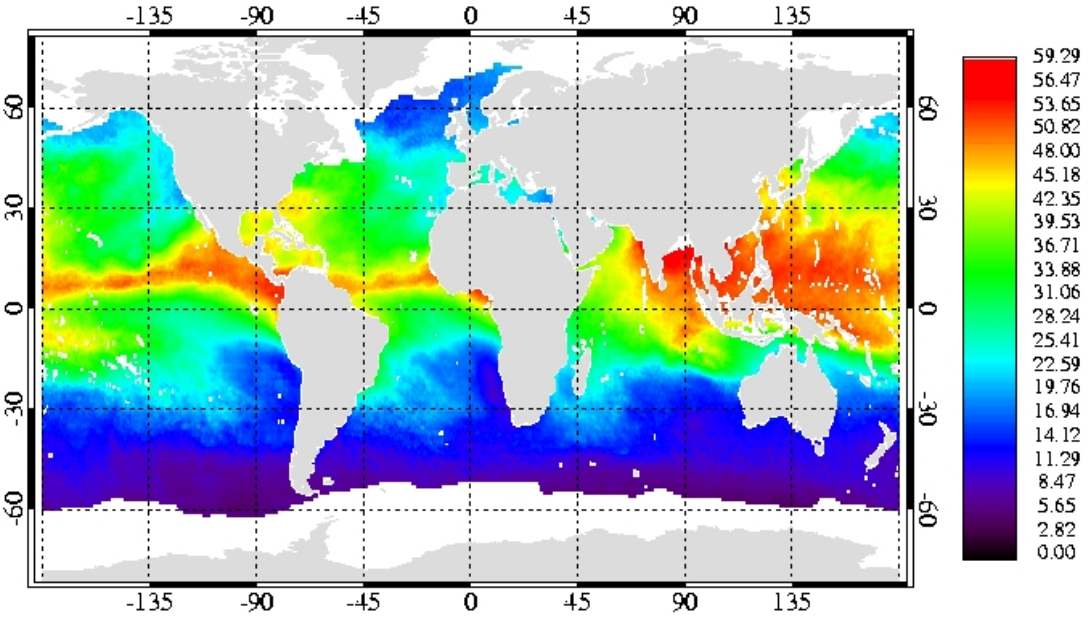

Figure 2.1: *Monthly mean clear–sky TPW [kg/m^2] for (A) January and (B) July 2004 clear–sky TPW derived from AMSU measurements. The grid size is 0.5°. Clear–sky is defined as a LWP of 0 kg/m^2 is observed.*

A: January

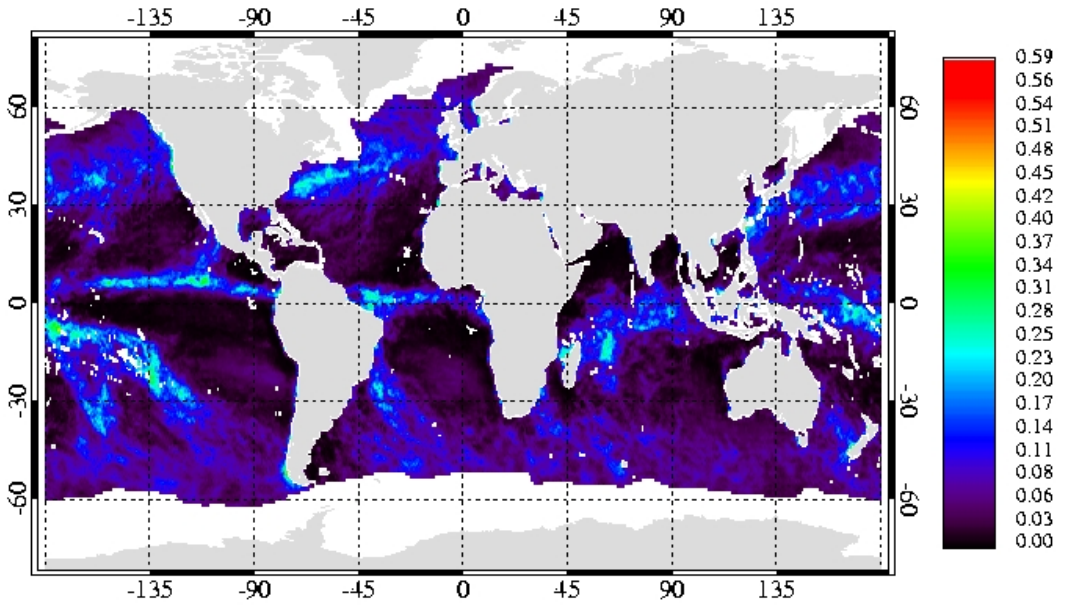

B: July

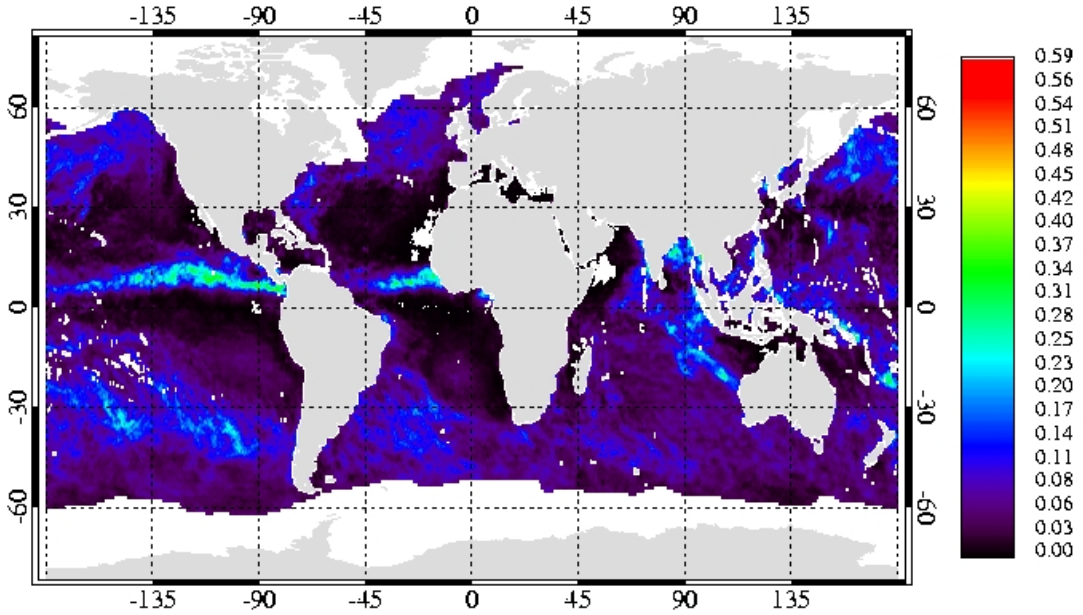

Figure 2.2: *Monthly mean LWP [kg/m^2] for (A) January and (B) July 2004 all sky LWP derived from AMSU measurements. The grid size is 0.5°. Only non–precipitating clouds inside the field of view are used.*

layer. The loss of energy therefore is lower.

Because of its strong greenhouse effect, the importance of a detailed knowledge of the water vapour distribution is prominent in the climate warming discussions. By means of a radiative transfer sensitivity study Bühler et al. (2004c) examine the influence of water vapour in clear sky atmosphere on outgoing longwave radiation (OLR). A water vapour increase of 20% in the tropics has the same reducing impact on the outgoing longwave radiation as a CO_2 doubling. Whereas a decrease of 20% shows the same impact on the OLR as a mean atmospheric temperature increase of 1K. The major parts of the OLR variability can be explained by changes in the mean atmospheric temperature, humidity and the CO_2.

Stephens and Tjemkes (1993) considered a linear relationship between the greenhouse effect G and the total precipitable water. The greenhouse effect is defined as the relation of the surface temperature T_s to the planetary temperature T_e. The temperatures can be expressed by the radiative effective optical depth using a grey body model. For the Earth's atmosphere this optical depth is expressed by the integrated total precipitable water, w.

$$G = \frac{T_s^4}{T_e^4} = a + b\,w \tag{2.1}$$

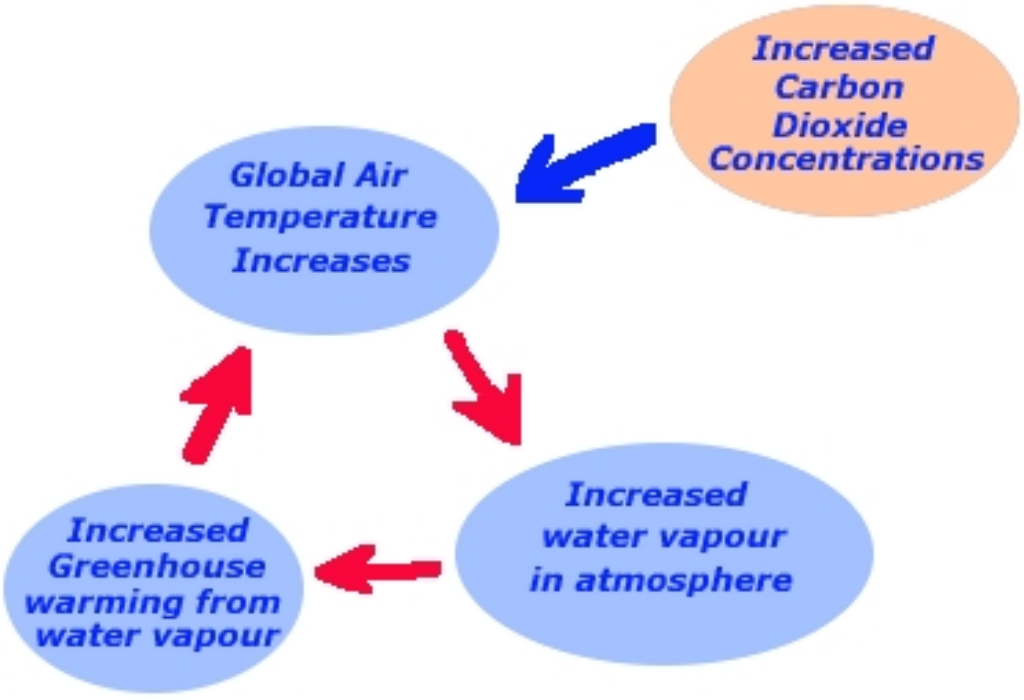

Figure 2.3: *Water vapour feedback characterises the greenhouse radiative forcing.*

The authors demonstrated that the slope factor b is largely governed by the variation of temperature with height in the atmosphere and that the intercept a is determined by a variety of factors including the assumed profile of water vapour as well as the concentrations of other greenhouse gases. Thus, the clear sky greenhouse effect is assessable from satellite by measurements of temperature and TPW. The correlation of the greenhouse effect, derived from Earth radiation budget and sea surface temperature observations, and using coincident SSM/I microwave observations of TPW for clear sky observations is given with 0.8. The retrieved greenhouse effect is not a direct measure of the water vapour feedback, which is not observed, because the true greenhouse effect is a consequence of numerous linked processes and feedbacks.

During the Cirrus Regional Study of Tropical Anvils and Cirrus Layers – Florida Area Cirrus Experiment (CRYSTAL–FACE) in July 2002 aircraft measurements in the infrared region were performed to estimate the greenhouse effect as a measure of the evaporative feedback of ocean and atmosphere. Marsden and Valero (2004) investigate the differences in the greenhouse effect due to water vapour absorption in cloudy compared to clear sky scenes. They conclude that convection and upper tropospheric moisture are the main determinants for the greenhouse efficiency.

Microwave retrieval techniques are based on the strong emission of the atmospheric water against the radiatively cold oceanic background. To investigate the TPW for cloud and clear scenes it is important to identify cloudy scenes. One advantage of microwave retrieval is the simultaneuously measurements of TPW and liquid water path (LWP). For these measurements ground based instruments are used as the truth. While TPW retrievals can be validated with colocated measurements from ground based sensors such as radiosondes, Global Positioning System (GPS) receiver, and Raman Lidar, retrieval validation of liquid water path is more complicated. During the last CLIWA–NET campaign (BBC) a ground based microwave intercomparison was performed to compare both instruments and the LWP retrieval algorithms. These algorithms are based on statistical correlations between brightness temperatures and LWP and TPW respectively. Resulting differences inbetween the various used algorithms are the cause of different cloud models and absorption schemes (see Löhnert and Crewell (2003)).

From radiosonde measurements the global vertical structure can be derived with a limited temporal and spatial resolution. Only ground based microwave radiometer with a profiling ability offer possibilities to derive the vertical structure in much higher temporal resolution. The vertically integrated water vapour is retrieved with time resolutions ranging from seconds to minutes depending on the radiometer sampling technique. Since ground based measurements represent point measurements, a regional TPW distribution can be maintained with a limited fidelity due to the limited distribution of contribution radiometers. Satellite based instruments offer better spatial coverage. Various techniques have been developed that are using different spectral bands to derive informations of the atmospheric water vapour, see Hauschildt and Macke (2004).

On board polar orbiting satellites infrared sensors like the High–resolution Infrared Radiation Sounder (HIRS) allow to derive the water vapour content in clear sky atmospheres only, because clouds are opaque in these spectral range. In the microwave spectrum non–precipitating clouds are translucent, so that sensors like the Special Sensor Microwave/Imager (SSM/I), the Spectral Sensor Microwave/Temperature (SSM/T–2) and the Advanced Microwave Sounding Unit (AMSU) offer the possibility to derive the TPW. These techniques are limited to ocean surfaces because the emission from the surface needs to be small and homogeneous within the radiometer field of view (FOV). These radiometer yield TPW products with a spatial resolution of about 60 km which is sufficient for resolving the TPW variability on a daily scale. Due to the polar orbits and limited swath the temporal variability of the water vapour fields related to synoptical processes can not be resolved.

Radiosondes offer humidity data for 50 years. The changes in equipment of one station during the years and the various radiosonde types introduce a temporal and spatial variability in the derived TPW fields. This uncertainty is investigated by Soden and Lanzante (1996) by comparing radiosonde upper–tropospheric humidity (UTH) with UTH derived from TIROS Operational Vertical Sounder (TOVS) measurements at 6.7 μm wavelength. The advantage of satellite measurements is that the basic technique is consistent over the globe. An error in the retrieval will lead to a systematic bias effecting the absolute numbers but the spatial variability is correct. Nevertheless, the retrieval of TPW or upper–tropospheric humidity with TOVS is limited to clear–sky scenes. The higher humidities in clouds and their vicinity are neglected, which leads to an underestimation of climatological water vapour. The dry bias in the upper–tropospheric humidity in TOVS estimates are assumed to be about 4%. This estimation is derived by comparing all radiosondes and those in clear–sky cases.

Lanzante and Gahrs (2000) introduced the temporal sampling bias (TSB) in UTH climatologies based on satellite data. They investigated the difference between continously observing radiosondes (6 times per day) and satellite based measurements which are maximum twice per day over an individual radiosonde station. A satellite UTH is available when at that time the atmosphere is cloud free. Thus, the satellite misses potentially moist cases and with two measurements per day, it cannot resolve diurnal cycle. The temporal sampling bias, TSB, ranges from -1 to 21 % relative humidity in the 500 hPa level for the different stations. The authors show further a latitudinal dependency of the clear–sky bias in the upper–troposphere. In the Tropics high convective towers hamper the satellite remote retrieval of humidity, the satellite misses the moistest cases. Considering radiosonde ascents at 63 stations during 1987-1991 the climatological mean values showed an underestimation in terms of relative humidity of 5 to 10%. Higher biases in upper tropospheric humidity occur in the Tropics. Trends in upper tropospheric humidity may be underestimated due to global warming; with increasing temperature the absolute humidity will increase but the relative humidity may be unchanged.

Geostationary orbits enable to monitor a region with a better temporal resolution compared to polar orbiting satellites. On METEOSAT–8, the first satellite of the Meteosat Second Generation (MSG), the Spinning Enhanced Visible and Infrared Imager (SEVIRI) measures infrared water vapour spectra with a spatial resolution of about 4 km at sub-satellite point

every 15 minutes. With this it is possible to derive a water vapour climatology with regards to the diurnal cycle. Furthermore, the use of two absorption and two window channels enables the derivation of the vertical distribution of water vapour. Similar to the HIRS instrument cloudy atmospheres are excluded in the SEVIRI retrieval.

Chapter 3

NAO

The NAO is the dominant mode of winter climate variability in the North Atlantic region ranging from central North America to Europe and much into Northern Asia. The NAO is a large scale seesaw in atmospheric mass between the subtropical high and the polar low. The corresponding index varies from year to year, but also exhibits a tendency to remain in one phase for intervals lasting several years.

Figure 3.1 shows the Winter (December to March) index of the NAO based on the difference of normalized sea level pressure (SLP) between Lisbon, Portugal and Stykkisholmur/Reykjavik,

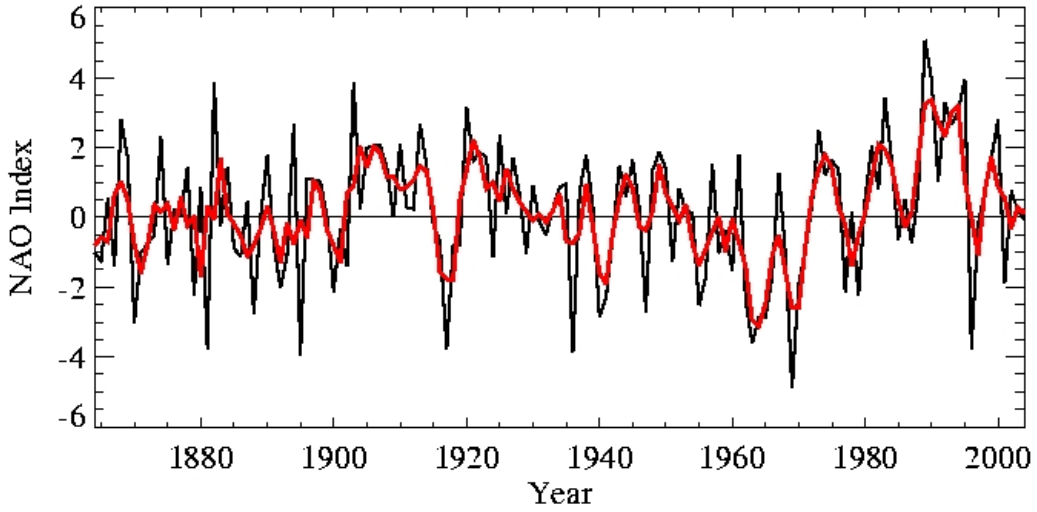

Figure 3.1: *The time series of the winter mean (December to March) NAO index after Hurrell is given in the upper panel. The red curve represents the 3-years running mean.*

Iceland since 1864. The SLP anomalies at each station were normalized by dividing each seasonal mean pressure with the long-term mean (1864–1983) standard deviation in order to avoid the series being dominated by the larger variability of the northern station. Positive values of the index indicate stronger-than-average westerlies over the mid latitudes.

For the time periods investigated in this study, 1994 to 2003, the NAO index is shown in

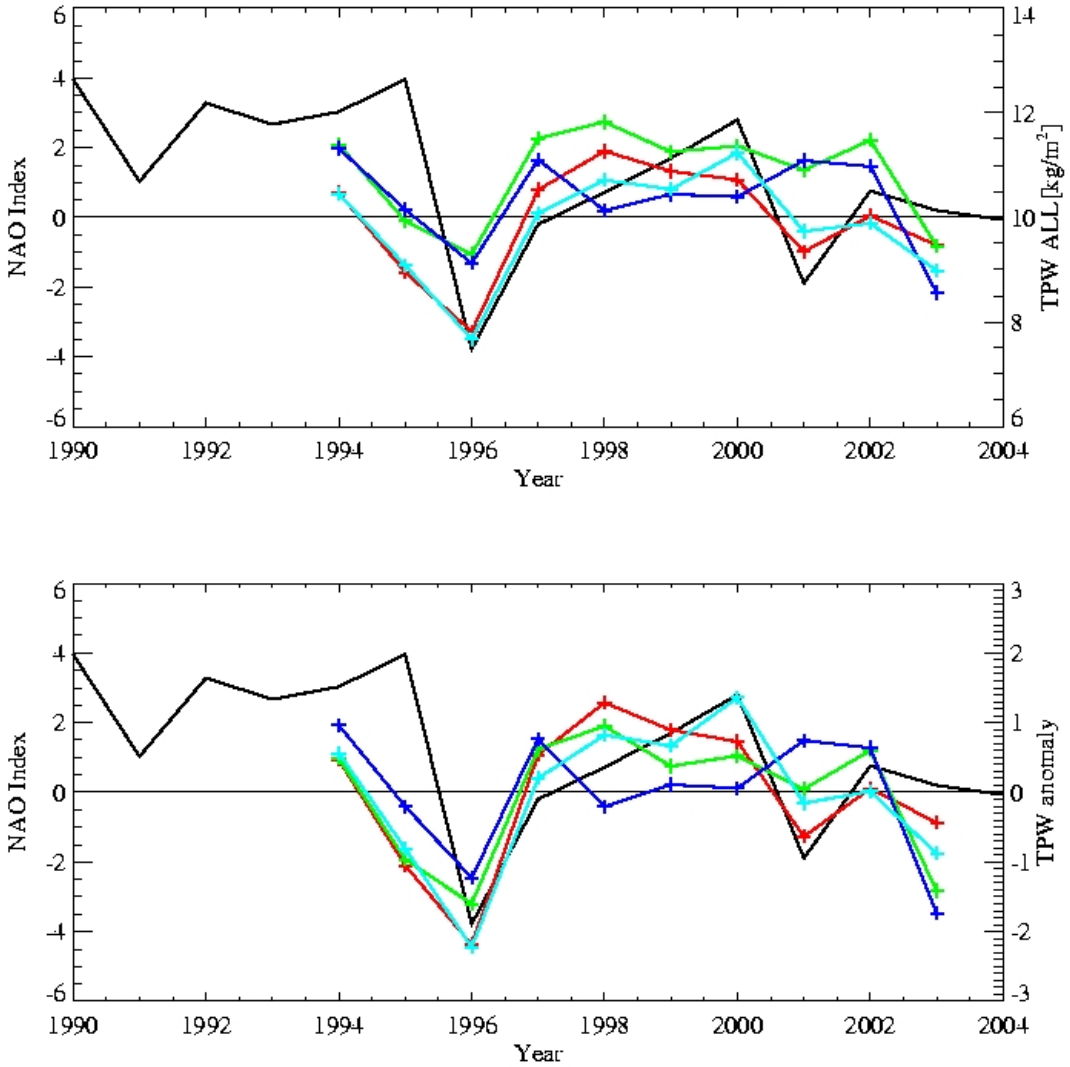

Figure 3.2: *Comparison of the all–sky TPW time serie and the NAO (top). The bottom panel shows the TPW anomaly and the NAO index. The coloured lines give the station TPW, Schleswig (red), Essen(green), Stuttgart (blue), and Lindenberg (cyan) .*

figure 3.2 together with the winter mean of the all–sky TPW for the German stations. The mean TPW roughly follows the NAO index. The large change in NAO from 1995 to 1996 from a positive index to negative values is visible in the TPW as a negative peak in the time series. For the stations Lindenberg and Schleswig the correlation of the NAO to the TPW is stronger than for the stations Essen and Stuttgart (table 3.1). The TPW anomaly follows the NAO index as well. For clear–sky TPW the stations show a lower relation to the NAO (figure

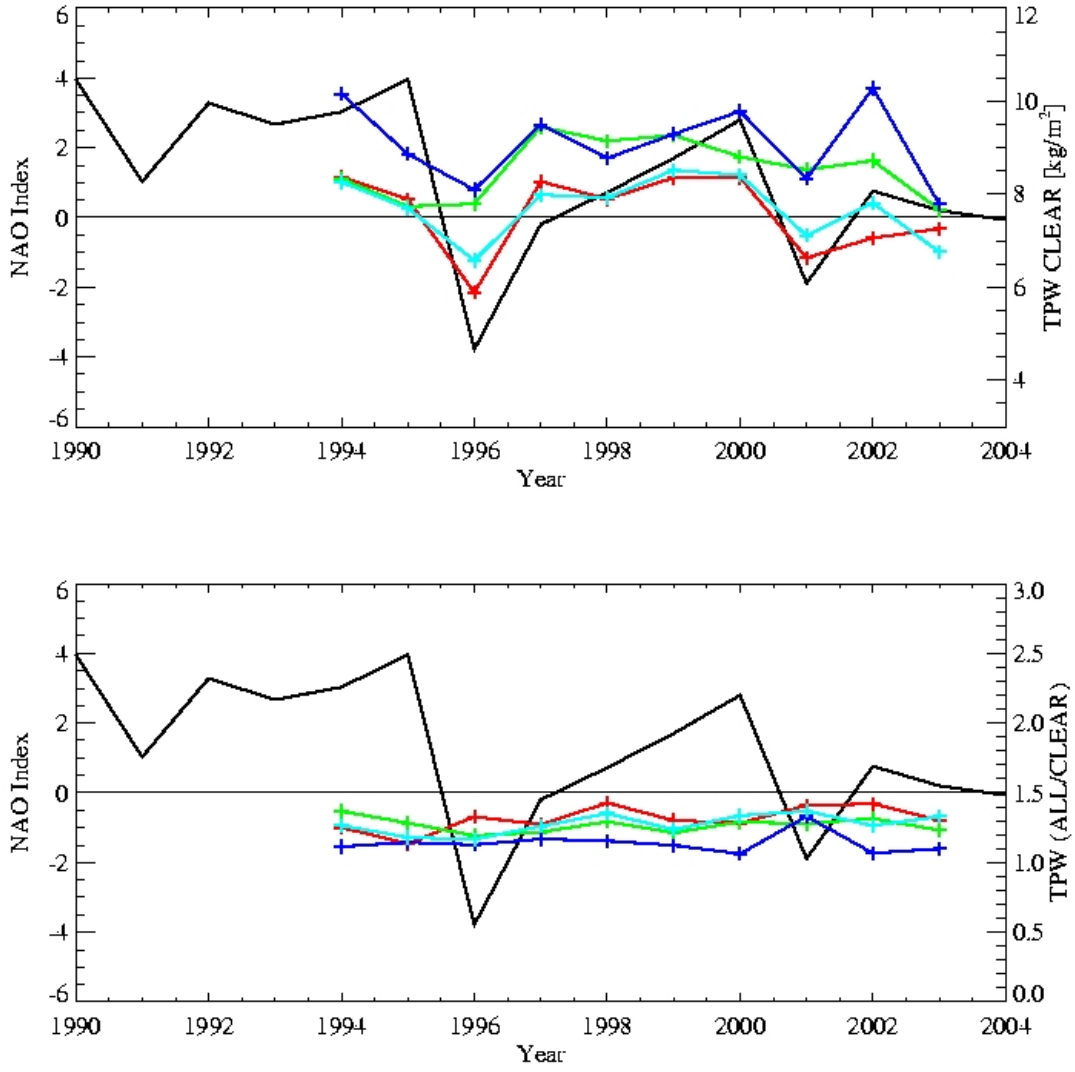

Figure 3.3: *Comparison of the TPW time serie and the NAO. The coloured lines give the station TPW, Schleswig (red), Essen(green), Stuttgart (blue), and Lindenberg (cyan) . Upper panel TPW clear, lower panel excess water vapour.*

3.3). The excess water vapour, the ratio of TPW in all–sky and clear–sky atmospheres, is not influenced by the NAO. The excess water vapour varies from station to station in the range of 1.1 to 1.4. The variability in clear– and all–sky TPW is not affecting the ratio. Only ten winter mean values are compared to the NAO which leads to insignificant correlations, as can be seen in the range of the correlation uncertainty, which is given in the table as well.

We can conclude that neither cold and dry winter (negative NAO values) nor warm and wet winter (positive NAO index) have a significant influence on the excess water vapour under cloudy conditions compared to clear conditions.

		Lindenberg						
		TPW	Temp	SLP	TPW Clear	TPW Cloud	Ratio (All/Clear)	TPW anomaly
NAO	cor	0.59	0.69	-0.50	0.72	0.60	-0.01	0.54
	err	0.56	0.50	0.65	0.40	0.54	0.85	0.5
		Schleswig						
		TPW	Temp	SLP	TPW Clear	TPW Cloud	Ratio (All/Clear)	TPW anomaly
NAO	cor	0.51	0.62	-0.64	0.82	0.44	-0.56	0.39
	err	0.63	0.52	0.51	0.28	0.69	0.58	0.6
		Essen						
		TPW	Temp	SLP	TPW Clear	TPW Cloud	Ratio (All/Clear)	TPW anomaly
NAO	cor	0.35	0.63	-0.12	0.09	0.50	0.57	0.28
	err	0.76	0.52	0.85	0.85	0.65	0.57	0.66
		Stuttgart						
		TPW	Temp	SLP	TPW Clear	TPW Cloud	Ratio (All/Clear)	TPW anomaly
NAO	cor	0.30	0.65	0.23	0.56	0.01	-0.42	0.32
	err	0.78	0.50	0.81	0.58	0.85	0.70	0.64

Table 3.1: *Correlation of the winter mean (December to March) NAO index after Hurrel and TPW, surface temperature, surface pressure, TPW clear, TPW cloud, ratio (ALL/CLEAR), and the TPW anomaly for the stations Schleswig, Lindenberg, Essen, and Stuttgart.*

Chapter 4

Ground and Satellite–based Retrieval Techniques

There are numerous techniques to determine the atmospheric water vapour from ground based, air borne and space borne sensors. By far the most in–situ measurements are taken from radiosonde humidity sensors. Laser-based measurements of water vapour absorption (Lyman-α) onboard research aircrafts provide continuous measurements during specific field campaigns, only. Most other methods are based on the relation of measured radiances to the water vapour concentrations. This relation is often derived by using numerous radiosonde profiles characterising the variability of the atmospheric state. In the following different retrieval techniques are shown and several intercomparison studies are summerised. A focus is set on the influence of clouds on the retrievals, the uncertainties of the methods and the attempts to quantify the water vapour inside the clouds. Most of the techniques find their limitations in the presence of clouds. In the infrared spectra clouds are opaque, so the retrieval of the total precipitable water is not possible. Some attempts are made to retrieve the water vapour above the clouds from infrared radiation measurements for cloud covered areas. The best opportunity to derive TPW in cloudy areas is given by microwave instruments. The methods are working for non-precipitating liquid water clouds, scattering of microwaves at large ice particles and raindrops weakens the relation between water content and radiances; from satellite the retrieval is limited to ocean areas.

4.1 Ground based Instruments and Techniques

Radiosonde measurements are an important database for weather and climate forecast models. They are often used as ground truth for validating humidity measurements based on other techniques and for the deduction of retrieval algorithms. The humidity sensors measure the relative humidity in the range $0-100$ % with an accuracy of about 2 %. Problems occur for dry and cold situations (e.g. in the upper–troposphere). The resolution of the relative humidity is too low for this cases (e.g. Revercomb et al. (2003), Turner et al. (2003), Bates and

Jackson (2001)). For global climatologies the different radiosondes with various sensor techniques yield to inhomogeneities in the water vapour fields (Westwater, 1997). A closer look on the various problems with radiosonde calibrations is given in Hauschildt and Macke (2004).

To assess differences between water vapour in clear and cloudy skies it is necessary to detect the cloud occurrences from temperature and humidity profiles. Auxiliary informations like cloud cover are important as the sonde does not necessary pass a cloud during the ascent. Various attempts to distinguish between clear and cloudy ascents are made.Thresholds and used to define the cloud layers (see Arabey (1975), Naud et al. (2003), Wang and Rossow (1995) and Wang et al. (1999)). In this study a scheme using the given cloud cover of the observer is used corresponding to a threshold in the dewpoint depression. If the minimum dewpoint depression of the ascent is below 0.5 K the radiosonde passes a cloud. A detailed analysis of the scheme is given in section 5.3.1.

Nevertheless, humidity and temperature profiles from radiosondes are commonly used in climate research. Many stations provide long timeseries of radiosonde data with several ascents per day. The more advanced microwave and lidar techniques are very limited in the covered region. Meanwhile, radiosondes are displaced by satellite and gps retrieved humidities in the assimilation schemes of the weather prediction models.

Radiosondes measurements are still the most important input for weather forecast models, despite their many disadvantages, for instance low temporal resolution, erroneous measurements especially of humidity, the inability to measure hydrometeors distribution, and their extremely high manpower costs. Strong efforts have been undertaken to develop alternative, ground based instruments for continuously monitoring the vertical structure of the atmosphere. Different types of active and passive sensors measure in different parts of the electromagnetic spectrum. Since the interaction of atmospheric constituents with atmospheric radiation changes with wavelength, spectrally diverse measurements contain different informations about the atmospheric composition.

Passive microwave radiometer measure the radiation emitted by water vapour in the atmospheric column in viewing direction of the instrument. At least measurements at two frequencies are needed to retrieve the TPW. Measuring the radiation at more frequencies enable the retrieval of a humidity profile. The lower layers provide the strongest emission, which is also the least attenuated, while the higher layers provide low emission, which is additionally highly attenuated by the lower layers before it reaches the sensor (see Elachi (1987).

4.2 Satellite Instruments and Techniques

Satellite remote sensing is based on radiation measurements modulated due to absorption, emission and scattering by the atmospheric constituents. The modulation depends on the

part of the radiation spectrum under consideration figure 4.1 shows atmospheric attenuation in the range from ultraviolet to radiowaves. In the far infrared the atmosphere is opaque whereas in the microwave region it is transparent except of two water vapour absorption lines (22.2 and 183 GHz) and two oxygen absorption bands (60 and 118 GHz). There are minor absorption bands related to ozone and other trace gases. Strong absorption in the infrared mostly due to H_2O and CO_2 is found. In the atmospheric water vapour window (8 - 12 μm) a strong ozone absorption line is disposed. For microwave radiation the atmosphere appears to be transparent beside a H_2O line at 22.235 GHz and 180 GHz and two O_2 lines at 53 GHz and 120 GHz. Remote sensing techniques for the retrieval of water vapour make use of spectral changes in molecular absorption.

The infrared satellite retrieval method are based on the split-window technique in which the difference in absorption between two nearby infrared channels is used to estimate the TPW. The greater the difference between the brightness temperatures, the more water vapor found above the pixel whose brightness temperatures are being measured (Kidder and Vonder Haar (1995, Chapter 6)). Typical wavelengths used for water vapour retrieval are 8.90 – 9.20 μm, 9.31 – 9.41 μm or 9.15 – 9.65 μm. With more channels close to one absorption line it is possible to retrieve additional informations about the vertical distribution of water vapour. Depending on the used wavelengths the signal is mostly emitted from a specific height. Each atmospheric layer is characterised by the peak in the weighting function.

Microwave radiometers offer the possibility to retrieve the TPW in clear and cloudy atmospheres. Passive microwave techniques measure the emission from the surface and the atmosphere. For the retrieval of atmospheric constituents it is compellent to know the background emission from the surface. Ocean surfaces appear cold and homogeneous in the microwave re-

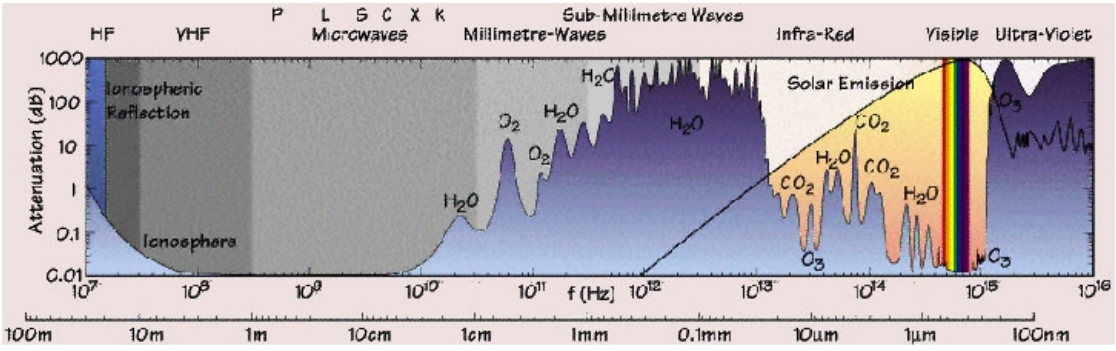

Figure 4.1: *The attenuation depending on the wavelength for the electromagnetic spectrum. The atmospheric absorption bands are labeled by the main absorbing gases.*

gion and their variability in emittance depends on the sea surface temperature, the roughness and the salinity. With ocean surface models the microwave emission can be assessed. Land surface emission is much stronger and depends on many variables which are inhomogeneous on small spatial scales. The retrieval of atmospheric properties is possible over ocean only. In the microwave region water vapour path and liquid water path is retrieved simultaneously using at least two frequencies; one close to the water vapour absorption line and one in the window where the radiation is related to the condensed water. An algorithm using AMSU channels is described in Grody et al. (2001). As for ground based microwave techniques described in section 4.1 scattering at large raindrops and ice particles weakens the efficiency of the algorithm and limits its application to nonprecipitating water clouds.

Humidity profiles can be obtained from measuring radiances at only the flanks of an appropriate absorption peak. Like for IR-measurements the measured radiance is related to an altitude by a corresponding weighting function.

Basically a two frequency scheme is used where one frequency is near the water vapour absorption line and another in the window channel. Numerous algorithms based on the frequencies available from SSM/I, SSM/T2, MSU and AMSU can be found in literature, a selection is described in the study of Wahl et al. (2003). Comparing the retrieved water vapour path to radiosonde and ground based microwave measurements shows a reasonable agreement. Ruprecht (1996) shows a bias for SSM/I TPW compared to radiosonde in a way that the satellite retrieval overestimates for low TPW and underestimates for high TPW retrieved with radiosondes.

English (1999) suggests a method for humidity and temperature profiling over land and bright surfaces with AMSU. The atmospheric humidity and temperature profiles can be derived within a acceptable error range. The influence of surface emission is stronger in the LWP retrieval then for the humidity retrieval. However, the humidity retrieval is sensitive to the LWP as well.

Other techniques like GPS Systems and combined retrievals using various frequencies are described in detail in Hauschildt and Macke (2004).

Chapter 5

Ground–based analysis

Radiosondes provide a suitable ground truth for humidity profiling of the atmosphere. The total precipitable water (TPW) is defined as the vertical integrated absolute humidity (from surface to 300 hPa). In this section ten years of radiosonde ascents with corresponding cloud cover observations at the German stations Lindenberg, Schleswig, Essen, and Stuttgart are studied. The radiosonde ascents are used to check whether the TPW in cloudy skies is significantly different compared to clear–sky situations, see section 5.1. The general behaviour of TPW in the mid–latitudes is investigated in section 5.2. Results are shown exemplarily for the station Lindenberg. A focus is set on the difference in TPW for different atmospheric layers (see section 5.4). Furthermore, the relation of all–sky to clear–sky TPW for all stations and both possible error sources and uncertainties are estimated.

5.1 Cloud to clear TPW differences

The first question to be accessed is whether there is more total precipitable water in cloudy–skies compared to clear–sky atmospheres. In the study of Gaffen and Elliot (1993) three years (1988-1990) of day time radiosoundings at 15 North hemispheric stations are used. The TPW is calculated from surface to 400 hPa. The data is categorised according to sky cloud cover from simultaneous suface visual cloud observations. The authors show significantly lower climatological TPW in clear–skies then in cloudy–skies. The variation in TPW with cloud cover is not only explainable by variations in air temperature, since an increase in cloud cover generally leads to a decrease in day time temperature.

To proof the climatological TPW difference between clear–skies and cloudy–skies Gaffen and Elliot (1993) categorise the TPW values by the observed cloud cover based on the WMO-category of cloud amount where 0 oktas is clear (CLR), 1 to 4 oktas is scattered (SCT), 5 to 7 is broken (BKN), and 8 oktas is overcast (OVC). Reports of sky obscured and fog were discarded in this analysis. The data were separated into classes according to cloud cover and

season. For each class the mean TPW has been calculated. The authors define the mean all–sky total precipitable water ($\overline{TPW}_{ALL}$) as:

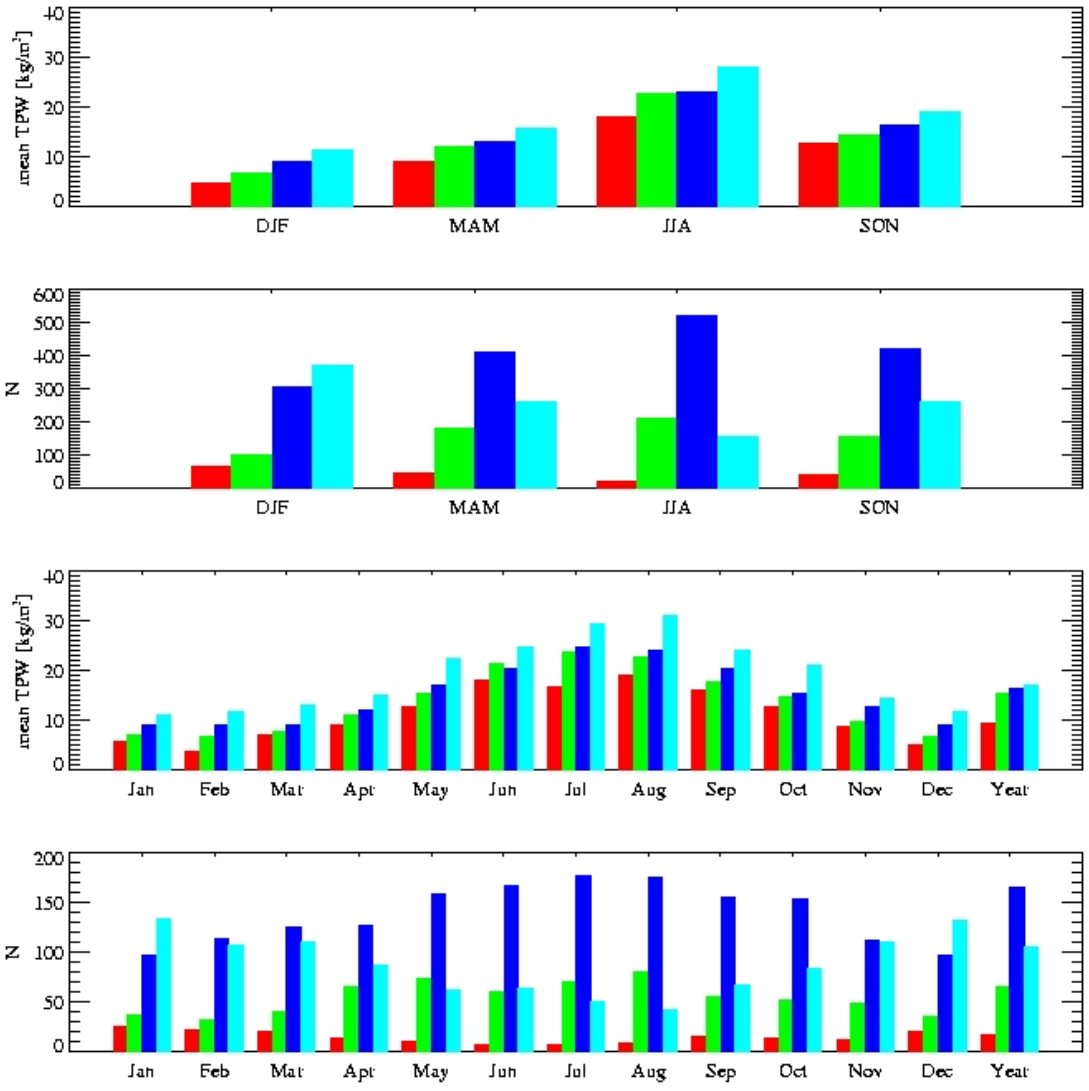

Figure 5.1: *10 years of data from Lindenberg sorted by the observed cloud cover: clear–sky in red, scattered cloudiness (1-4 octas) in green, broken cloudiness (5-7 octas) in blue, and overcast in cyan. From Top to bottom: Seasonal mean TPW in the cloud classes, number of cases per cloud class per season, monthly mean TPW per cloud classes and the number of cases per class. The last block in the monthly dispartment gives the yearly mean (the number of cases is given by the ordinate number times 10).*

$$\overline{TPW}_{ALL} = \frac{N_{CLR}\overline{TPW}_{CLR} + N_{SCT}\overline{TPW}_{SCT} + N_{BKN}\overline{TPW}_{BKN} + N_{OVC}\overline{TPW}_{OVC}}{N_{CLR} + N_{SCT} + N_{BKN} + N_{OVC}} \quad (5.1)$$

were the subscripts refer to the cloud classes and N is the number of samples used to calculate the mean. Three additional parameters are defined to quantify the bias in climatological

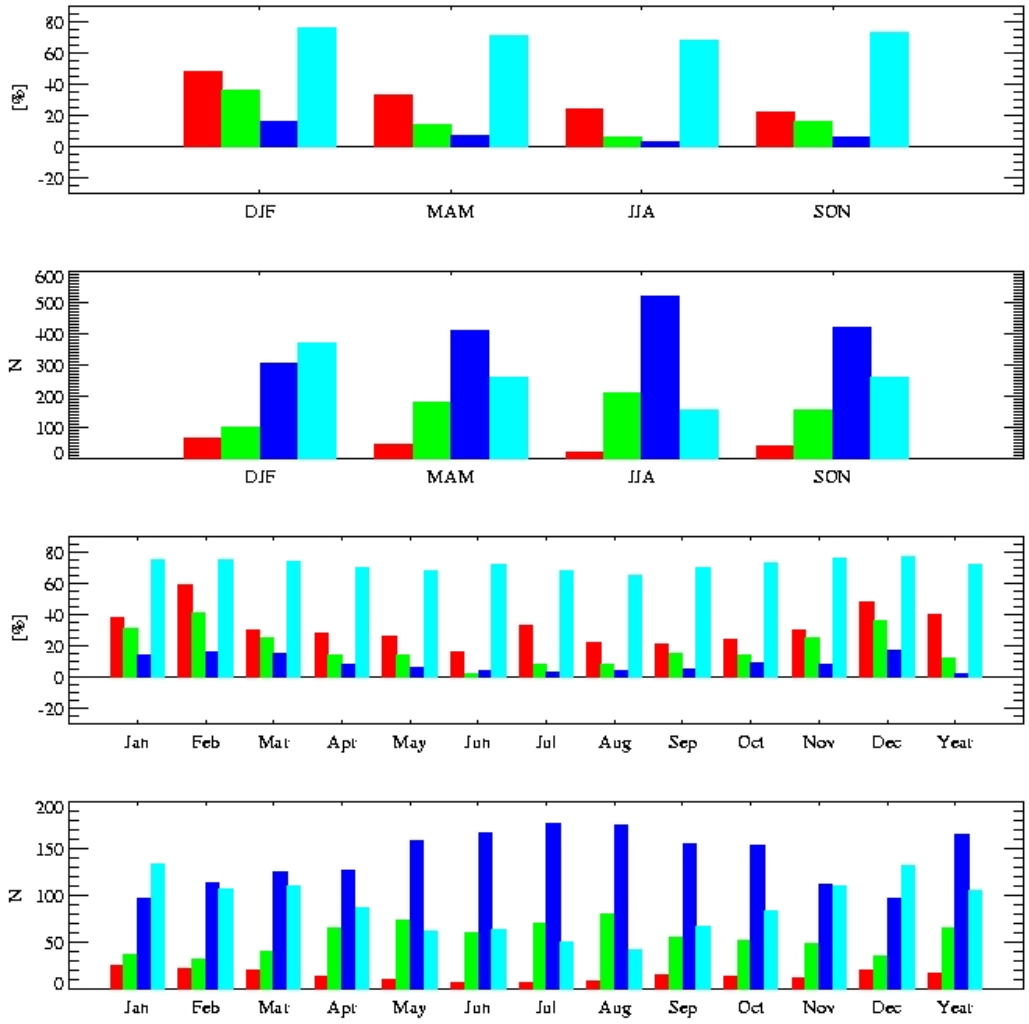

Figure 5.2: *The bias estimators and the probability according to Gaffen and Elliot (1993): the b_0 in red, b_4 in green, b_7 in blue, and the probability in cyan. From Top to bottom: Seasonal bias estimators, number of cases per cloud class (see figure 5.1) per season, monthly bias estimators and the number of cases per class. The last block in the monthly dispartment gives the yearly mean (the number of cases is given by the ordinate number times 10).*

($\overline{TPW}$) values.

$$B_0 = \frac{\overline{TPW}_{CLR}}{\overline{TPW}_{ALL}}\,, \tag{5.2}$$

$$B_4 = \frac{\dfrac{N_{CLR}\,\overline{TPW}_{CLR} + N_{SCT}\,\overline{TPW}_{SCT}}{N_{CLR} + N_{SCT}}}{\overline{TPW}_{ALL}}\,, \tag{5.3}$$

$$B_7 = \frac{\dfrac{N_{CLR}\,\overline{TPW}_{CLR} + N_{SCT}\,\overline{TPW}_{SCT} + N_{BKN}\,\overline{TPW}_{BKN}}{N_{CLR} + N_{SCT} + N_{BKN}}}{\overline{TPW}_{ALL}}\,. \tag{5.4}$$

The subscripts $(0, 4, 7)$ in equation 5.2 to 5.4 denote the maximum cloud cover included. For example B_0 expressed as a percentage gives the percent by which $\overline{TPW}_{ALL}$ is underestimated when only clear–sky observations are included. B_0 and B_7 therefore define the extreme cases. The probability P of a radiosonde passing through a cloud is estimated by the product of the the probability of encountering a cloud for a given cloud cover category and the probability of occurrence of the that category, summed over all categories,

$$P = \sum_{k=0}^{8} \frac{k}{8}\,\frac{n_k}{N}\,. \tag{5.5}$$

Here the index k is the cloud–cover in oktas, n_k is the number of observations per category and N is the total number of observations.

Gaffen and Elliot (1993) analysed 3 years of radiosoundings. The amount of data per cloud category was low. Our data set including only four German stations but 10 years of radiosoundings will lead to more robust mean values and enables estimating monthly means. In figure 5.1 the mean TPW per cloud class and the number of cases included are shown both for seasonal and monthly mean. The annual cycle of TPW related to the air temperature is observed. Each month shows an increase in TPW with increasing cloudiness. Broken cloudiness is the most frequently observed cloud class for the German area. The number of clear–sky observations is low. An annual cycle in clear–sky observations in found for Lindenberg with a higher occurrence in winter time and a decrease towards summer. In summer the number of overcast observations is lower than for the rest of the year.

The bias indices defined in equation 5.2 - 5.4 are shown in figure 5.2. B_0 is always larger than B_7 which is expected because the extreme situations are used. For B_0 only clear–sky values are used to define the relation whereas for B_7 moist atmospheres with up to seven oktas observed cloud cover are used. Similar to Gaffen and Elliot (1993) the general behaviour of the bias indices is: $B_0 > B_4 > B_7$. The probability of a radiosonde to pass a cloud is shown in

figure 5.2 as well. For Lindenberg the probability is larger than 70 % and decreases slightly towards summer. In appendix A results for Schleswig, Stuttgart, and Essen are shown.

Results for all stations are summerised in the following tables. In table 5.2 and 5.3 the monthly mean TPW and the number of cases comprising the mean for the four stations. The results for the seasonal means are given in table A.1 in the appendix A. The bias indices and the probability of the radiosonde to pass a cloud are given in table 5.4 on monthly basis and in table A.2 (see appendix A) on seasonal basis. In summer the number of clear–cases are rare. For all stations the probability for the radiosonde to pass a cloud is larger than 50 %. For the station Schleswig the number of clear–sky observation in summer is very low. Schleswig is close to both North and Baltic sea. In summer a land–sea–circulation occurs due to the stronger warming over land than over the seas and convective clouds are formed. The observation time, 12 UTC which is 14:00 local time is located around the main convective time.
For the station Stuttgart the number of clear–sky observations is small as well. Here local circulations are responsible for frequently occurring convective clouds at noon time.
The German stations are located in the same latitude. Therefore, we do not expect any latitudinal differences in TPW like **??** report on their northern hemisphere stations. The all–sky annual mean TPW is about 16 kg/m^2, the regional variablity is less than 1 kg/m^2. The annual cycle of the all–sky mean is defined by the minimum value in February of about 9.5 kg/m^2 and the maximum value in July of 25 kg/m^2. The increase of TPW due to the presence of clouds is observed for all stations. Overcast scenes obtain nearly three times the clear–sky TPW.

	Jan		**Feb**		**Mar**		**Apr**		**May**		**Jun**	
	TPW	**N**	**TPW**	**N**	**TPW**	**N**	**TPW**	**N**	**TPW**	**N**	**TPW**	**N**
Lindenberg												
CLR	5.90	25	3.80	22	7.18	21	9.04	14	12.97	10	18.08	8
SCT	7.09	37	6.70	32	7.87	40	11.31	66	15.48	74	21.49	60
BKN	9.24	97	9.06	114	9.14	126	12.12	128	17.28	159	20.52	167
OVC	11.18	134	11.90	107	13.00	111	15.14	88	22.33	62	24.81	64
ALL	9.57	293	9.47	275	10.27	298	12.69	296	17.73	305	21.57	299
	Jul		**Aug**		**Sep**		**Oct**		**Nov**		**Dec**	
CLR	16.87	7	19.06	9	16.12	16	12.77	14	8.91	12	5.03	20
SCT	23.77	71	22.86	81	17.83	56	14.82	52	9.77	49	6.85	35
BKN	24.88	178	24.18	175	20.31	156	15.52	154	12.93	112	9.17	97
OVC	29.61	50	31.16	42	24.27	68	21.15	84	14.51	110	11.72	132
ALL	25.21	306	24.64	307	20.53	296	16.83	304	12.83	283	9.78	284

Table 5.1: *Monthly mean TPW in kg/m^2 in the cloud classes (CLR = clear, SCT = scattered (1-4 octas), BKN = broken (5-7 octas), OVC = overcast) and without regards to cloudiness (ALL) for Lindenberg. N gives the number of observations comprising the mean.*

	Jan		**Feb**		**Mar**		**Apr**		**May**		**Jun**	
	TPW	**N**	**TPW**	**N**	**TPW**	**N**	**TPW**	**N**	**TPW**	**N**	**TPW**	**N**
Schleswig												
CLR	5.09	3	4.07	10	6.32	12	8.37	10	17.85	10	–	0
SCT	6.49	49	5.10	35	7.20	56	9.33	59	12.83	77	18.32	60
BKN	8.85	119	8.57	130	8.70	132	11.64	153	15.56	169	18.91	185
OVC	12.32	107	13.29	91	13.21	97	16.32	67	22.68	47	23.60	52
ALL	9.73	278	9.56	266	9.80	297	12.14	289	16.04	303	19.61	297
	Jul		**Aug**		**Sep**		**Oct**		**Nov**		**Dec**	
CLR	28.58	3	22.33	5	22.36	3	14.59	3	6.37	4	4.77	6
SCT	20.84	74	20.99	88	16.79	62	11.28	59	8.90	48	6.20	55
BKN	22.58	193	22.87	183	18.65	169	15.42	176	11.23	132	9.44	107
OVC	27.43	37	29.63	30	25.98	65	21.17	65	15.89	96	13.53	107
ALL	22.81	307	22.99	306	19.90	299	15.84	303	12.36	280	10.28	275

	Jan		**Feb**		**Mar**		**Apr**		**May**		**Jun**	
	TPW	**N**	**TPW**	**N**	**TPW**	**N**	**TPW**	**N**	**TPW**	**N**	**TPW**	**N**
Essen												
CLR	5.16	12	4.70	17	6.04	18	8.91	9	14.37	5	27.38	2
SCT	7.32	47	7.25	45	8.33	50	9.60	67	14.84	63	18.41	70
BKN	10.01	118	9.51	95	10.46	132	11.98	153	16.17	141	19.90	158
OVC	13.25	93	13.32	81	15.73	74	17.44	61	20.66	66	25.78	38
ALL	10.44	270	10.04	238	11.20	274	12.48	290	16.91	275	20.40	268
	Jul		**Aug**		**Sep**		**Oct**		**Nov**		**Dec**	
CLR	20.78	9	22.79	12	15.31	5	11.68	10	8.85	6	4.28	16
SCT	23.18	91	21.76	91	17.25	59	12.50	52	9.90	48	7.22	38
BKN	23.88	137	23.54	125	19.57	139	16.53	128	12.71	101	10.59	99
OVC	27.68	43	30.10	42	24.52	62	20.73	75	16.38	106	14.12	116
ALL	24.13	280	23.93	270	20.13	265	16.75	265	13.59	261	11.26	269

Table 5.2: *Monthly mean TPW in kg/m^2 in the cloud classes (CLR = clear, SCT = scattered (1-4 octas), BKN = broken (5-7 octas), OVC = overcast) and without regards to cloudiness (ALL) for Schleswig and Essen. N gives the number of observations comprising the mean.*

	Jan		**Feb**		**Mar**		**Apr**		**May**		**Jun**	
	TPW	**N**	**TPW**	**N**	**TPW**	**N**	**TPW**	**N**	**TPW**	**N**	**TPW**	**N**
Stuttgart												
CLR	5.12	16	4.97	8	7.68	11	4.41	1	16.03	1	17.09	2
SCT	7.61	37	7.46	37	7.73	41	10.47	44	15.07	56	20.63	64
BKN	9.88	86	9.41	94	10.85	77	12.79	98	16.85	99	20.98	97
OVC	10.80	98	11.77	69	13.43	77	14.51	47	21.75	58	23.92	37
ALL	9.58	237	9.68	208	11.02	206	12.64	190	17.71	214	21.37	200
	Jul		**Aug**		**Sep**		**Oct**		**Nov**		**Dec**	
CLR	18.71	2	17.13	2	16.77	3	10.45	6	8.33	6	6.31	4
SCT	22.15	85	22.61	78	16.01	52	12.79	46	9.56	24	8.17	27
BKN	26.04	91	24.10	92	19.55	97	16.13	108	12.57	87	10.83	96
OVC	27.89	36	29.70	25	25.01	49	20.42	59	14.75	93	12.41	86
ALL	24.74	214	24.15	197	19.93	201	16.43	219	13.07	210	11.04	213

Table 5.3: *Monthly mean TPW in kg/m^2 in the cloud classes (CLR = clear, SCT = scattered (1-4 octas), BKN = broken (5-7 octas), OVC = overcast) and without regards to cloudiness (ALL) for Stuttgart. N gives the number of observations comprising the mean.*

	Jan	Feb	Mar	Apr	May	Jun	Jul	Aug	Sep	Oct	Nov	Dec
Lindenberg												
CLR/OVC	0.53	0.32	0.55	0.60	0.58	0.73*	0.57*	0.61*	0.66	0.60	0.61	0.43
SCT/OVC	0.63	0.56	0.61	0.75	0.69	0.87	0.80	0.73	0.73	0.70	0.67	0.58
BKN/OVC	0.83	0.76	0.70	0.80	0.77	0.83	0.84	0.78	0.84	0.73	0.89	0.78
B0	0.38	0.60	0.30	0.29	0.27	0.16	0.33*	0.23*	0.21*	0.24	0.31	0.49
B4	0.31	0.42	0.26	0.14	0.14	0.02	0.08	0.09	0.15	0.15	0.25	0.37
B7	0.14	0.16	0.16	0.08	0.07	0.04	0.03	0.04	0.05	0.10	0.08	0.17
P	0.75	0.76	0.74	0.70	0.68	0.72	0.68	0.65	0.70	0.73	0.76	0.77
Schleswig												
CLR/OVC	0.41*	0.31	0.48	0.51	0.79	–	1.04*	0.75*	0.86*	0.69*	0.40*	0.35*
SCT/OVC	0.53	0.38	0.55	0.57	0.57	0.78	0.76	0.71	0.65	0.53	0.56	0.46
BKN/OVC	0.72	0.65	0.66	0.71	0.69	0.80	0.82	0.77	0.72	0.73	0.71	0.70
B0	0.48*	0.57	0.36	0.31	-0.11	–	-0.25*	0.03*	-0.12*	0.08*	0.48*	0.54*
B4	0.34	0.49	0.28	0.24	0.16	0.07	0.07	0.08	0.14	0.28	0.30	0.41
B7	0.17	0.20	0.17	0.10	0.08	0.04	0.03	0.03	0.08	0.09	0.15	0.20
P	0.79	0.77	0.73	0.72	0.68	0.73	0.69	0.66	0.74	0.76	0.78	0.76
Essen												
CLR/OVC	0.39	0.35	0.38	0.51*	0.70*	1.06*	0.75*	0.76	0.62*	0.56	0.54*	0.30
SCT/OVC	0.55	0.54	0.53	0.55	0.72	0.71	0.84	0.72	0.70	0.60	0.60	0.51
BKN/OVC	0.76	0.71	0.67	0.69	0.78	0.77	0.86	0.78	0.80	0.80	0.78	0.75
B0	0.51	0.53	0.46	0.29*	0.15*	-0.34*	0.14*	0.05	0.24*	0.30	0.35*	0.62
B4	0.34	0.35	0.31	0.24	0.12	0.09	0.05	0.09	0.15	0.26	0.28	0.44
B7	0.14	0.17	0.15	0.11	0.07	0.04	0.03	0.05	0.07	0.09	0.14	0.19
P	0.75	0.72	0.72	0.71	0.72	0.69	0.65	0.64	0.72	0.72	0.78	0.78
Stuttgart												
CLR/OVC	0.47	0.42*	0.57	0.30*	0.74*	0.71*	0.67*	0.58*	0.67*	0.51*	0.56*	0.51*
SCT/OVC	0.70	0.63	0.58	0.72	0.69	0.86	0.79	0.76	0.64	0.63	0.65	0.66
BKN/OVC	0.91	0.80	0.81	0.88	0.77	0.88	0.93	0.81	0.78	0.79	0.85	0.87
B0	0.47	0.49*	0.30	0.65*	0.09*	0.20*	0.24*	0.29*	0.16*	0.36*	0.36*	0.43*
B4	0.28	0.27	0.30	0.18	0.15	0.04	0.11	0.07	0.19	0.24	0.29	0.28
B7	0.09	0.11	0.13	0.05	0.08	0.03	0.03	0.03	0.08	0.09	0.10	0.08
P	0.76	0.75	0.73	0.73	0.72	0.67	0.63	0.62	0.70	0.72	0.81	0.81

Table 5.4: *Monthly ratios of the mean TPW in a cloud class (CLR = clear, SCT = scattered (1-4 octas), BKN = broken (5-7 octas)) towards the overcast mean TPW (OVC) for each station. The bias indices (dimensionless), and the probability of a sounding passing through a cloud as defined in the equations 5.2 to 5.5 are given. A dash is given when no clear–sky observations are done, ratios and indices based on less then 10 observations are marked (*).*

5.2 TPW under all–sky and clear–sky conditions

In this section the difference in mean TPW for clear– and all–sky atmospheres for different temporal scales is investigated. The final task is to obtain a conversion scheme to relate the clear–sky TPW climatologies derived from satellite measurements to the all–sky TPW. It is decisive to assess the variability at different time scales. For this purpose the radiosondes and synoptical data at four German weather stations are used. Observations are deployed for the years 1994 to 2003. Geographically, the stations are close to each other. Observations are not independent neither on temporal nor on spatial scale. Thus, the degree of dependence is examined.

In Figure 5.3 station–to–station correlations are shown relative to Lindenberg for the stations Schleswig, Stuttgart, and Essen. The largest correlation is found for the surface temperature, surface pressure and the height of the 500 hPa level. The TPW shows lower correlations ranging from 0.65 to 0.76. In table 5.5 the correlation coefficients for the combinations of two stations are given. For geographically close stations the correlations are larger, as we are looking at nearly the same airmass. Since Stuttgart is located at a higher surface level, a bias in the near surface parameters is observed. In the following the station Lindenberg because it shows the highest occurrence of clear–sky observations at noon time, compared to the other stations.

	Lindenberg				**Essen**				**Stuttgart**			
	SLP	**H500**	**Temp**	**TPW**	**SLP**	**H500**	**Temp**	**TPW**	**SLP**	**H500**	**Temp**	**TPW**
Schleswig	0.94	0.92	0.94	0.76	0.89	0.90	0.89	0.75	0.75	0.84	0.89	0.65
	Schleswig				**Essen**				**Stuttgart**			
	SLP	**H500**	**Temp**	**TPW**	**SLP**	**H500**	**Temp**	**TPW**	**SLP**	**H500**	**Temp**	**TPW**
Lindenberg	0.94	0.92	0.94	0.76	0.88	0.89	0.89	0.71	0.82	0.91	0.91	0.73
	Schleswig				**Lindenberg**				**Stuttgart**			
	SLP	**H500**	**Temp**	**TPW**	**SLP**	**H500**	**Temp**	**TPW**	**SLP**	**H500**	**Temp**	**TPW**
Essen	0.89	0.90	0.89	0.75	0.88	0.89	0.89	0.71	0.93	0.93	0.91	0.79
	Schleswig				**Lindenberg**				**Essen**			
	SLP	**H500**	**Temp**	**TPW**	**SLP**	**H500**	**Temp**	**TPW**	**SLP**	**H500**	**Temp**	**TPW**
Stuttgart	0.75	0.84	0.89	0.65	0.82	0.91	0.92	0.73	0.93	0.93	0.91	0.79

Table 5.5: *Correlation coefficients of the DWD stations Schleswig, Lindenberg, Essen, and Stuttgart for the TPW given, the surface temperature, the surface pressure and the height of the 500 hPa level.*

5.2.1 TPW statistics for Lindenberg

To examine the behaviour of the TPW in all–sky situations 10-years of radiosonde profiles derived at the DWD station Lindenberg have been investigated. Time series of surface pressure, surface temperature, the height of the 500 hPa level, cloud cover and the TPW are shown in figure 5.4. The annual cycle in the TPW is clearly visible as it follows strongly the

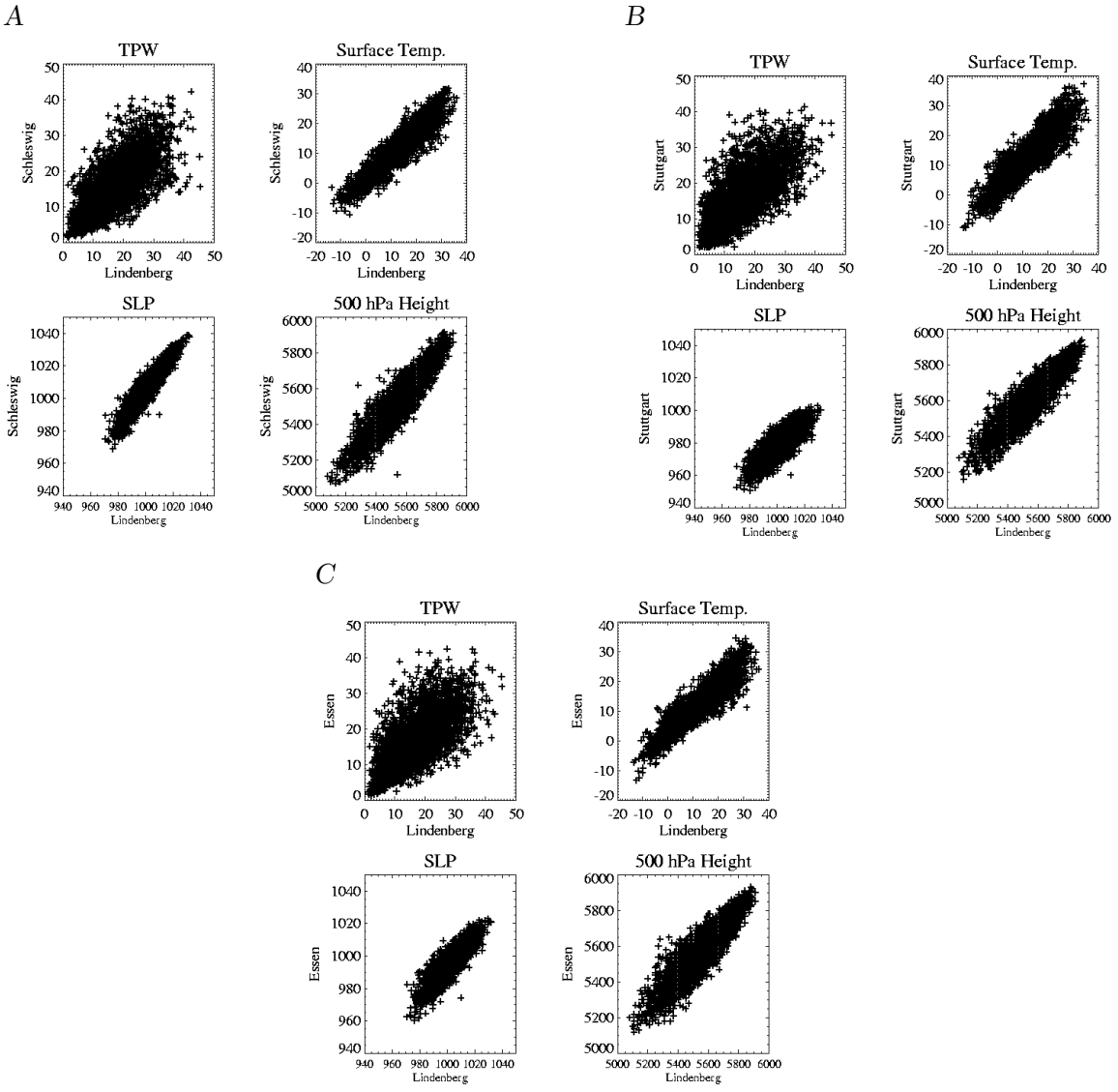

Figure 5.3: *Correlation of TPW given in $kg\,m^{-2}$ (upper left), the surface temperature in $^\circ C$ (upper right), the surface pressure in $h\,Pa$ (lower left) and the height of the 500 hPa level in m for the DWD stations Schleswig (y-axis) (A), Stuttgart (B), and Essen (C) and Lindenberg (x-axis). The correlation coefficients are given in table 5.5*

temperature. From the ten years the mean annual cycle is calculated for all quantities (see figure 5.5). The variability of surface pressure and the height of the 500 hPa level is larger in winter than in summer. The weather situation is dominated by the passage of low pressure systems. The frontal systems are related to different airmasses coinciding with higher (lower) 500-hPa level in warm (cold) air. In contrast the variability in the TPW is larger in summer

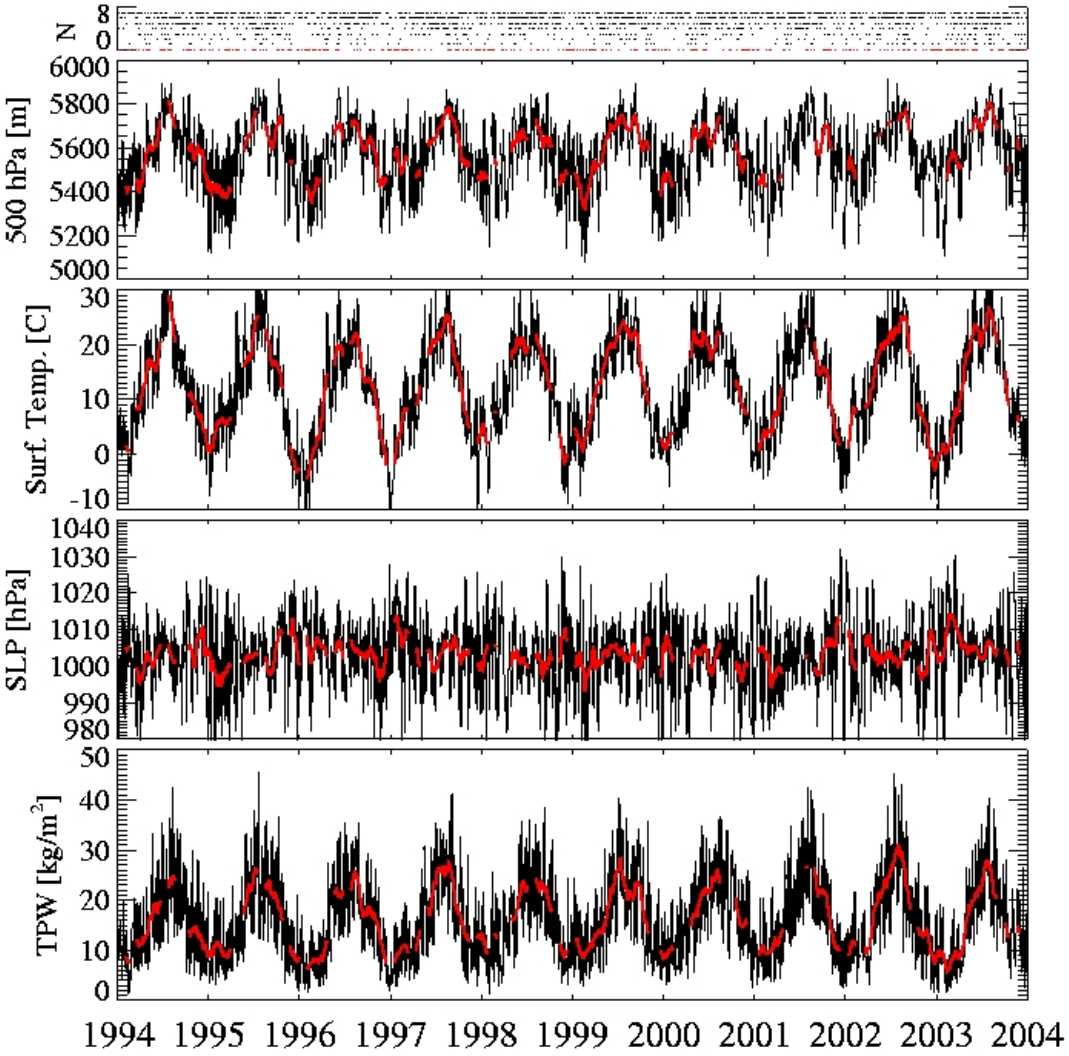

Figure 5.4: *10-years time series of the noon radiosonde ascents performend at the DWD station Lindenberg. The various panel top to bottom show: the cloud cover in octas (red accentuate the clear–sky), the height of the 500 hPa level, the temperature at the surface, surface pressure and the total precipitable water derived from the humidity profile. The red line denotes the 30-days running mean.*

due to the strong coupling to temperature, since warm air can contain more humidity than cold air. The daily anomalies are shown in figure 5.6. The anomalies of the sea level pressure and 500 hPa level have the same direction, e.g. a positive sea level pressure anomalies corresponds to higher temperatures and to a positive 500 hPa level height anomalies. The variability in the TPW follows this structure, but the derivation from the mean is small compared to the temperature anomalies.

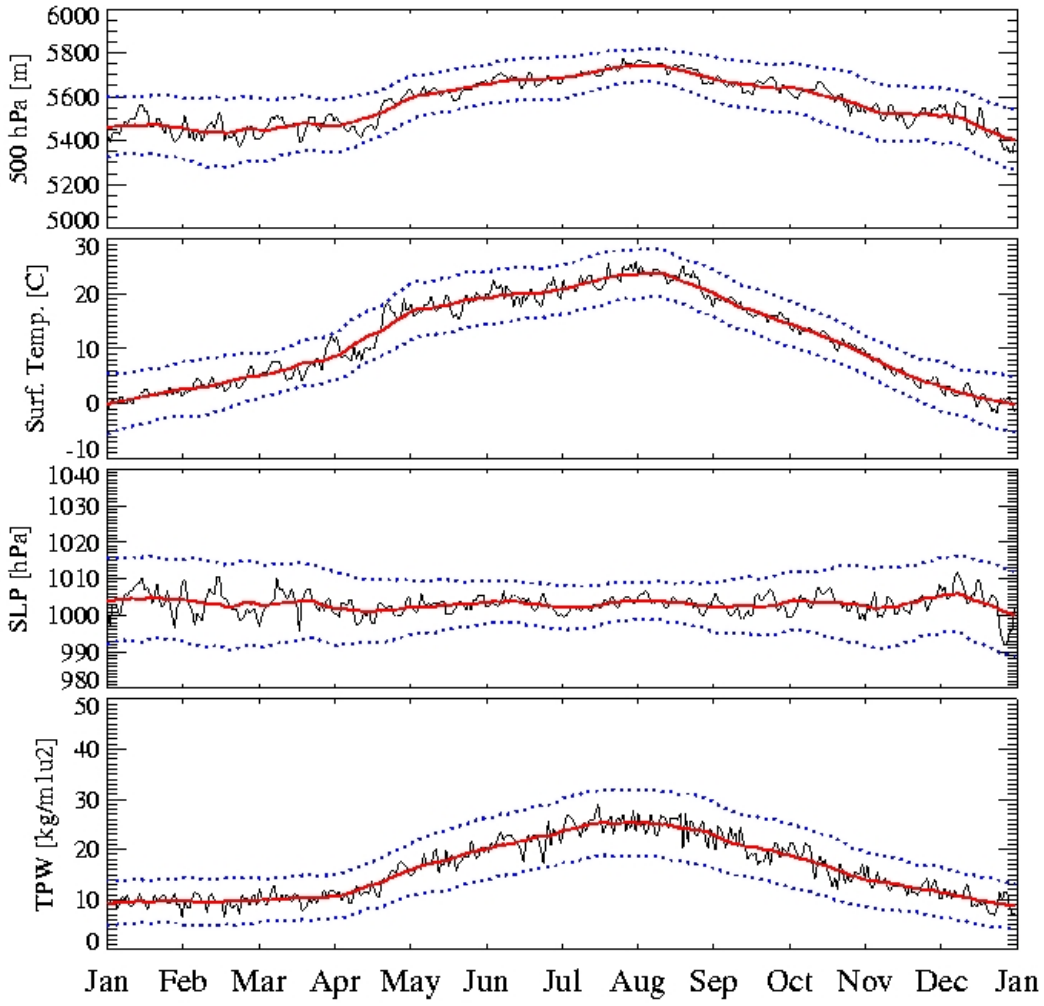

Figure 5.5: *Annual cycles derived from the 10-years time series from Lindenberg in figure 5.4, from top to bottom: the height of the 500 hPa level, the temperature at the surface, surface pressure and the total precipitable water derived from the humidity profile. The red line denotes the running mean. The blue dotted lines give the standard deviation of the quantity.*

On a seasonal basis the distributions of the surface pressure for Lindenberg shows a tendency towards high pressure in cases of clear skies. However the number of clear–sky observations at noon are limited (figure 5.7). The distinction in clear and cloudy ascents is achieved by the observed cloud cover in the synoptical data. For cloud cover below 5 octas the ascent is set to clear and above 5 octas the minimum dewpoint depression below 500 hPa has to be below 0.5 K for a cloud effected ascent. A more detailed description is given in chapter 5.3. In summer the 2 m temperature shows a tendency of clear–sky days to higher temperature whereas for other seasons no preference is obvious. In winter for the station Schleswig (not

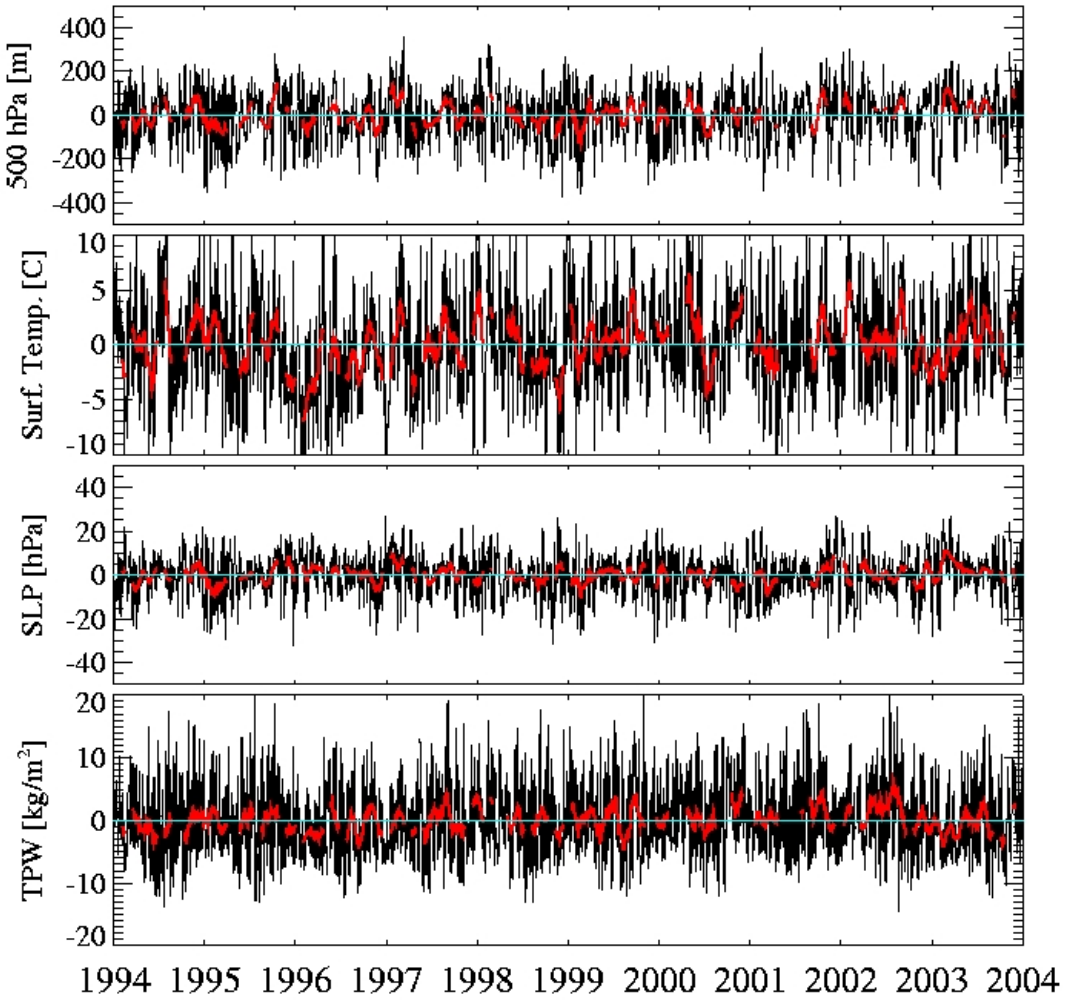

Figure 5.6: *The anomalies of the time series shown in figure 5.4. The various panel top to bottom show: the height of the 500 hPa level, the temperature at the surface, surface pressure and the total precipitable water derived from the humidity profile. The red line denotes the 30-days running mean.*

shown) colder temperatures are connected to clear–sky cases. In spring and autumn, no preferred situations can be detected (figures 5.8).
The 2 m relative humidity shows no preferred value in clear–sky situations. Nevertheless, the observed humidities are at the lower end of the distribution. The shape of the distribution is changing throughout the year. In spring the distribution is broad with a slight maximum for relative humidities smaller then 60 %. In summer the maximum of the distribution is shifted

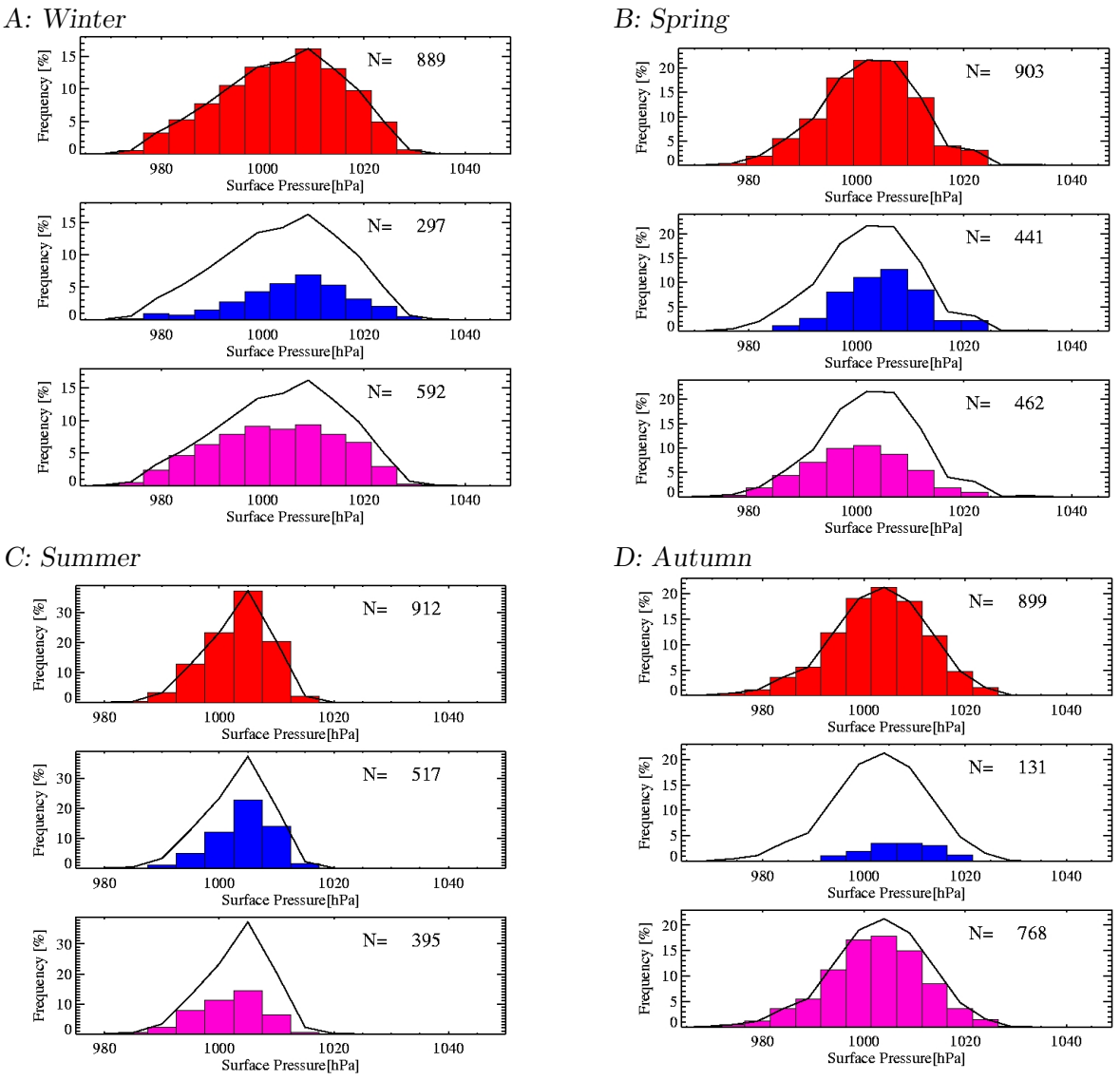

Figure 5.7: *Distribution of the surface pressure for winter (A), spring (B), summer (C), and autumn (D) derived from noon radiosonde ascents at Lindenberg. Upper panel shows all cases, middle panel cloud free cases and the lowest cloudy–sky cases. The solid line gives the distribution over all cases.*

towards larger relative humidities, in winter to values just below 100 % (figure 5.9).
The shape of the TPW distribution follows the temperature, which is to be expected due to the ability of air to contain different amounts of water vapour depending on temperature (figures 5.10). Table 5.6 and table 5.7 are summerising the main parameters describing the seasonal distributions.

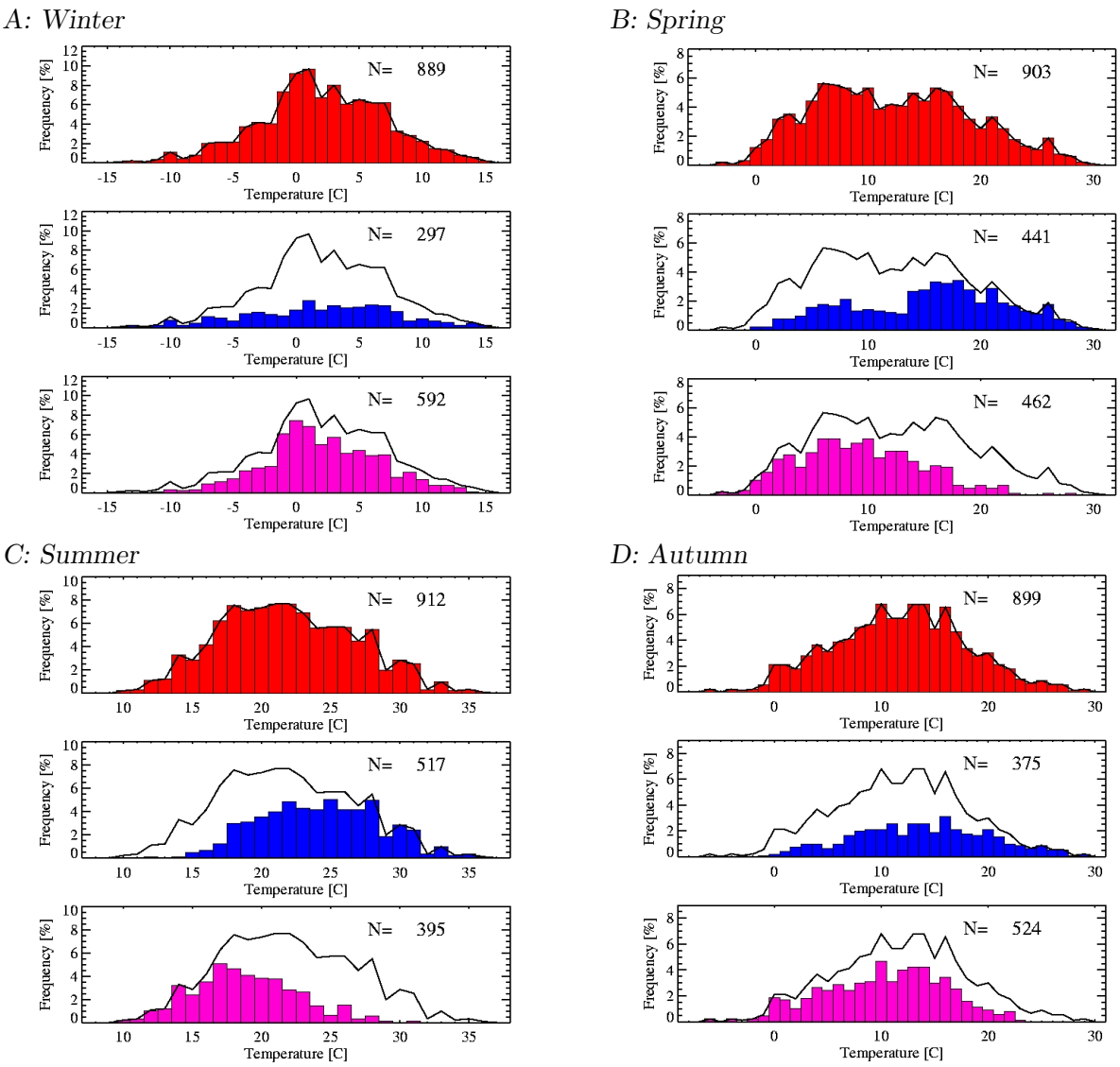

Figure 5.8: *Distribution of the 2-m temperature for winter (A), spring (B), summer (C), and autumn (D)) derived from noon radiosonde ascents at Lindenberg. Upper panel shows all cases, middle panel cloud free cases and lowest the cloudy–sky cases. The solid line gives the distribution over all cases.*

It follows that the frequency distributions of the meteorological parameter (sea level pressure, relative humidity, temperature and TPW) mainly vary with season with the median of the distribution depending on the existence of clouds. This encourages us to investigate the excess water vapour in cloudy scenes on climatological scales.

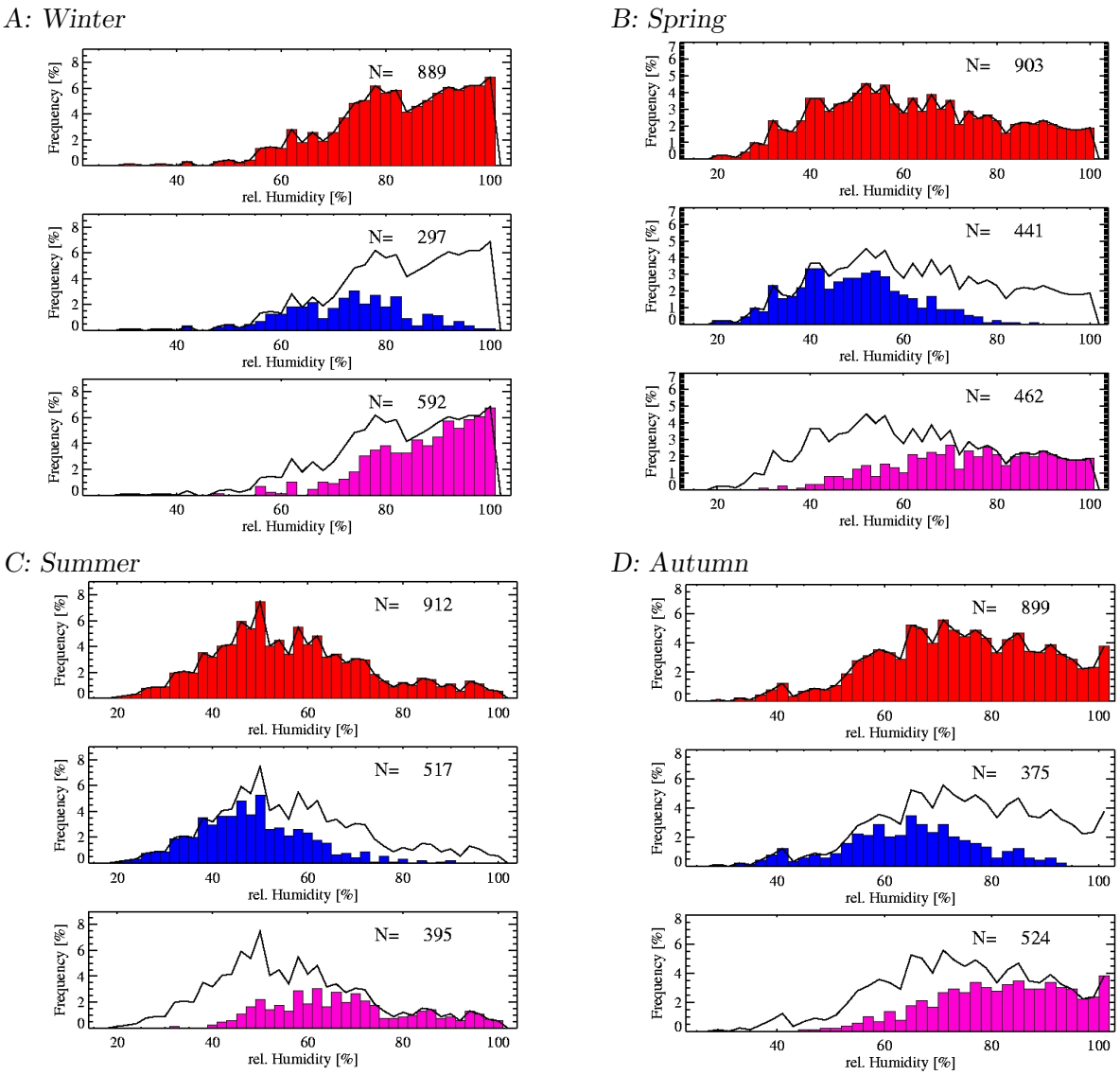

Figure 5.9: *Distribution of the relative humidity for winter (A), spring (B), summer (C), and autumn (D) derived from noon radiosonde ascents at Lindenberg. Upper panel shows all cases, middle panel cloud free cases and the lowest cloudy–sky cases. The solid line gives the distribution over all cases.*

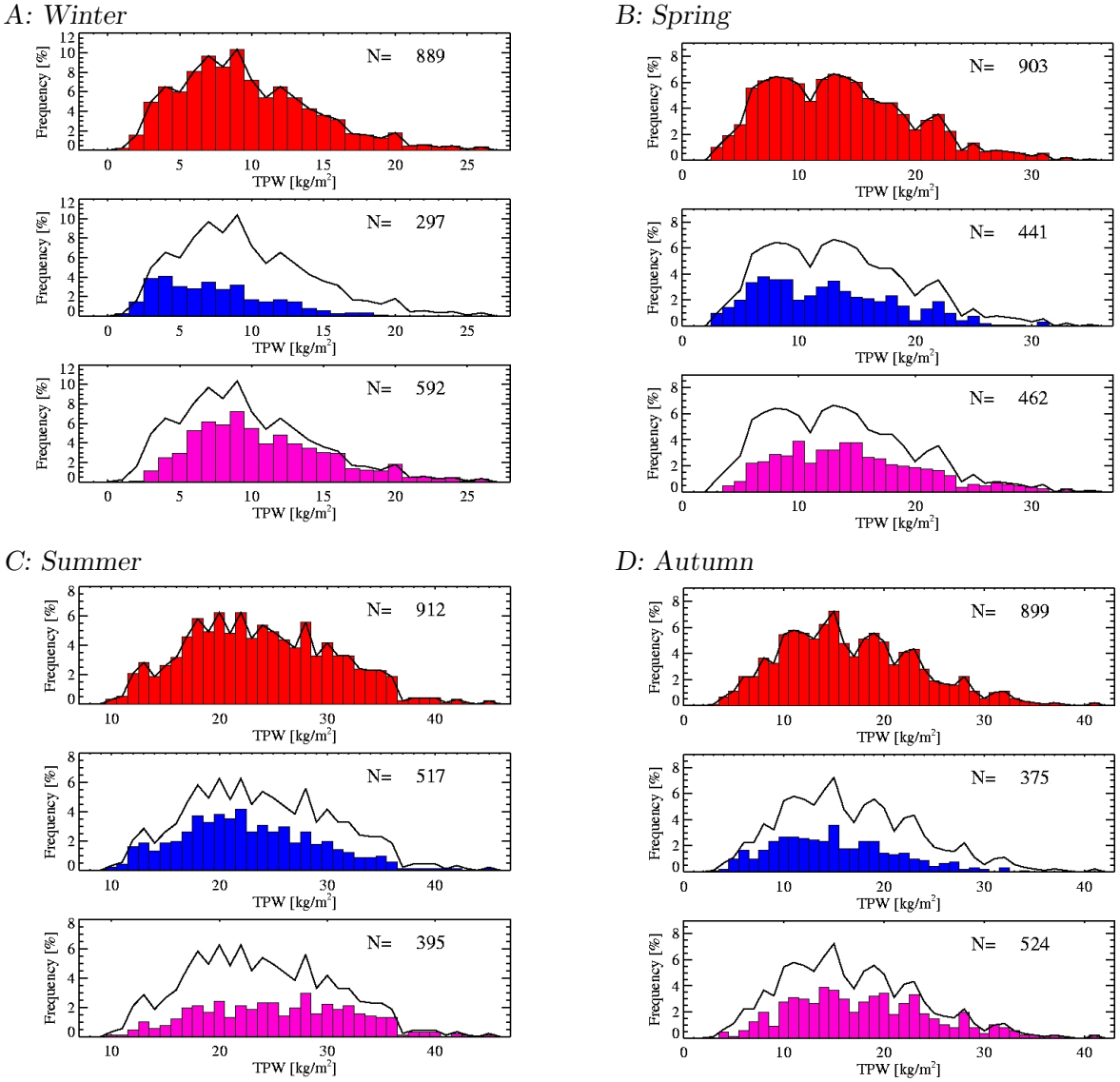

Figure 5.10: *Distribution of the total precipitable water for winter (A), spring (B), summer (C), and autumn (D) derived from noon radiosonde ascents at Lindenberg. Upper panel shows all cases, middle panel cloud free cases and the lowest cloudy–sky cases. The solid line gives the distribution over all cases.*

Season	Case	N	Median	Mean	Variance	Skewness	Kurtosis
TPW							
winter	total	889	8.918	9.667	22.025	0.749	0.354
	clear	297	6.871	7.386	14.592	0.687	-0.091
	cloud	592	9.802	10.812	21.856	0.749	0.230
spring	total	903	12.828	13.588	36.963	0.595	-0.080
	clear	441	11.847	12.584	35.516	0.567	-0.352
	cloud	462	13.931	14.547	36.536	0.651	0.079
summer	total	912	23.379	23.824	44.969	0.286	-0.441
	clear	517	21.888	22.627	39.881	0.391	-0.164
	cloud	395	25.066	25.390	47.409	0.102	-0.643
autumn	total	899	15.793	16.749	46.018	0.546	-0.013
	clear	375	14.507	15.007	37.036	0.494	-0.198
	cloud	524	17.414	17.995	48.797	0.500	-0.118
Temperature							
winter	total	889	1.800	1.969	24.648	-0.138	-0.015
	clear	297	2.400	1.873	34.753	-0.270	-0.375
	cloud	592	1.700	2.017	19.622	0.053	-0.092
spring	total	903	11.800	12.233	46.979	0.226	-0.716
	clear	441	16.300	15.420	45.814	-0.218	-0.757
	cloud	462	8.950	9.192	29.209	0.336	-0.223
summer	total	912	21.600	21.833	23.729	0.189	-0.498
	clear	517	24.100	24.180	18.336	0.072	-0.529
	cloud	395	18.500	18.761	14.162	0.313	-0.106
autumn	total	899	11.900	11.708	38.357	0.005	-0.284
	clear	375	13.900	13.771	41.258	-0.023	-0.537
	cloud	524	10.600	10.231	31.118	-0.239	-0.450
Surface pressure							
winter	total	889	1004.800	1003.857	140.877	-0.245	-0.591
	clear	297	1007.100	1006.255	116.239	-0.435	0.005
	cloud	592	1002.900	1002.654	149.114	-0.125	-0.767
spring	total	903	1003.200	1002.514	79.370	-0.126	-0.018
	clear	441	1005.300	1004.985	62.218	0.049	0.340
	cloud	462	1000.300	1000.156	84.504	-0.053	-0.379
summer	total	912	1003.900	1003.200	31.363	-0.479	0.050
	clear	517	1005.100	1004.381	26.035	-0.541	0.495
	cloud	395	1002.300	1001.655	34.196	-0.306	-0.339
autumn	total	899	1003.400	1002.954	86.150	-0.273	0.073
	clear	375	1005.000	1004.708	74.872	-0.390	0.084
	cloud	524	1001.700	1001.700	90.597	-0.157	0.107

Table 5.6: *The statistical parameters of the TPW, Temperature and surface pressure distribution for all–sky, cloudy and clear atmospheres.*

Season	Case	N	Median	Mean	Variance	Skewness	Kurtosis
relative Humidity							
winter	total	889	83.488	82.300	165.363	-0.707	0.242
	clear	297	73.399	72.339	142.679	-0.462	0.542
	cloud	592	89.482	87.297	102.128	-0.859	0.414
spring	total	903	60.328	62.112	365.837	0.199	-0.877
	clear	441	48.784	49.165	155.820	0.245	-0.346
	cloud	462	75.253	74.471	253.654	-0.288	-0.770
summer	total	912	54.437	56.718	268.941	0.540	-0.116
	clear	517	47.638	48.263	140.845	0.499	0.472
	cloud	395	66.198	67.784	220.826	0.364	-0.684
autumn	total	899	74.412	74.474	228.537	-0.245	-0.498
	clear	375	64.969	64.574	160.995	-0.190	-0.235
	cloud	524	82.381	81.559	156.714	-0.380	-0.598
Dewpoint							
winter	total	889	4.000	4.450	6.987	0.879	0.461
	clear	297	3.900	4.174	5.636	1.030	1.108
	cloud	592	4.000	4.588	7.618	0.792	0.179
spring	total	903	4.000	4.176	4.796	0.953	1.065
	clear	441	3.600	3.744	3.392	0.906	1.464
	cloud	462	4.100	4.589	5.797	0.803	0.422
summer	total	912	3.500	3.715	3.846	0.924	1.400
	clear	517	3.100	3.363	2.774	0.812	0.435
	cloud	395	4.100	4.174	4.885	0.763	1.127
autumn							
	total	899	3.600	3.876	4.426	0.812	0.457
	clear	375	3.600	3.802	3.663	0.698	0.363
	cloud	524	3.600	3.929	4.974	0.835	0.347

Table 5.7: *The statistical parameters of the relative humidity and dewpoint temperature distribution for all–sky, cloudy and clear atmospheres.*

5.3 The excess water vapour

5.3.1 Distinction of clear and cloudy cases from radiosoundings

When discussing the differences in all–sky to clear–sky total precipitable water the question arises, how reliable the identification of clear sky cases is. From ground–based observations the cloud cover is given in the synoptical data set. But for partly cloudy situations, the radiosonde does not necessarily pass a cloud. As an example, for 4 octas the sky is half cloud covered, the likelyhood of the radiosonde to find a whole exceeds 50% because the observer may overestimate the cloud cover near the horizon due to his view on the cloud vertical extend. Additional to the cloud cover from synoptical observations a parameter from the ascent is chosen for the distinction of clear sky cases.

The basic criteria from cloud detection is taken from the synoptical data. If no cloud cover

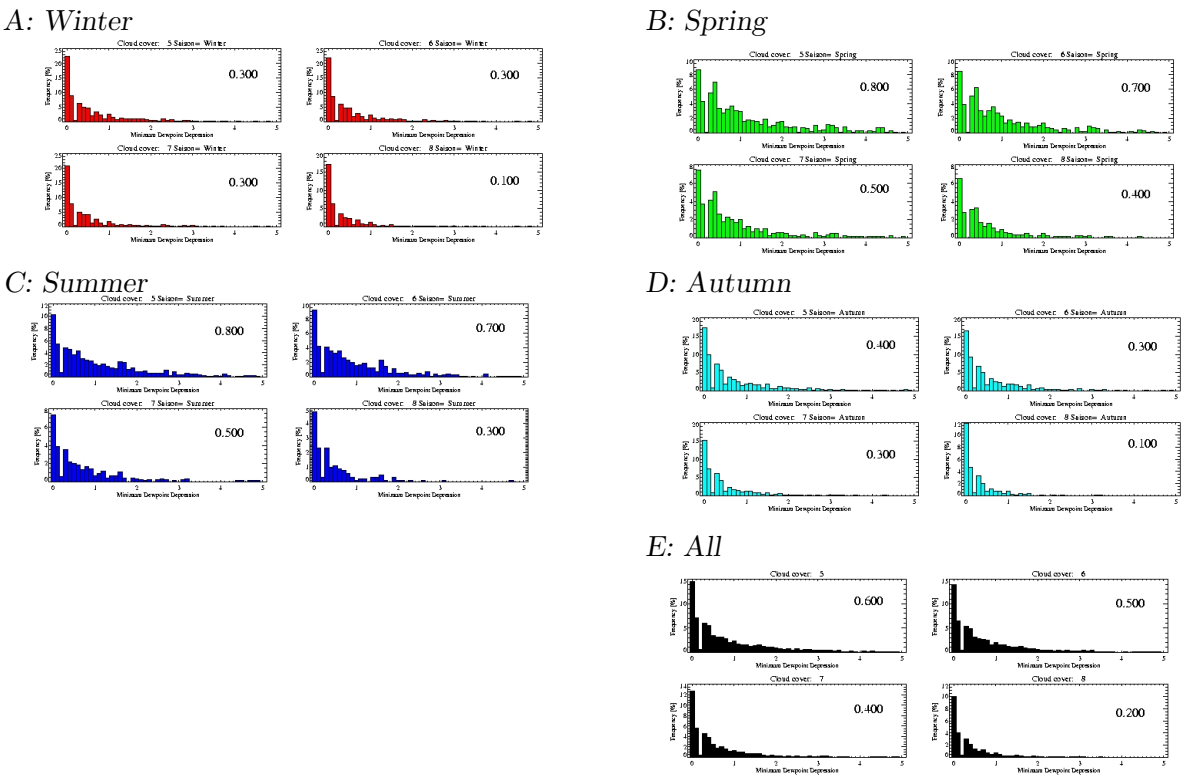

Figure 5.11: *Distribution of the minimum dewpoint difference of radiosonde ascents for winter (A), spring (B), summer (C), autumn (D), and for the whole data set derived from noon radiosonde ascents at Lindenberg. Separations are made by the observed cloud cover from the synoptical data set. Upper left (right) is for greater or equal 5 (6) octas, lower left for greater and equal 7 octas, and lower right for overcast cases. The numbers give the median of the distribution.*

information is in the synoptical data set, then the minimum of the dewpoint difference profile below 500 hPa is compared to a threshold. A cloud is present when the dewpoint depression is below 0.5 K. The *no criteria* case in the following figures calculates the clear–sky TPW for the ascents where cloud cover value in the synoptical information is 0, or for no cloud cover value the dewpoint depression exceeds 0.5 K.

The dewpoint depression threshold is chosen for various reasons. From the distribution of

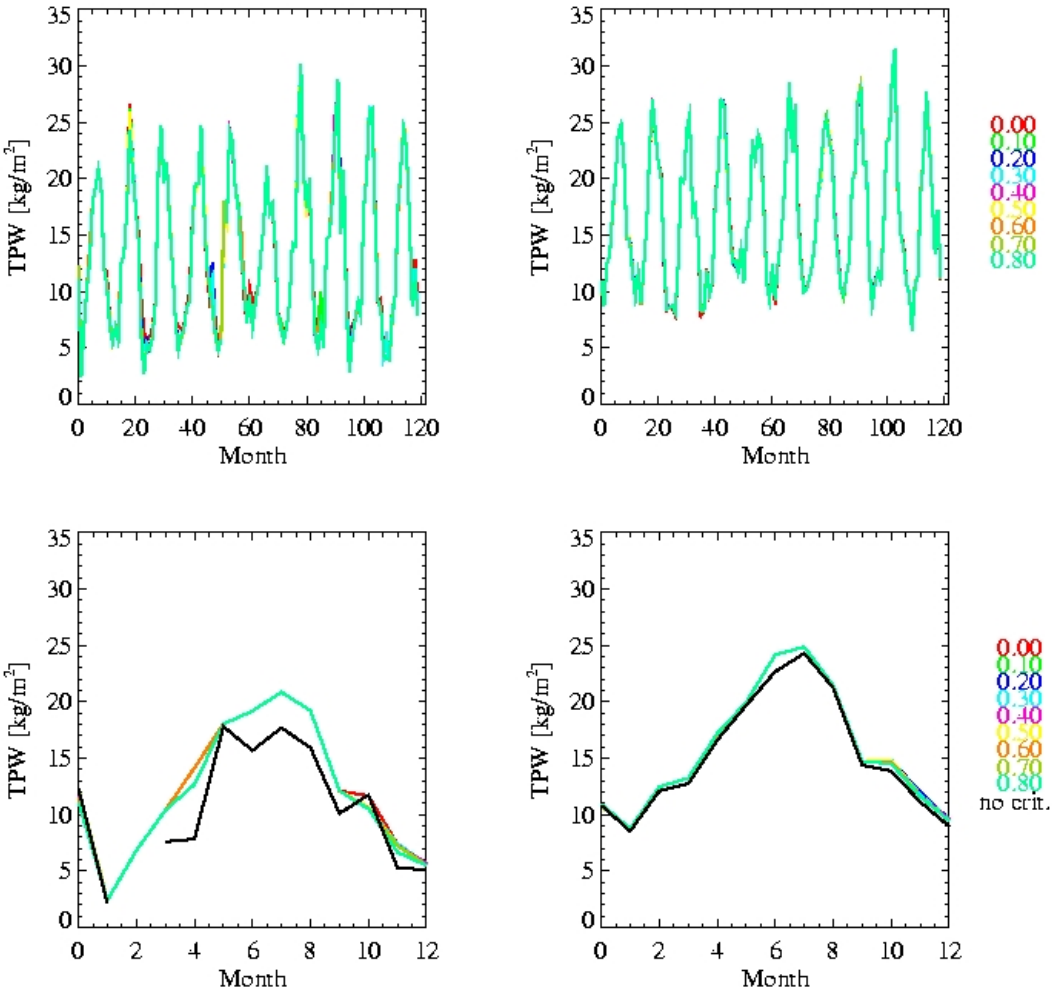

Figure 5.12: *Monthly mean clear–sky (left) and cloudy–sky (right) TPW depending on the distinction criteria. Upper row for 10 years and lower panel for the first 13 months. Colours denote the dewpoint depression threshold. The dewpoint depression is used for cloud covers above 5 octas. No criteria denotes clear sky as zero octas and if no cloud flag is given (dummy value) then the minimum dewpoint depression below 500 hPa is lower then 0.5 K.*

minimum dewpoint depression below the 500 hPa level of radiosonde ascent in overcast cases varies between 0.1 and 0.4 depending on the season (see figure 5.11). Including 7 octas in the overcast case the median lies between 0.1 and 0.5. For station Schleswig the median of the dewpoint depression distributions lies between 0.4 and 1.0. Furthermore the dependency of the monthly mean for clear–sky TPW on different dewpoint depression thresholds is shown in figure 5.12. Varying the dewpoint depression in the range of 0.3 to 0.6 does not effect the mean value significantly. Therefore, the threshold is set to 0.5. This choice ensures a

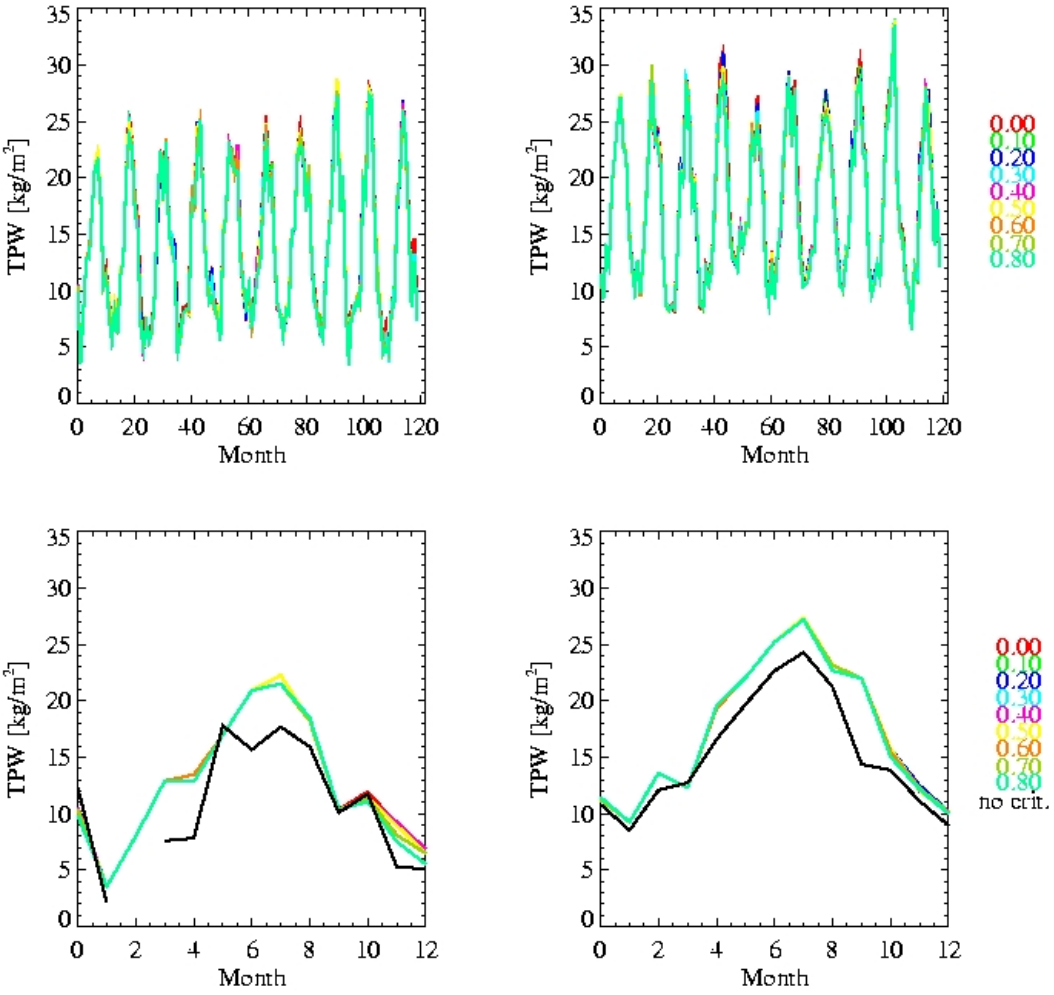

Figure 5.13: *Monthly mean clear–sky (left) and cloudy–sky (right) TPW depending on the distinction criteria. Upper row for 10 years and lower panel for the first 13 months. Colours denote the dewpoint depression threshold. The dewpoint depression is used for cloud covers above 7 octas. No criteria denotes clear sky as zero octas and if no cloud flag is given (dummy value) then the minimum dewpoint depression below 500 hPa is lower then 0.5 K.*

sufficient number of monthly mean values for all stations.

For broken cloudiness the radiosonde does not necessarily pass a cloud. Thus, the larger absolute humidities inside the clouds are missed. The monthly mean clear–sky TPW is underestimated. Therefore a cloud cover of 5 octas is set as a threshold to define clear–sky

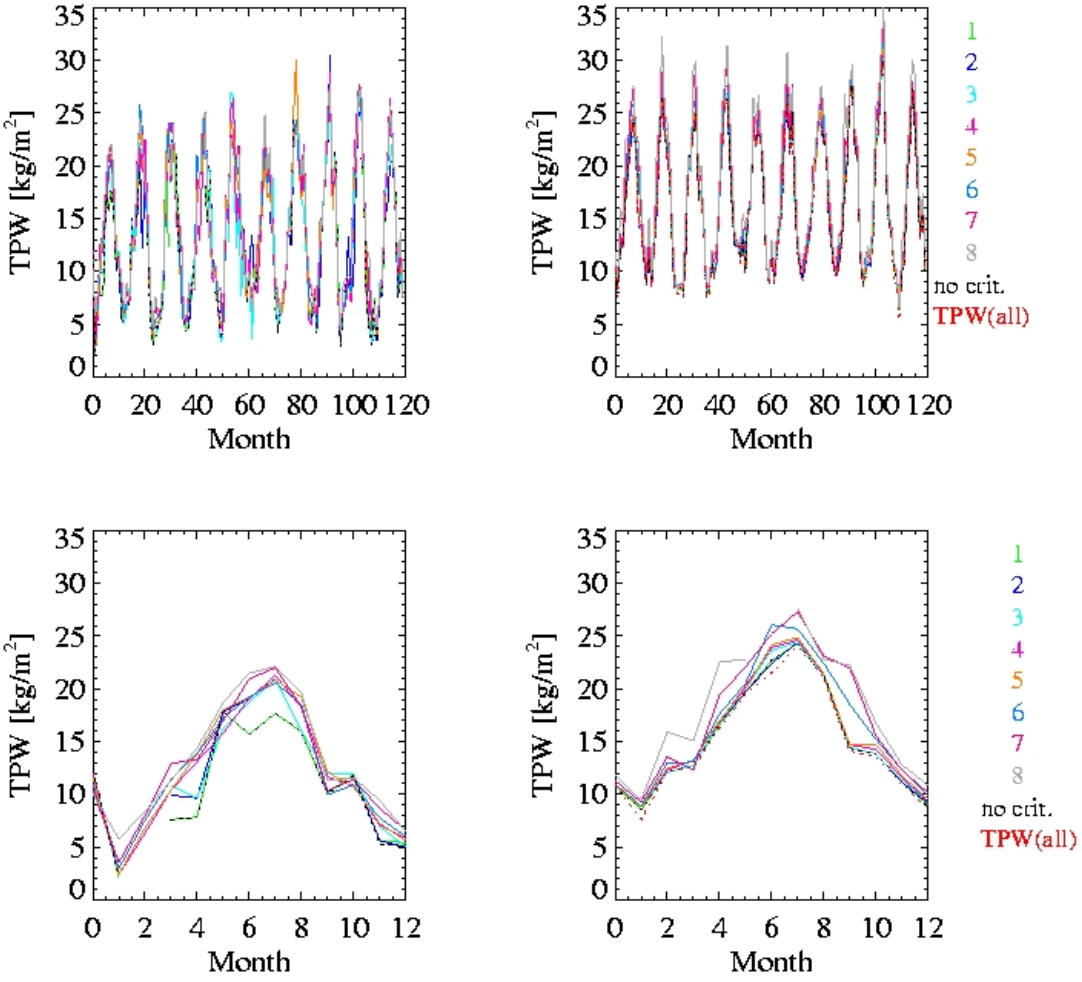

Figure 5.14: *Monthly mean clear–sky (left) and cloudy–sky (right) TPW depending on the starting cloud cover for the dewpoint depression threshold. The monthly means represent the mean over the different dewpoint depression thresholds given in figure 5.12. Upper row for 10 years and lower panel for the first 13 months. Colours denote cloud cover as given by the observer used as a threshold for the dewpoint depression criteria. No criteria denotes clear sky as zero octas and if no cloud flag is given (dummy value) then the minimum dewpoint depression below 500 hPa is lower then 0.5 K. In red the all–sky TPW is given; this value is not effected by the thresholding.*

ascents with an additional dewpoint depression threshold. For this study, the minimum value of the dewpoint depression up to 500 hPa is used as a identifier for cloud levels as described before. When the minimum is below 0.5 K it is assumed that a cloud is passed by the radiosonde. Figure 5.12 shows the retrieved time series for the clear–sky TPW and the cloudy–sky TPW for varying dewpoint depression thresholds using a detection scheme for cases where the cloud cover exceed 5 octas (and 7 octas in figure 5.13). The monthly mean clear–sky TPW is larger in all cases compared to the no criteria case. Low clear–sky TPW values are corrected by larger TPW in cases with broken cloudiness. The same effect is observed for cloudy–sky cases. Here, the monthly means are larger in the two–threshold scheme compared to the no–criteria case. Cases of broken cloudiness, where the radiosonde does not pass a cloud are excluded from the mean value.

Figure 5.14 compares the mean values over different dewpoint depression thresholds for one starting cloud cover. The largest mean TPW values are derived for cloud cover thresholds of 7 and 8 octas. Here only extreme cases are detected as clouds. For cloud covers below 5 octas the number of month where no clear–sky or cloudy–sky TPW is derived is as high as for the *no criteria* case. From this point and from comparing the different TPW timeseries the cloud cover threshold is set to 5 octas. Furthermore, the threshold in dewpoint depression is set to 0.5 K.

Mean values of TPW are calculated when more than 3 ascents fullfill the criteria. For different stations the number of data points are the same. Differences mainly occur in the number of clear–sky days per monthly mean.

5.3.2 All–sky vs clear–sky TPW

The TPW frequency distribution shown in the previous section are significantly different for clear and cloudy conditions. For monthly and seasonal means of clear–sky and all–sky cases the behaviour of TPW is examined. Figure 5.15 shows the relation of clear–sky monthly mean TPW to cloudy–sky TPW and to all–sky TPW for station Lindenberg. Only a few months show a large TPW in clear–sky compared to cloudy or all–sky situations. Here, the clear–sky cases are related to warm air masses at high pressure conditions, whereas the cloudy–sky cases are related to cold air advection corresponding to frontal systems in low pressure systems. Colder air contains less water vapour. Therefore, the ratio of the all–sky TPW to the clear–sky TPW denoted as the excess water vapour is slightly below 1 for these cases. One example for a month with larger clear–sky TPW than all–sky TPW is May 1997 shown in figure 5.16.

During winter the clear– to cloudy–sky difference in TPW is larger than during summer. The difference between air masses related to frontal systems passing the station are stronger in winter compared to summer. However, for the retrieval of correction terms the number of

clear–sky cases per month is too low.

Looking at yearly means for each month (figure 5.15, lower panel) the remaining 12 points give the annual cycle of the TPW. Large excess water vapour values which appear for small clear–sky TPWs are reduced.

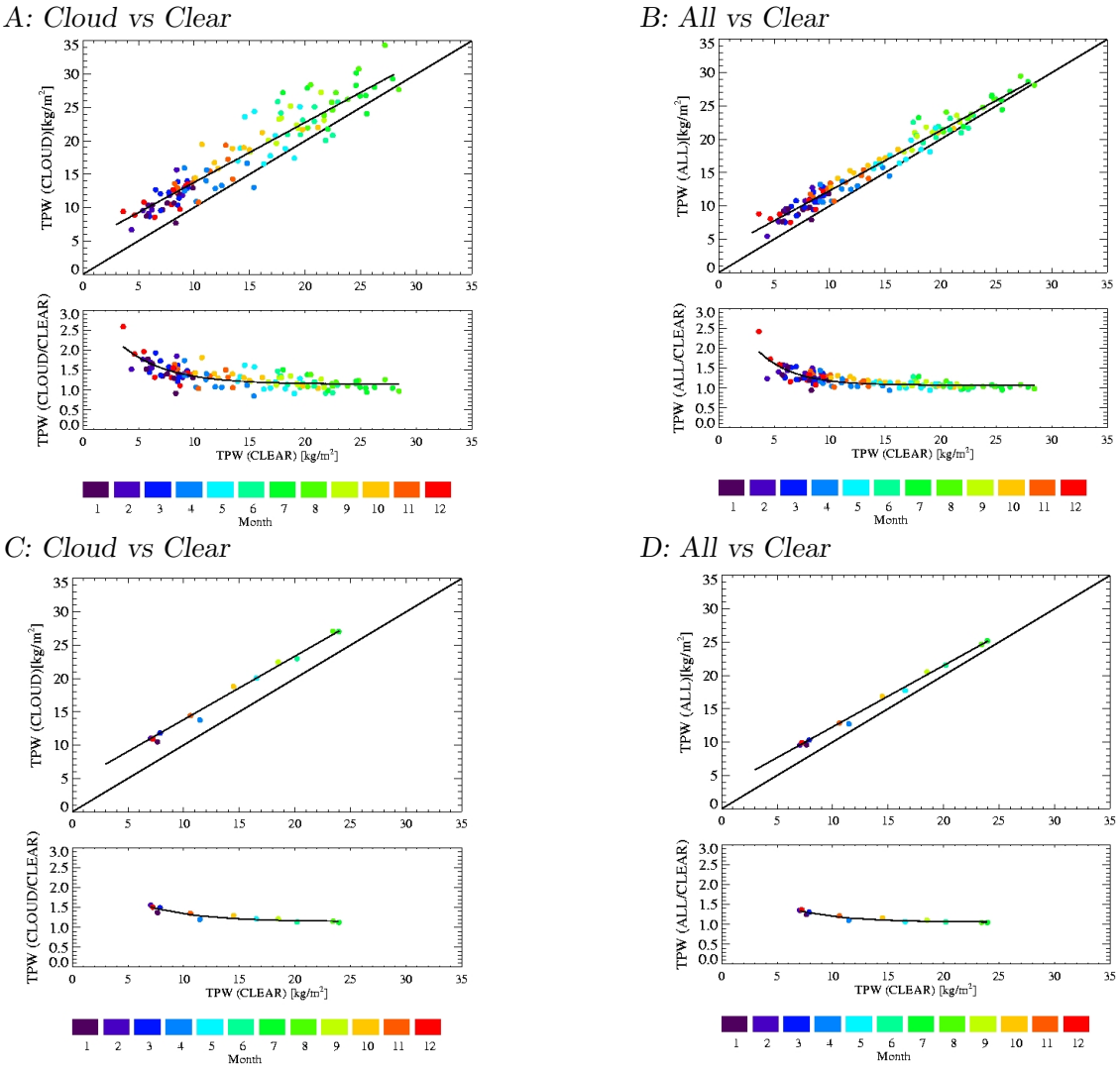

Figure 5.15: *Monthly means for the 10 years of Lindenberg radiosonde measurements. A: The monthly mean TPW in clear–sky cases versus the cloudy–sky cases (upper panel) and versus the ratio (cloud/clear) (lower panel). B: The clear–sky TPW is shown in relation to the all–sky TPW. C: The yearly mean TPW for every month in clear–sky cases versus the cloudy–sky cases (upper panel) and versus the ratio (cloud/clear) (lower panel). D: The clear–sky TPW is shown in relation to the all–sky TPW. Colors denote the month.*

The relation of clear TPW to cloudy–sky TPW or all–sky TPW respectively is linear in TPW clear, whereas the relation to the ratio all–to–clear is exponential and can be fitted with :

$$Y \;=\; a_0\, a_1^x \;+\; a_2\;. \tag{5.6}$$

The parameters a_0 to a_2 are given in table 5.8.

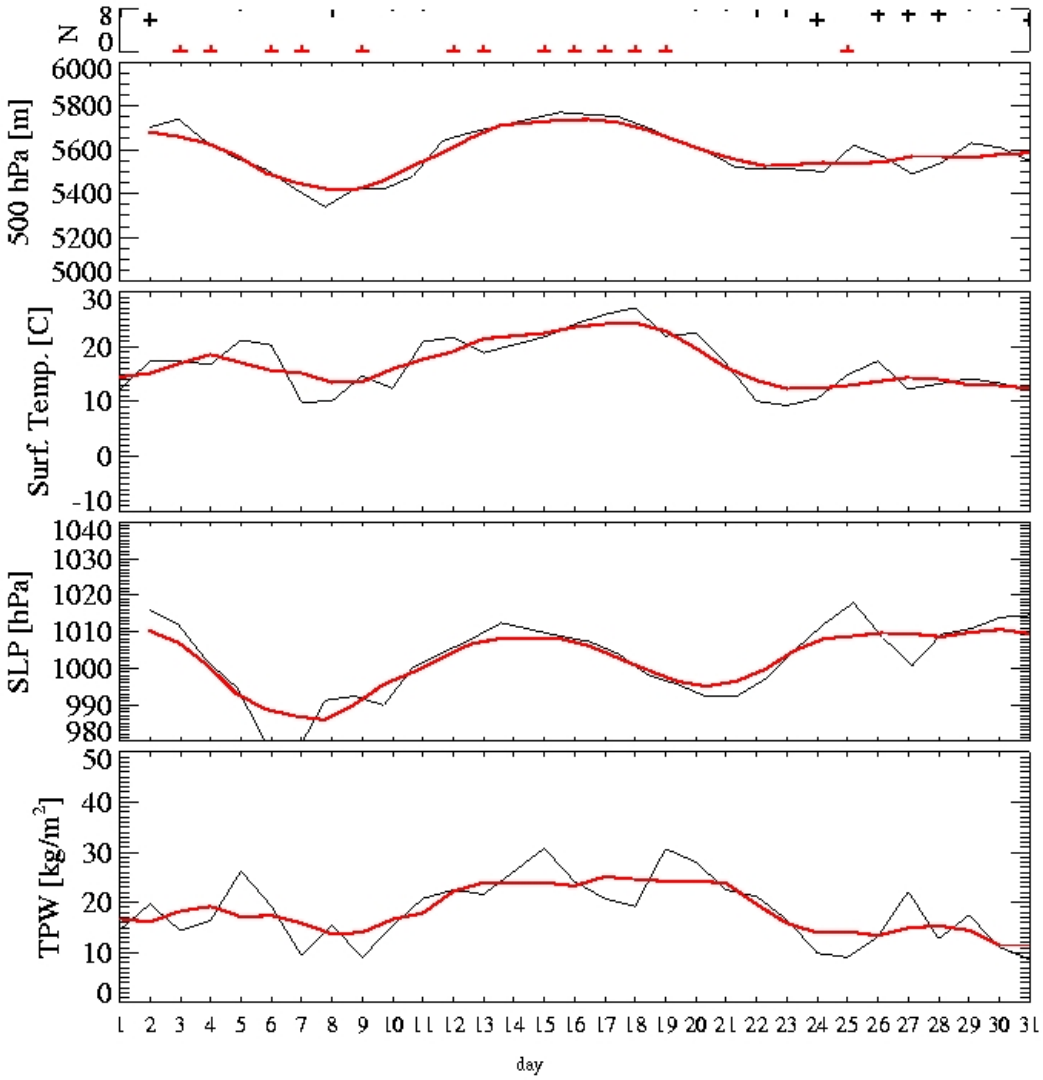

Figure 5.16: *Time series of noon radiosonde ascents performend at DWD station Lindenberg in May 1997. The various panel top to bottom show: the cloud cover in octas (red accentuate the clear–sky), height of the 500 hPa level, temperature at the surface, surface pressure and total precipitable water derived from the humidity profile. The red line denotes the 5-day running mean.*

For different stations the regression functions look slightly different (figure 5.17). This is caused by different behaviours of the ratio in the low clear–sky TPW cases. Which in turn is mainly affected by the different number of clear–sky observations per month. For the regression parameters see table 5.8.
The relation of TPW (Cloud) or TPW (ALL) to TPW (Clear) shows good correspondence. For large clear–sky TPW all stations show an excess water vapour of 1.1, whereas differences occur for low clear–sky TPW. From a clear–sky TPW of 10 kg/m^2 up to larger TPW the factor decreases from 1.3 to 1.1. This decrease does not depend on the integration time.

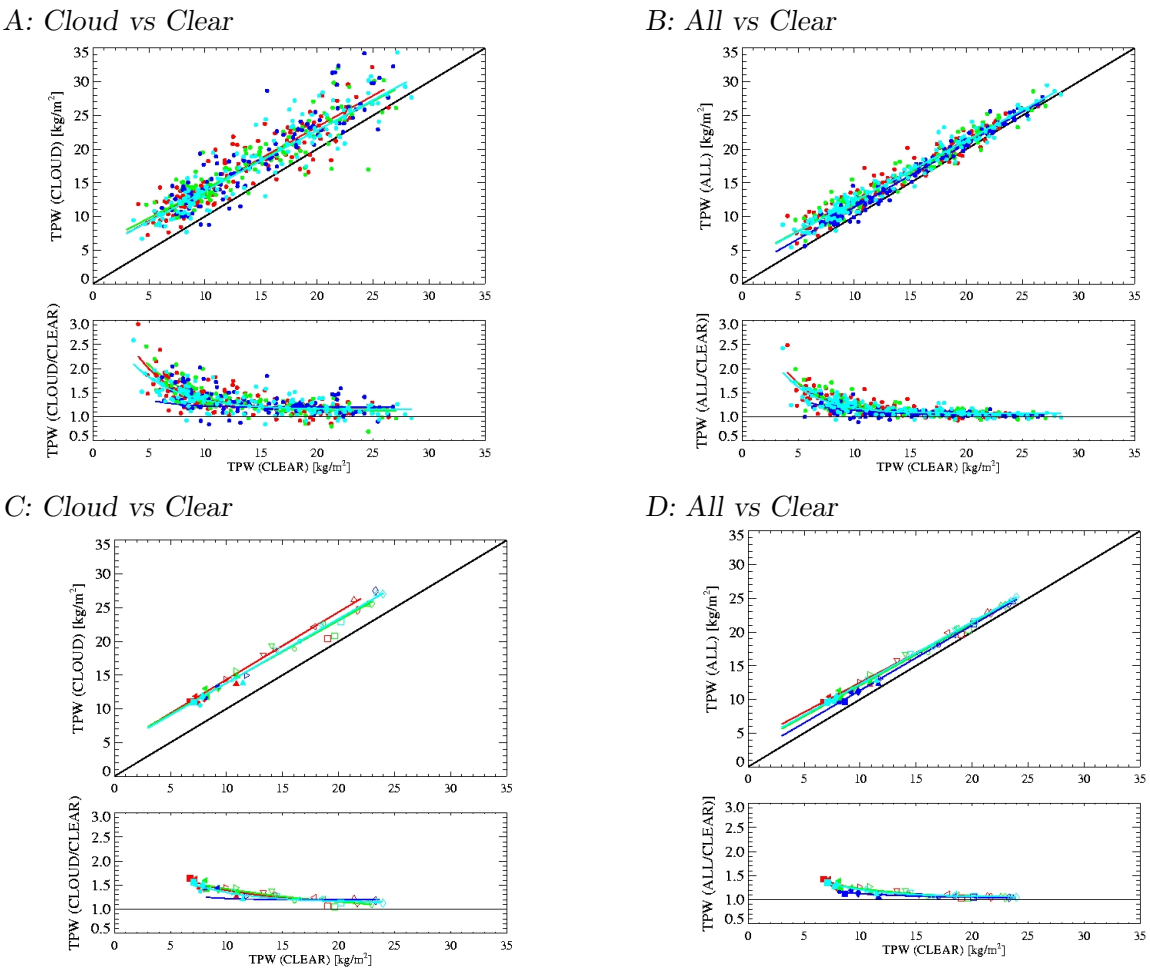

Figure 5.17: *Monthly means for 10 years of radiosonde measurements for Schleswig (red), Essen (green), Stuttgart (blue), and Lindenberg (cyan).* ***A****: Monthly mean TPW in clear–sky cases versus cloudy–sky cases (upper panel) and versus the ratio (cloud/clear) (lower panel).* ***B****: Clear–sky TPW is shown in relation to all–sky TPW.* ***C****: Yearly mean TPW for every month in clear–sky cases versus cloudy–sky cases (upper panel) and versus the ratio (cloud/clear) (lower panel).* ***D****: Clear–sky TPW is shown in relation to all–sky TPW. Symbols in* ***C*** *and* ***D*** *represent the month.*

Yearly means for all months, seasonal means (see figure 5.18) and monthly means show the same behaviour. For lower clear–sky TPW the increase in excess water vapour is stronger, but the number of cases is limited and the spread of monthly means is broader. Except for Stuttgart all stations show an increase of excess water vapour for low clear–sky TPW (from 10 to 5 kg/m^2) up to 1.5. Stuttgart does not observe these values. Therefore a retrieval below 7 kg/m^2 is not possible.

Regression function enable the assessment of the underestimation in TPW for an observed clear–sky monthly mean. In Figure 5.19 the difference in all– to clear–sky TPW is shown versus the mean clear–sky TPW. For different stations the amount of water vapour for all–sky situations is about 2 kg/m^2 larger than for clear–sky case. For low mean clear–sky TPW the difference to all–sky cases is largest.

5.3.3 Sensitivity study

The sensitivity of the regression on different parameters, like number of data points, number of ascents included in determing the mean value and the total data amount is investigated here. Figure 5.20 shows the variability of the regression resulting from randomly chosen data points. For Lindenberg data the number of cases is reduced to 25%, 50%, 75% and 90%. The different regressions look quite similar. Differences occur in the extreme end of the data range. Here the number of available points is low, and reducing the points will affect the

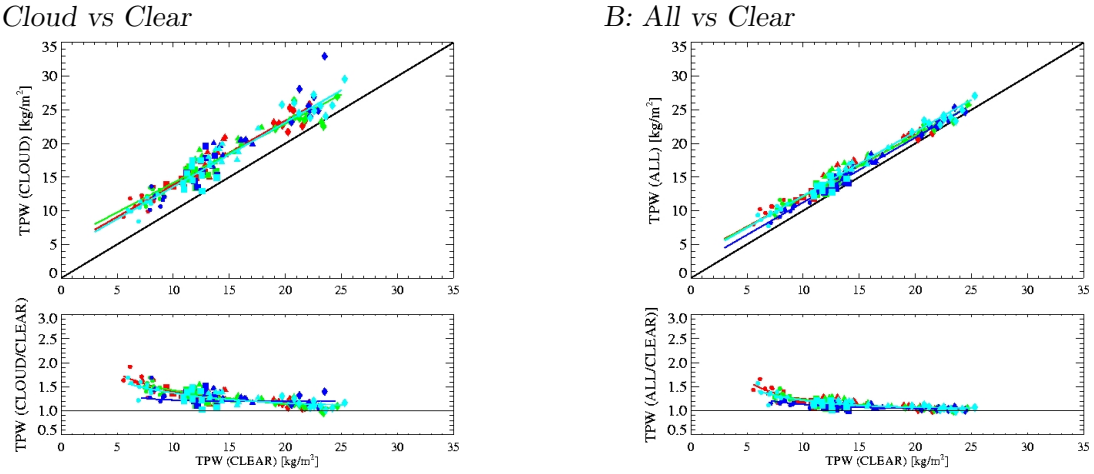

Figure 5.18: *Seasonal means for 10 years of radiosonde measurements for Schleswig (red), Essen (green), Stuttgart (blue), and Lindenberg (cyan).* ***A****: Seasonal mean TPW in clear–sky cases versus cloudy–sky cases (upper panel) and versus the ratio (cloud/clear) (lower panel).* ***B****: Clear–sky TPW is shown in relation to all–sky TPW. Symbols represent the season; winter (circle), spring (square), summer (diamond), and autumn (triangle).*

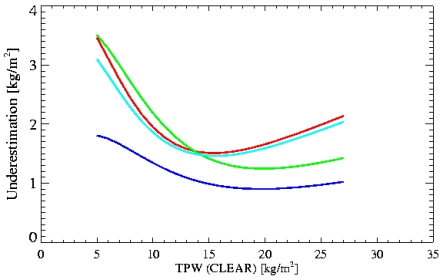

Figure 5.19: *Underestimation retrieved for four German stations. In color: Schleswig (red), Essen (green), Stuttgart (blue), and Lindenberg (cyan)*

slope of the regression.

Figure 5.21 shows how the mean values of TPW are affected by reduced amounts of data. From the total noon ascents smaller samples are chosen for calculating the regression function.The resulting distribution of mean values and the regressions are shown. Obviously, the regression functions are stable. The introduced variability is small. Random samples containing 60% of Lindenberg data were also used to show the spread in the regression lines. The variability of the resulting functions is shown in figure 5.22. Differences in the slope of the linear regression clear– to all–sky TPW occur. For the relation of the excess water vapour the functions spread out for cases with low clear–sky TPW. Here the number of cases

Case	N	Cor	RMS	Chi^2	A0	A 1	A 2
Lindenberg							
Year	12	0.96	0.03	0.012	1.4438	0.22813	1.057
Season	40	0.85	0.056	0.167	1.174	0.197	1.050
Month	120	0.79	0.09	1.696	2.741	0.323	1.08
Schleswig							
Year	12	0.93	0.039	0.026	2.034	0.262	1.064
Season	40	0.87	0.56	0.207	1.863	0.239	1.056
Month	120	0.78	0.099	2.12	3.318	0.337	1.079
Stuttgart							
Year	12	0.86	0.023	0.076	0.049	0.016	1.031
Season	40	0.75	0.037	0.068	0.662	0.189	1.034
Month	120	0.62	0.072	0.789	1.098	0.242	1.036
Essen							
Year	12	0.89	0.039	0.029	0.874	0.133	1.002
Season	40	0.83	0.05	0.15	0.828	0.123	0.991
Month	120	0.79	0.086	1.424	2.55	0.272	1.052
All Station							
Year	48	0.89	0.043	0.127	2.41	0.297	1.062
Season	160	0.81	0.058	0.771	1.604	0.24	1.052
Month	480	0.77	0.093	6.616	2.864	0.319	1.063

Table 5.8: *Parameter describing the fitted function given in equation 5.6 for different stations and resulting of all available monthly means and the mean over all single months.*

is small and the variability is high. Reducing the data amount will result in different slopes for the regression.

The variability of the functional relation between the excess water vapour and the clear–sky TPW based on the cloud cover is shown in figure 5.23. The observed cloud cover for this cases is used as a threshold. The noice in the retrieval is larger when including TPWs where small cloud covers are observed in the calculation of the clear–sky mean. But the derived fitting functions are not influenced.

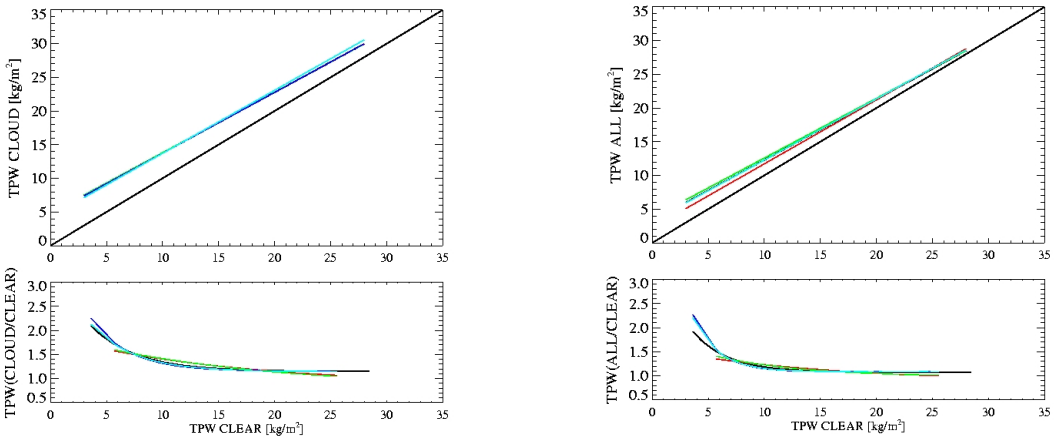

Figure 5.20: *Variability of the functions introduced by different number of data points: 25% (red), 50% (green), 75% blue, 90% cyan and all data in black.*

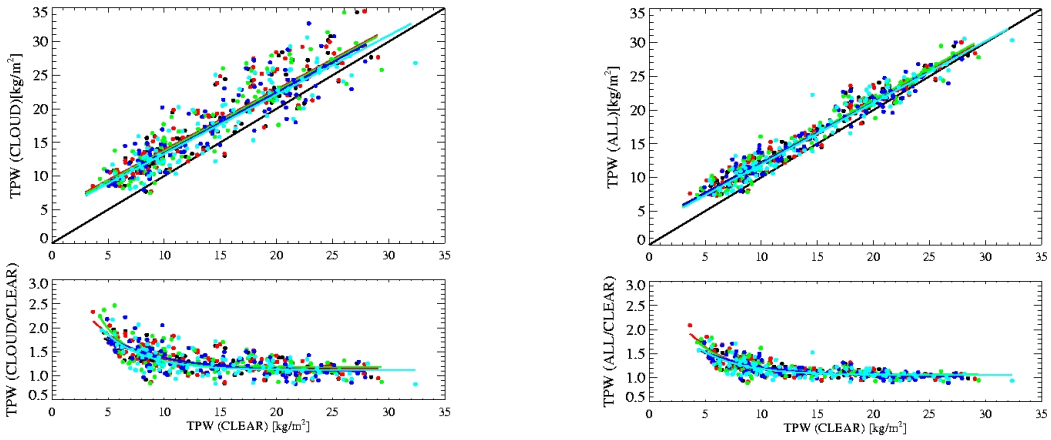

Figure 5.21: *Dependency of clear–sky TPW to cloudy–sky TPW (left) or all–sky TPW (right) towards the amount of available data. All data used (black), 90% (red), 80% (green), 70% (blue), and 50%(cyan)*

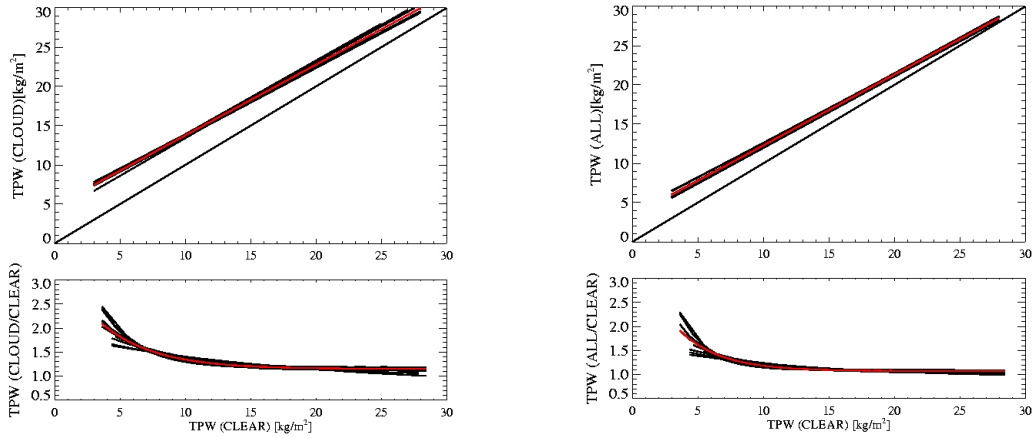

Figure 5.22: *Randomly chosen 60% of daily data, in red the regression derived from all data is denoted.*

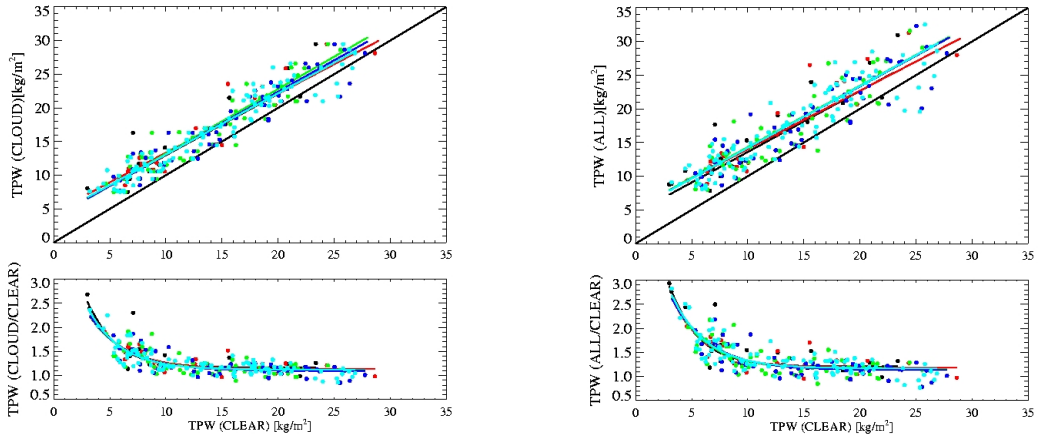

Figure 5.23: *Dependency of clear–sky TPW to cloudy–sky TPW (left) or all–sky TPW (right) towards the definition of clear–sky. Given cloud cover from observer: cloud free (black), one octa (red), two octas (green), three octas (blue), and four octas (cyan)*

5.3.4 Excess water vapour for Europe

In chapter 5.3.2 TPW variability for a single station is investigated. The function describing the relation of the excess water vapour, expressed by the ratio of all to clear–sky TPW is analysed. The stability of the function is mainly driven by the number of cases included in the derivation of the regression. Regional variability does not influence the excess water vapour function much. The linear relationship of all–sky to clear–sky TPW shows a stronger dependency on the number of cases than on the different regions. In the following, investigation of excess water vapour is performed for several European stations shown in figure 5.24. These station data consist of radiosonde ascents. Unfortunately, there are no synoptical informations included. Therefore, a threshold for the selection of cloudy cases is applied. The dewpoint depression is used to distinguish between clear– and cloudy–sky situations. It is assumed that the dewpoint depression falls below 0.5 K in cloud cases. This threshold is derived from an analysis of all German station ascents which included synoptical observations. The uncertainty of this assumption should not effect the validity of the results much. For the DWD data set over 80% of overcast radiosonde profiles show a dewpoint difference below 0.5 K. In section 5.3.1 the uncertainty in mean TPW introduced by thresholds for cloud detection is shown to be small. The influence of cloud distinction on excess water vapour is small as well, see figure 5.23. Here the amount of octas as threshold is varied.

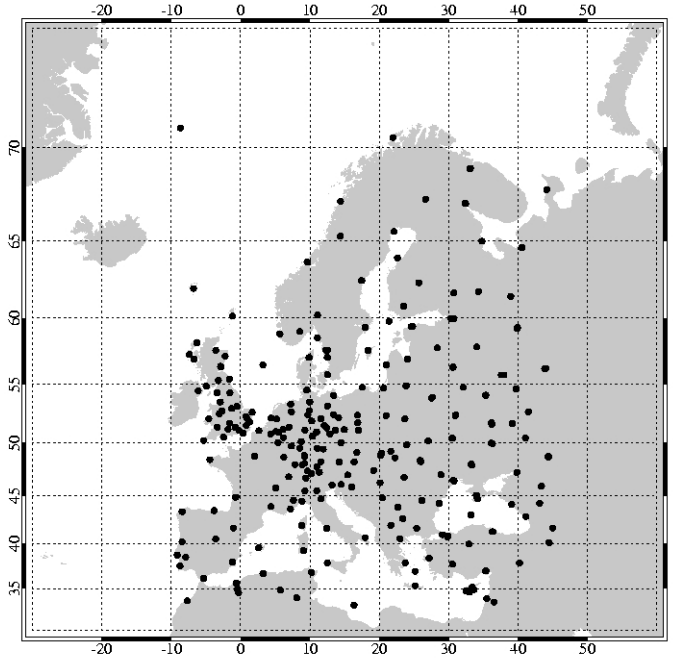

Figure 5.24: *Geographical distribution of European stations. Atmospheric profiles are not continously present for all stations in the years 1990 to 2000.*

For all stations in figure 5.24 the monthly mean TPW relation is shown in figure 5.25. For large clear–sky TPW excess water vapour is low, whereas excess water vapour is high for small clear–sky TPWs. Here, the differences in air masses corresponding to clear– and cloudy–sky situations are larger as is the variability in excess water vapour. This variability is driven by regional and seasonal differences.

Largest differences in air masses most obviously occur in the vicinity of frontal systems. To investigate this in more detail, the data set is divided based on the pressure at the lowest level. Surface pressures below 1003 hPa are denoted as low pressure cases. Surface pressures above 1023 hPa are flagged as high pressure cases. Figure 5.26 shows a higher number of data points in the low case. A wider range of clear-sky TPW is observed. The dependency of excess water vapour is more prominent in the low pressure case.

Seasonal variability influences the variability in excess water vapour in cases with small clear–sky TPW. The observed mean clear-sky TPW is subject to annual variablity. In summer (figure 5.28) larger values are reached than during the other seasons. The maximum excess water vapour is smaller during summer than in winter time (figure 5.27), which is related

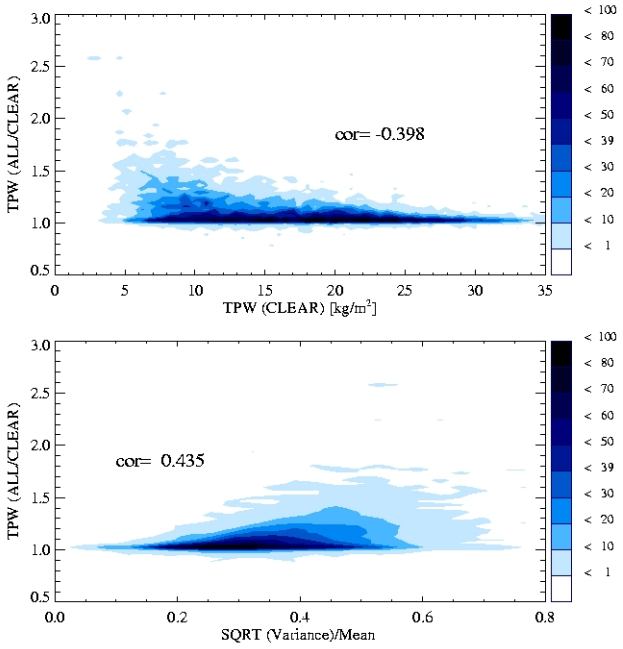

Figure 5.25: *Relation of monthly mean TPW in all–sky depending on clear–sky TPW. Radiosonde profiles under investigation are European stations and four German stations. The upper panel shows the ratio (all to clear–sky TPW) versus clear–sky TPW. The lower panel shows the ratio versus the normalised standard deviation. Colours denote the percentage of occurrence.*

to the larger differences of the air masses related to frontal systems. The best regressions are derived for spring and autumn (figure 5.28). Correlations between clear–sky TPW and excess water vapour are summerised in table 5.9.

The excess water vapour is derived without cloud informations from coinciding synoptical observations. The distributions show more noise due to miss detections in the thresholding scheme. On this larger regional scale the dependency of the excess water vapour on surface pressure is shown to be small. For low pressure systems the correlation to the excess water vapour is larger than under high pressure conditions. Under low pressure conditions the difference in cloud to clear situations is dominated by the passing of frontal systems. The effects of frontal systems on the TPW is further investigated in section 6.

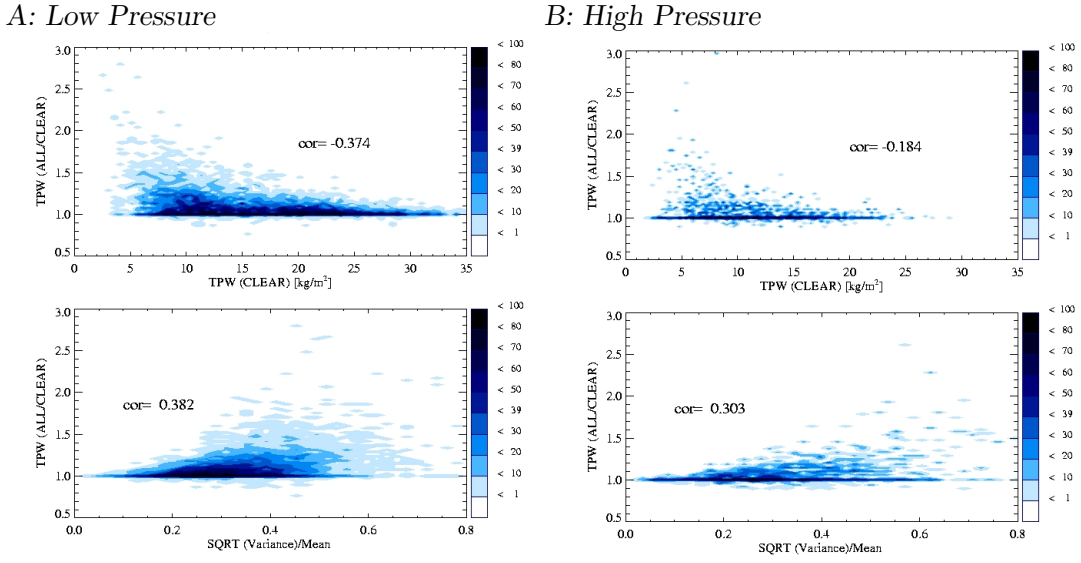

Figure 5.26: *Same as figure 5.25 but the surface pressure is lower then 1003 hPa (left) and for surface pressures higher then 1023 hPa (right).*

A: Winter: Low Pressure

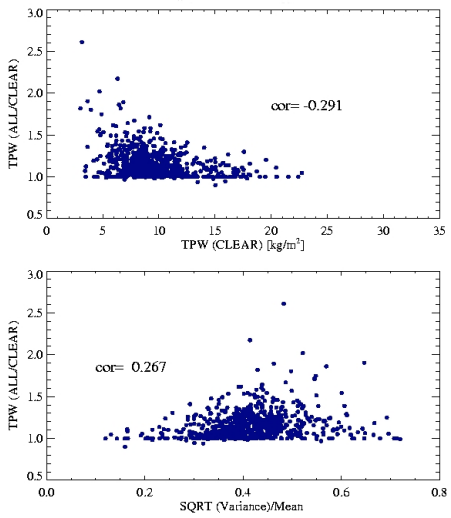

B: Winter: High Pressure

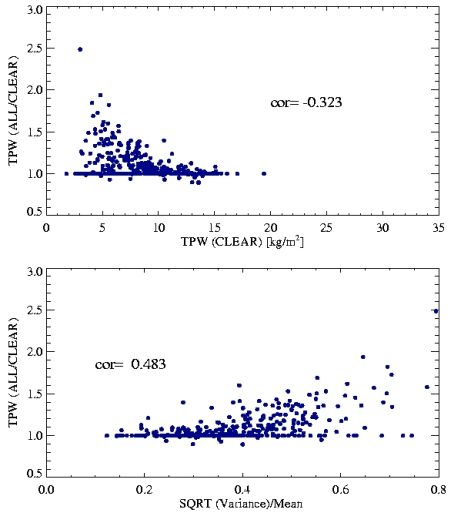

C: Spring: Low Pressure

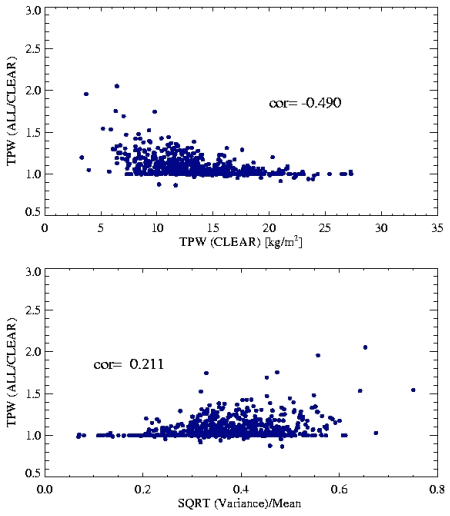

D: Spring: High Pressure

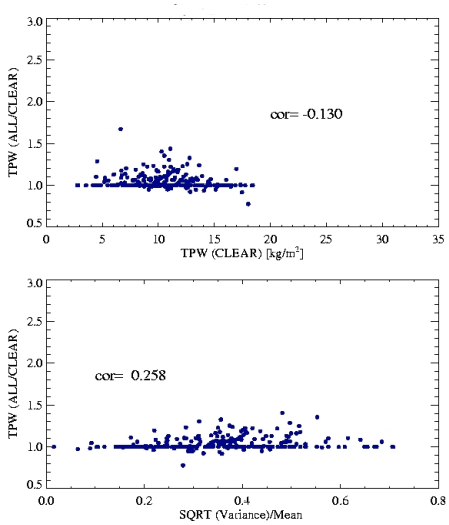

Figure 5.27: *Same as figure 5.26 but for winter (A and B) and autumn (C and D).*

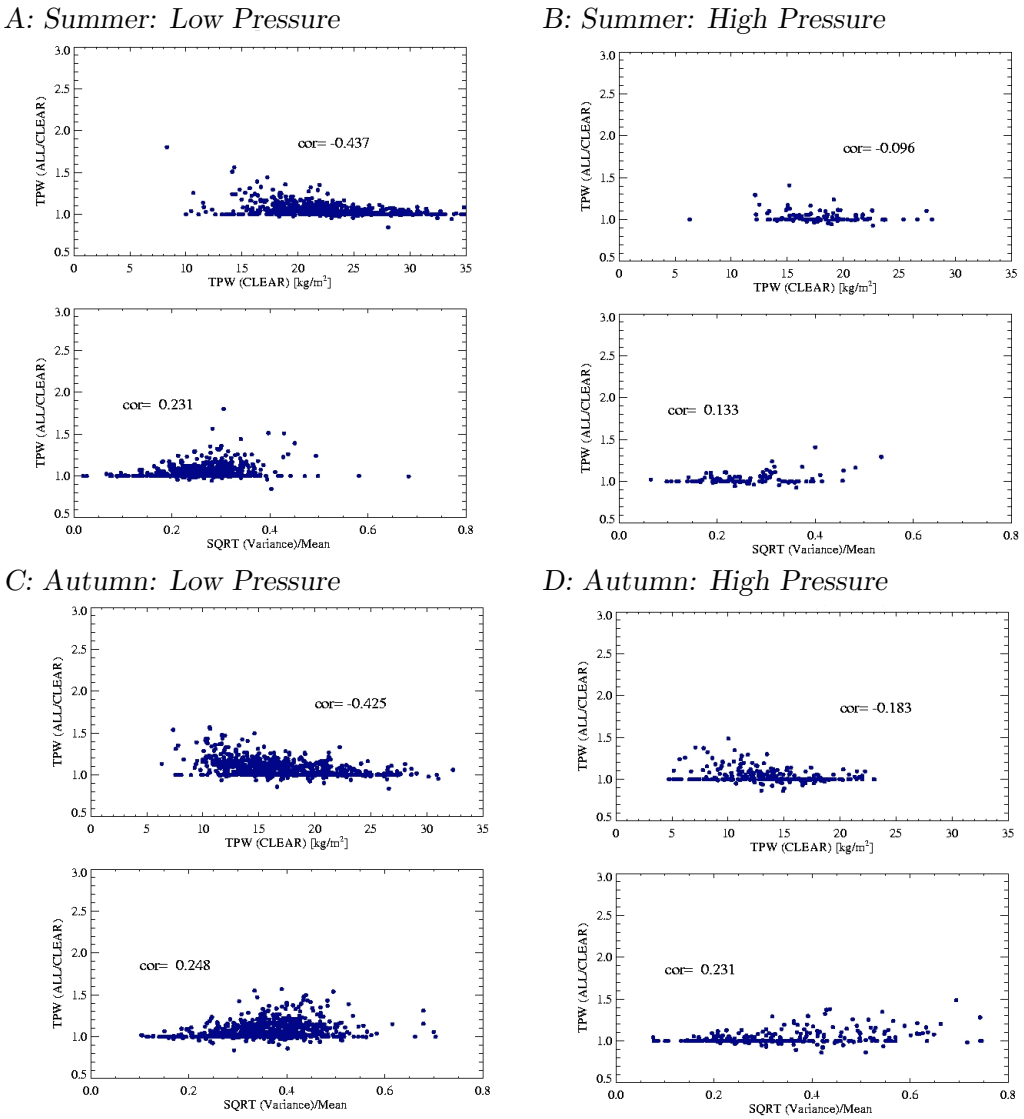

Figure 5.28: *Same as figure 5.26 but for summer (A and B) and autumn (C and D).*

Time	Pressure	Cor(Ratio, TPW(Clear))	Cor(Ratio, sdev/mean)
All		-0.57	0.58
	High	-0.28	0.44
	Low	-0.55	0.52
	Rest	-0.43	0.52
Spring		-0.57	0.34
	High	-0.19	0.27
	Low	-0.62	0.22
	Rest	-0.35	0.33
Summer		-0.66	0.52
	High	-0.39	0.35
	Low	-0.55	0.33
	Rest	-0.58	0.54
Autumn		-0.56	0.35
	High	-0.4	0.42
	Low	-0.55	0.27
	Rest	-0.34	0.25
Winter		-0.5	0.5
	High	-0.44	0.55
	Low	-0.43	0.37
	Rest	-0.33	0.58

Table 5.9: Correlation coefficients for the relations given in figures 5.25 to 5.28.

5.4 The vertical distribution of excess water vapour

Marsden and Valero (2004) show an increase in upper–tropospheric humidity in cloudy at-

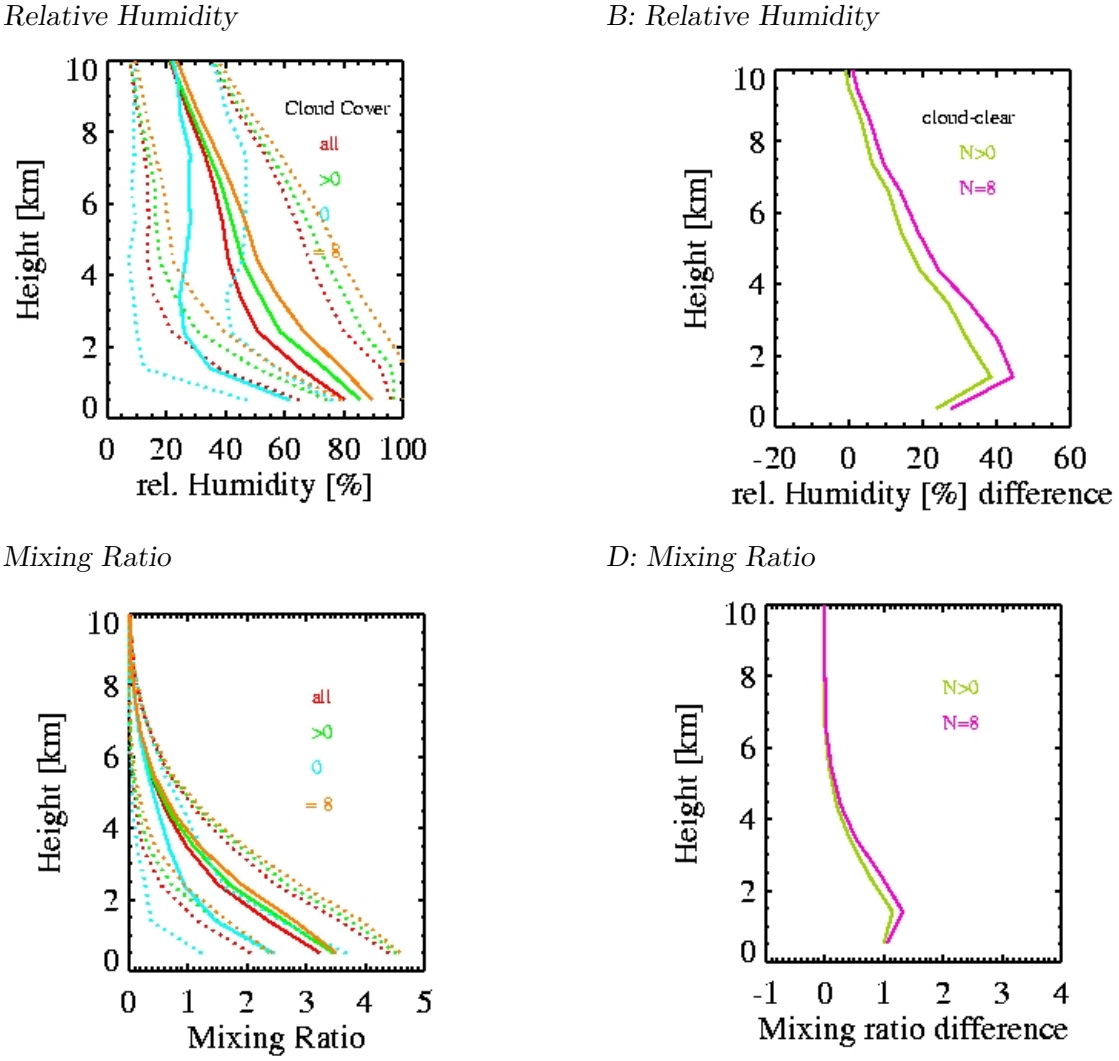

Figure 5.29: *Mean vertical profiles for January. A: mean profile (solid line) and standard deviation (dashed lines) of relative humidity for clear–sky cases (cyan), cloudy (dark green), total cloud cover (orange), and all profiles (red). B: humidity difference profiles for mean cloudy to mean clear profile; all cloudy cases (green) and total cloud cover (magenta). C: mean profile (solid line) and standard deviation (dashed lines) of mixing ratio (in [g/kg]) for clear–sky cases (cyan), cloudy (dark green), total cloud cover (orange), and all profiles (red). D: mixing ratio difference profiles for mean cloudy to mean clear profile; all cloudy cases (green) and total cloud cover (magenta).*

mospheres compared to clear sky situations. For calculations of greenhouse radiative forcing the humidity profile is important. An increase in upper–tropospheric humidity has a higher impact on the radiative forcing then an increase in the lower atmosphere. Therefore, differ-

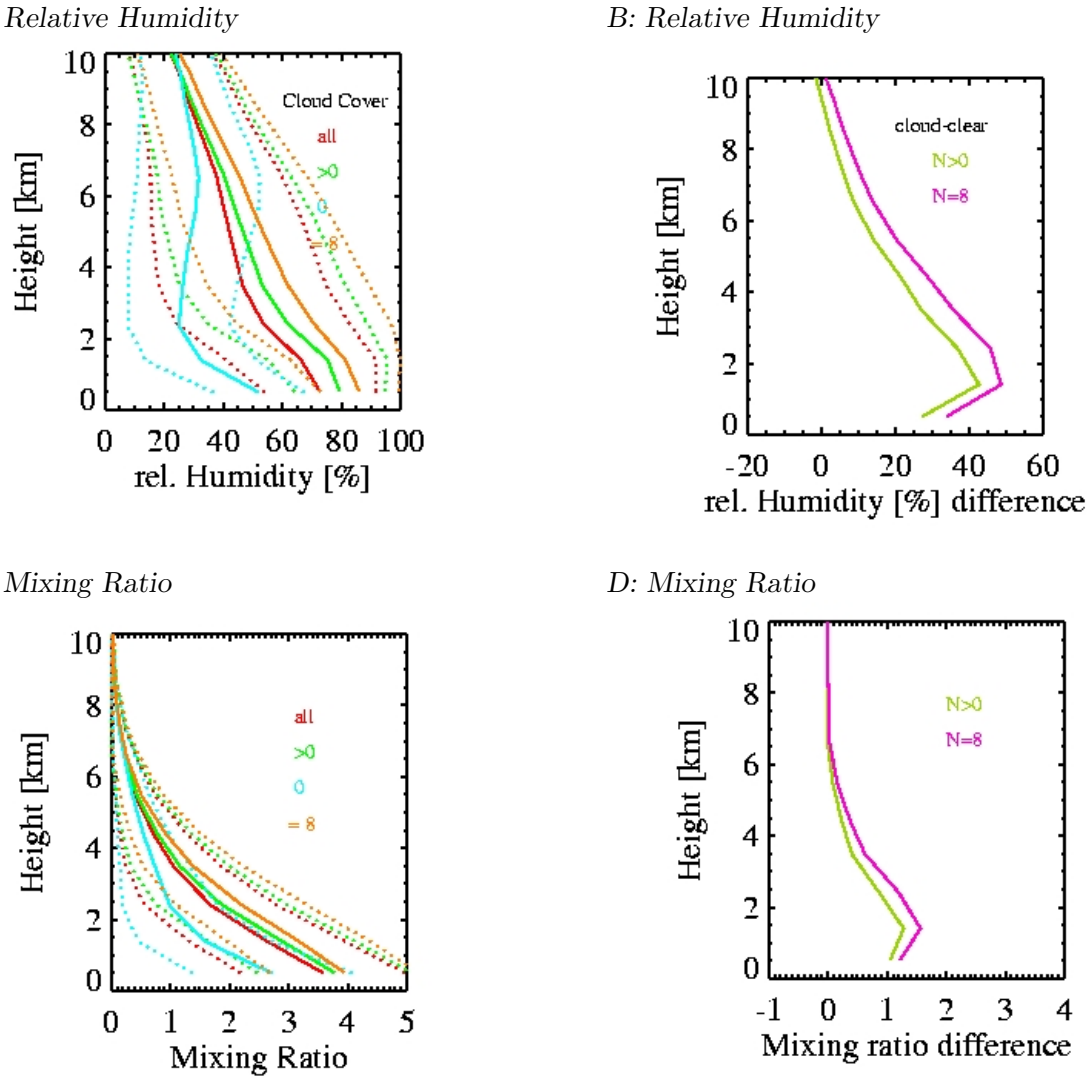

Figure 5.30: *Mean vertical profiles for April. A: mean profile (solid line) and standard deviation (dashed lines) of relative humidity for clear–sky cases (cyan), cloudy (dark green), total cloud cover (orange), and all profiles (red). B: humidity difference profiles for mean cloudy to mean clear profile; all cloudy cases (green) and total cloud cover (magenta). C: mean profile (solid line) and standard deviation (dashed lines) of mixing ratio (in [g/kg]) for clear–sky cases (cyan), cloudy (dark green), total cloud cover (orange), and all profiles (red). D: mixing ratio difference profiles for mean cloudy to mean clear profile; all cloudy cases (green) and total cloud cover (magenta).*

ences in the humidity profiles between cloudy and clear skies are investigated here.

To answer the question whether there is a dominant height, where in cases of cloudiness the

A: Relative Humidity

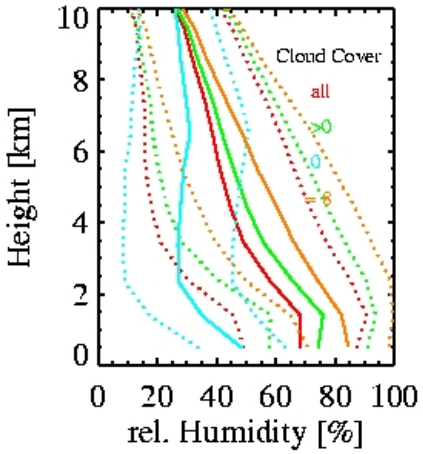

B: Relative Humidity

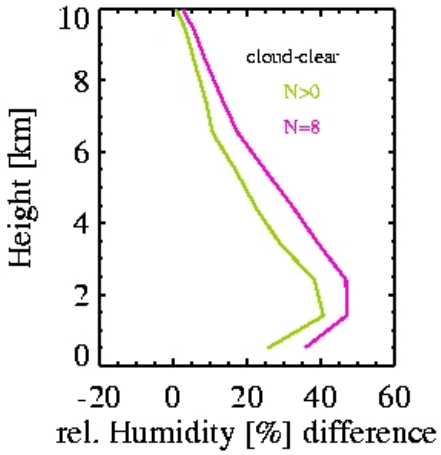

C: Mixing Ratio

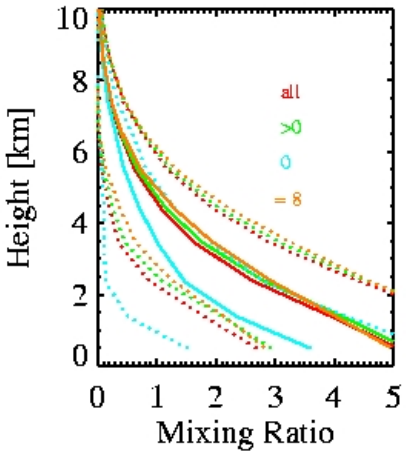

D: Mixing Ratio

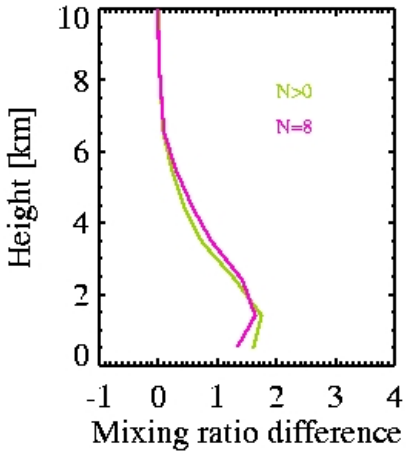

Figure 5.31: *Mean vertical profiles for July. A: mean profile (solid line) and standard deviation (dashed lines) of relative humidity for clear–sky cases (cyan), cloudy (dark green), total cloud cover (orange), and all profiles (red). B: humidity difference profiles for mean cloudy to mean clear profile; all cloudy cases (green) and total cloud cover (magenta). C: mean profile (solid line) and standard deviation (dashed lines) of mixing ratio (in [g/kg]) for clear–sky cases (cyan), cloudy (dark green), total cloud cover (orange), and all profiles (red). D: mixing ratio difference profiles for mean cloudy to mean clear profile; all cloudy cases (green) and total cloud cover (magenta).*

humidity is enlarged, monthly mean vertical relative humidity profiles are investigated. The humidity difference (mean cloudy to mean clear) is largest in 1.5 km height. This level is nearly constant throughout the year, but the vertical extend is larger in summer, whereas in winter and spring the maximum relative humidity occurs in a small vertical extend. In

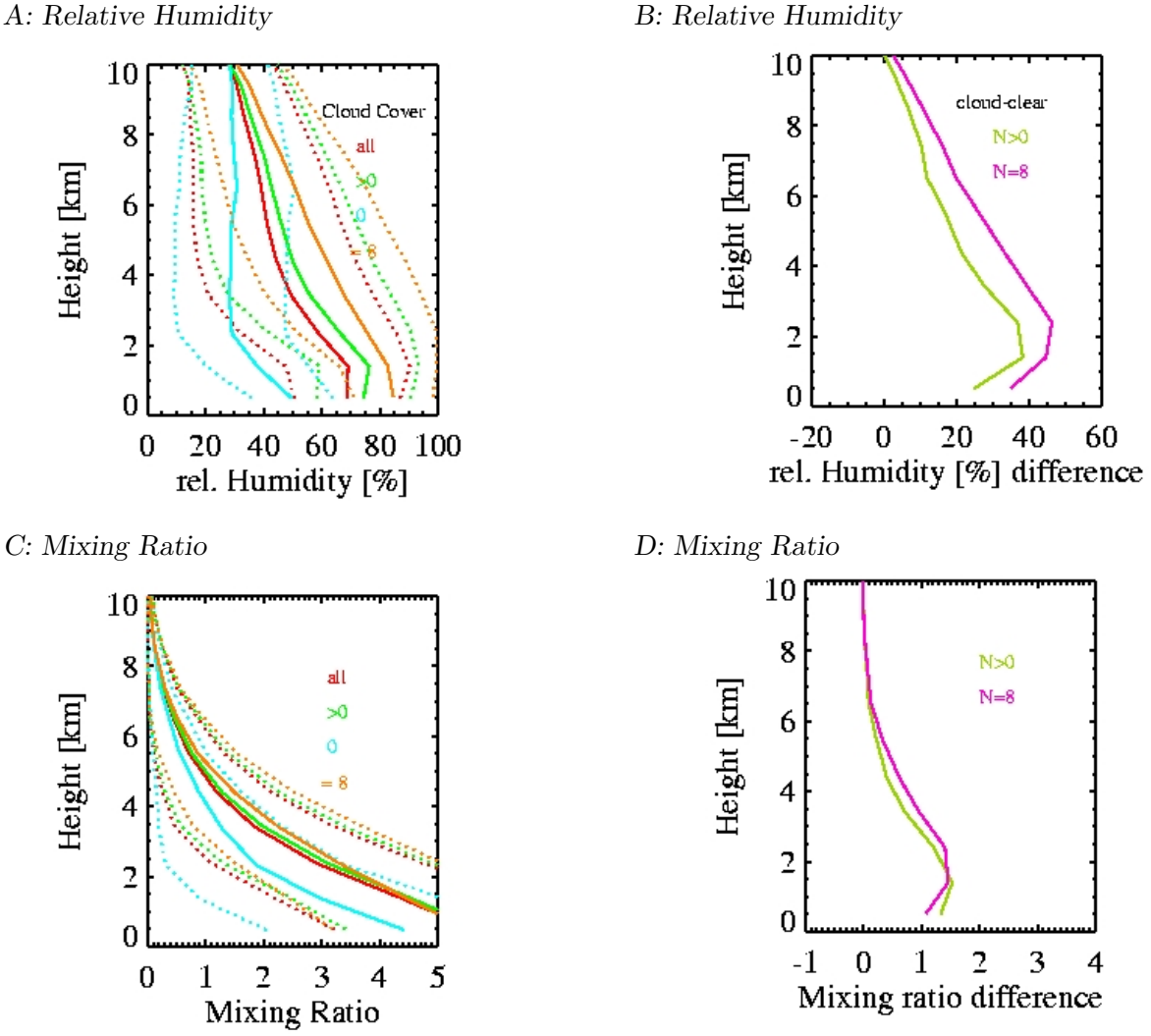

Figure 5.32: *Mean vertical profiles for October. A: mean profile (solid line) and standard deviation (dashed lines) of relative humidity for clear–sky cases (cyan), cloudy (dark green), total cloud cover (orange), and all profiles (red). B: humidity difference profiles for mean cloudy to mean clear profile; all cloudy cases (green) and total cloud cover (magenta). C: mean profile (solid line) and standard deviation (dashed lines) of mixing ratio (in [g/kg]) for clear–sky cases (cyan), cloudy (dark green), total cloud cover (orange), and all profiles (red). D: mixing ratio difference profiles for mean cloudy to mean clear profile; all cloudy cases (green) and total cloud cover (magenta).*

the cloud layer the excess water vapour (cloud - clear relative humidity) is about 50 %. The cloudy-sky profile contains more humidity un to the tropopause. Below the cloud layer the excess water vapour is about 20 %, and in the upper troposphere additional 10 % relative humidity occurs, as is shown in figures 5.29 to 5.32.

The relative humidity increases with temperature. One can argue that the observed differences in excess water vapour profiles are related to temperature differences between clear and cloudy situations. Therefore the mixing ratio, which gives water vapour per dry air, is shown as well. An increase in mixing ratio over the whole profile is found for cloudy skies compared to clear sky observations. The maximum here is found in the cloud layer but up to 6 km height an increase in water vapour is found. In July and October the increase is in higher levels than in January and April.

Differences in the distributions of sea level pressure and the height of the 500 hPa level depending on cloudiness are shown in section 5.2.1. Figure 5.33 shows that the relation between surface pressure (500 hPa level height) and TPW is depending on cloudiness. For Lindenberg clear–sky cases show the maximum occurrences of low TPW under higher surface pressure situations coinciding with a higher 500 hPa level. Cloudy cases dominate under lower surface pressure situations and under lower 500 hPa level situations.

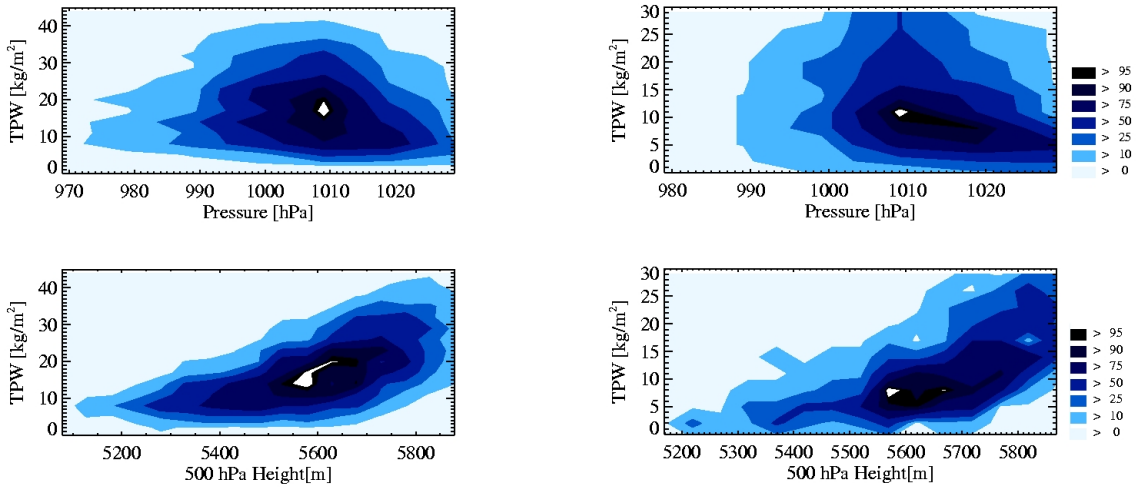

Figure 5.33: *Upper row: Frequency distribution of surface pressure related to TPW for all radiosonde ascents at noon time. Lower row: Frequency distribution of 500 hPa level height related to TPW. Right for clear–sky and left for cloudy conditions. In colours the percentage of occurrence is given.*

5.4.1 Layered excess water vapour

The relative humidity and mixing ratio is enlarged over the whole profile as shown in the previous section. The relation of retrieved excess water vapour towards mean clear–sky TPW was shown for total column water vapour. But does this ratio vary with height? With satellite retrievals of TPW for different layers is possible. The corresponding heights are related to the signal weighting functions of the used frequencies. Figure 5.34(A) shows the relation of clear–sky to all–sky TPW for surface layer reaching up to 850 hPa. For large clear–sky TPW, all–sky cases do not differ in monthly mean TPW. In the height of cloud layers (Figure 5.34 (B) and 5.35 (A and B)) excess water vapour is largest. For the upper most layer from 300 hPa to 200 hPa, the measured TPW is low and the variability in the monthly all–sky means is large. For all layered excess water vapour the ratio is close to 1.1 for larger clear–sky TPW and and increases towards lower clear–sky TPW values.

The excess water vapour as a function of clear–sky TPW is similar for the total TPW and for the layered TPW. Largest excess water vapour values are found in and below the cloud layers. Which is explained by the transport of humidity from the surface to higher level due to convection.

A: 1000 hPa to 850 hPa

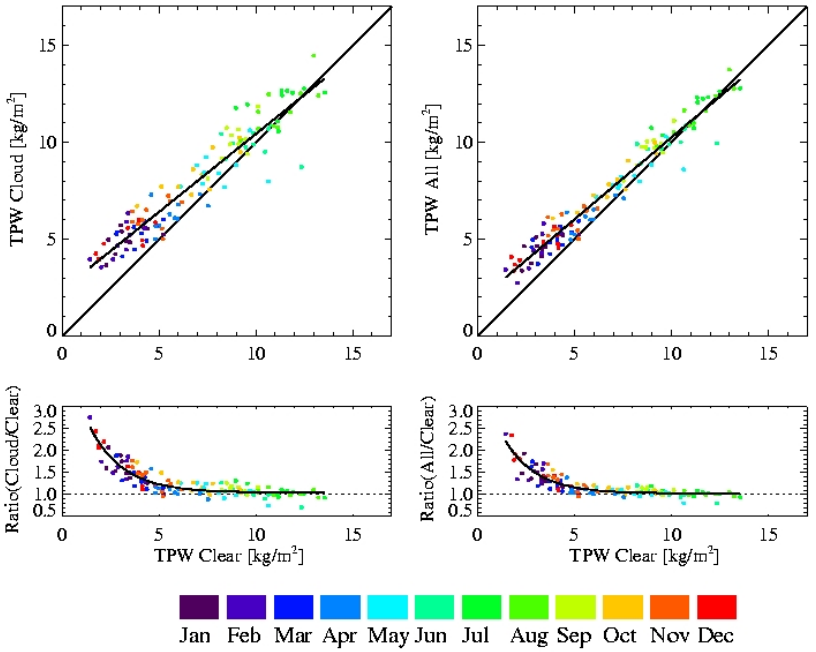

B: 850 hPa to 700 hPa

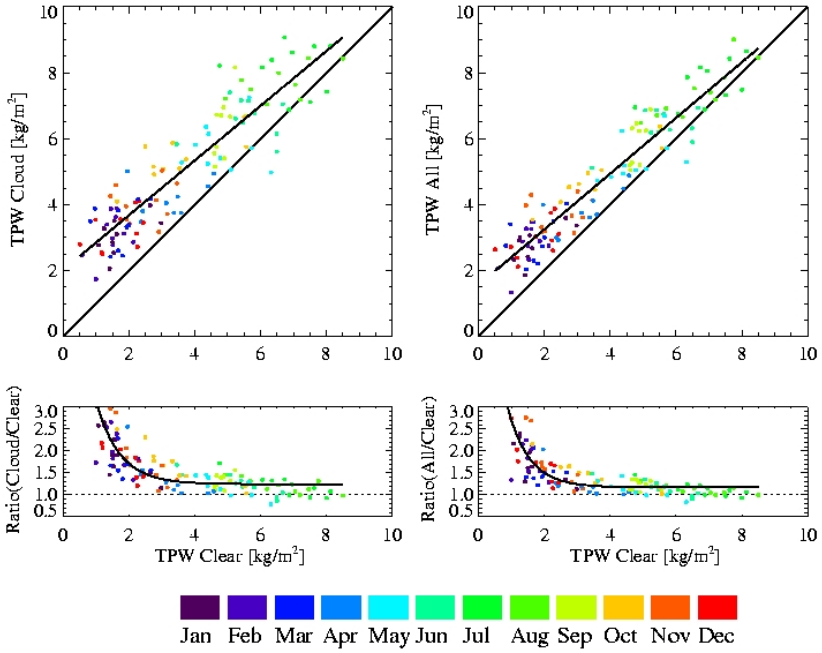

Figure 5.34: *Monthly means for 10 years of Lindenberg radiosonde measurements for the layer 1000 hPa to 850 hPa (A) and 850 hPa to 700 hPa (B). Monthly mean TPW in clear–sky cases versus cloudy–sky cases (upper panel) and versus the ratio (cloud/clear) (lower panel) (left). Clear–sky TPW is shown in relation to all–sky TPW (right). Colors denote the month.*

A: 700 hPa to 500 hPa

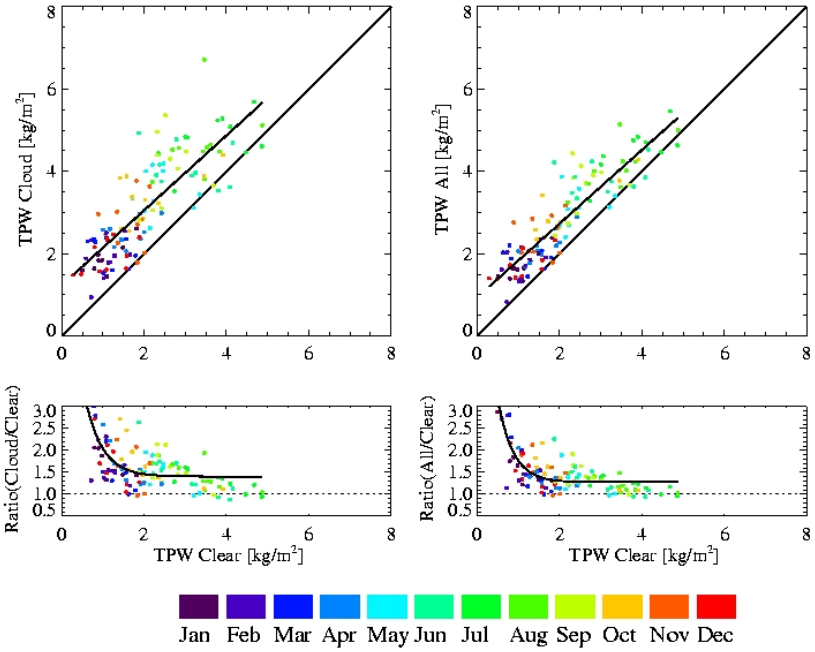

B: 500 hPa to 300 hPa

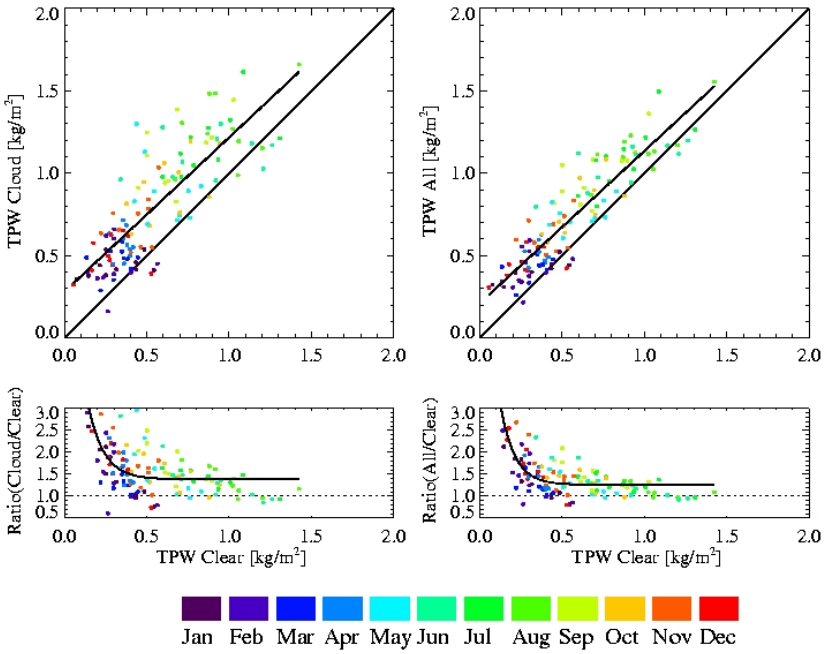

Figure 5.35: *Monthly means for 10 years of Lindenberg radiosonde measurements for the layer 700 hPa to 500 hPa (A) and 500 hPa to 300 hPa (B). Monthly mean TPW in clear–sky cases versus cloudy–sky cases (upper panel) and versus the ratio (cloud/clear) (lower panel) (left). Clear–sky TPW is shown in relation to all–sky TPW (right). Colors denote the month.*

A: 300 hPa to 200 hPa

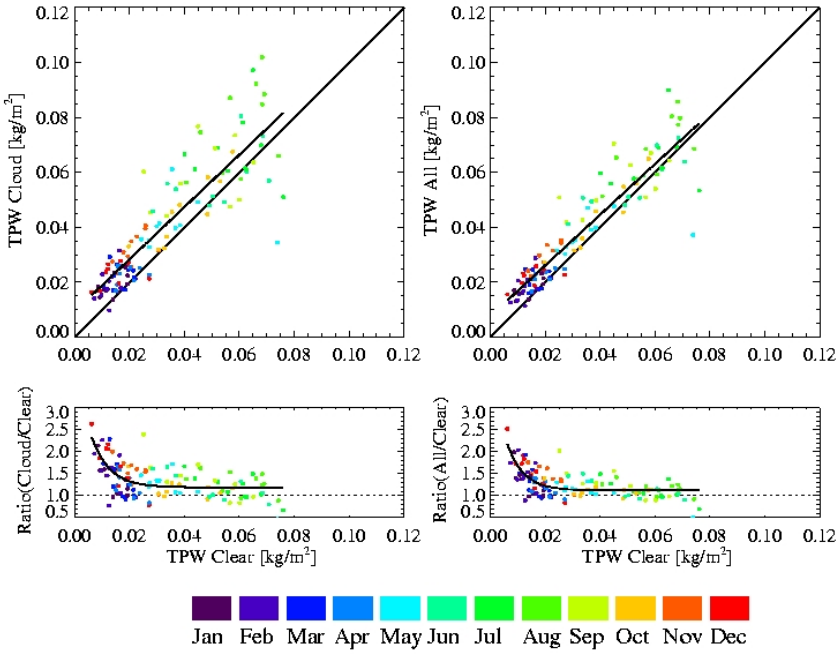

Figure 5.36: *Monthly means for 10 years of Lindenberg radiosonde measurements for the layer 300 hPa to 200 hPa (A). Monthly mean TPW in clear–sky cases versus cloudy–sky cases (upper panel) and versus the ratio (cloud/clear) (lower panel) (left). Clear–sky TPW is shown in relation to all–sky TPW (right). Colors denote the month.*

5.5 Concluding Remarks

The clear–sky TPW is significantly lower than TPW in cloudy atmospheres. The amount of water vapour added by the clouds is about 10% of the clear–sky TPW. The excess water vapour defined as the ratio of TPW in all–sky to the TPW in clear–sky situations is derived for German stations. The functional relation between the excess water vapour and the clear–sky TPW on monthly mean basis is described by an exponential function. The excess water vapour decreases with increasing clear–sky TPW. The underestimation in TPW by neglecting cloudy scenes is about 10%–20%. The same functional relation is found for the European area. The relation is much more noisy due to missing cloud informations.
The cloud layers are identified in the mixing ratio and relative humidity profile. Looking at layered TPW the largest excess water vapour is found in the cloud levels. However, the functional relation of the excess water vapour depending on the clear–sky TPW is found for all layers.

Chapter 6

Satellite observed low pressure systems

One explanation for the larger excess water vapour values in the mid–latitudes is the difference in airmasses passing through a region related to low pressure systems. The monthly mean excess water vapour is the mean over different synoptical situations. In this section a case study on the distribution of vertical integrated water vapour in the vicinity of North Atlantic low pressure systems is given. Two situations are chosen for a deeper discussion. The strongest difference in air temperature of the air masses related to the frontal systems occurs in winter and spring. Therefore, the first case is a low pressure system at the 28th of January 2001 over the central Atlantic. The second case is chosen in early spring. It spans three days in which low pressure systems form and move eastward across the Atlantic.

For the following case studies some remarks in advance should be made. The surface pressure chart is taken from the archive of www.wetterzentrale.de. The charts are provided by the UK Met Office. The pressure field shows the observation from 0 UTC. The AVHRR channel 3 field is taken from the Dundee receiving station. Channel 3 measures generally at 1.6μm during day time and at special occasions at 3.7μm. During day time the observations are mainly the backscattered sunlight, whereas at 3.7μm the thermal emission of the surface is included. The AMSU fields show a composit of all morning overpasses which leads to problems in interpreting the overlap regions because the atmosphere is not stationairy. The TPW and LWP retrieval from microwave emission is possible only for ice free ocean. SST values lower than 2°C are not used. The surface state data like pressure, SST and atmospheric temperature are provided by NCEP-NCAR reanalysis. The data are available on a 2.5° longitude latitude grid.

6.1 First case: 28–29 January 2001

The UK-Met Office chart of January the 29th 2001 0 UTC (see figure 6.1 left) shows a low pressure system east of Newfoundland. A ridge spans about 30° West northward. A cold

front occurs at 40° West. The NOAA AVHRR channel 3 afternoon overpass is shown in figure 6.1. The cloud fields are related to the frontal systems. During the day, the low pressure system has moved eastwards.

Figure 6.2 shows the AMSU observed quantities and the NCEP–NCAR reanalysis data as used for the AMSU retrieval. The near-surface air temperature shows the ridge as warmer air moving north. The SST shows a strong zonal distribution in the central Atlantic. Near the coasts and in the vicinity of ocean currents a stronger gradient is found. The TPW and LWP show a strong cloud band with large LWP values in the center. The cloud field stretches from Greenland southward in relation with the occlusion front shown in figure 6.1 but with a slight displacement towards the north east due to the different observing times. More to the south the fronts are separated in warm and cold front. The total precipitable water shows larger values in the areas where LWP is observed. Over the oceans the source of humidity in the atmosphere is unlimited. The vertical transport of humidity is due to turbulence. The ability of air containing humidity is coupled to the air temperature. If clouds do not contribute to the TPW the temperature distribution should dominate the TPW field. However, the structure of both air and sea surface temperature is not clearly visible in the TPW fields.

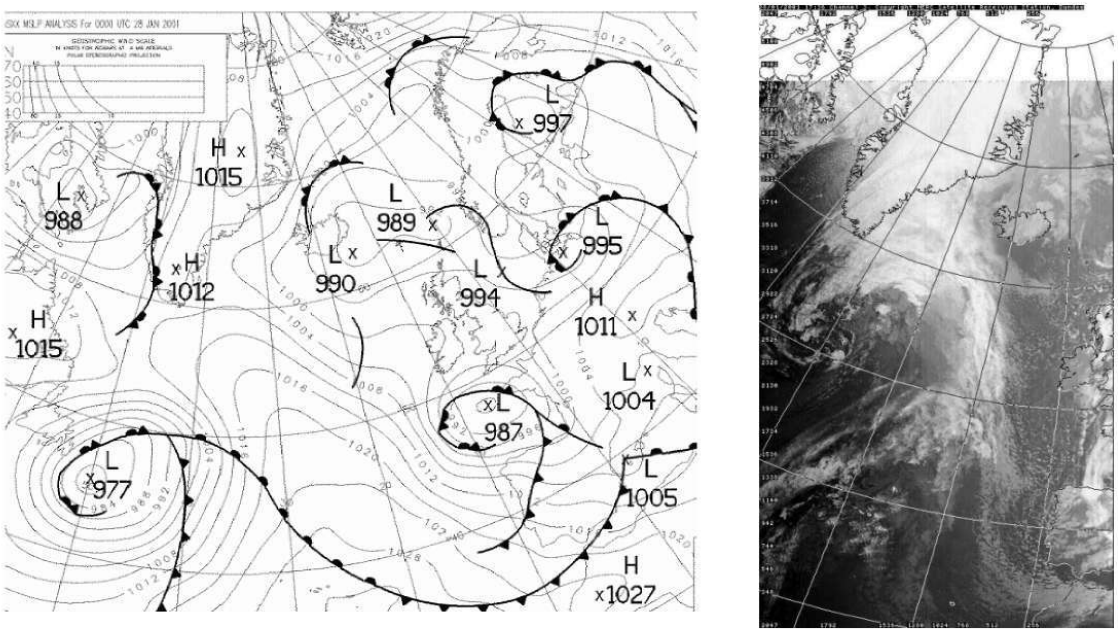

Figure 6.1: *Synoptical situation for the 28th, January 2001. On the left the 0 UTC surface chart of the UK–Met Office is shown. On the right the NOAA AVHRR channel 3 afternoon overpass is shown.*

Figure 6.3 shows the 1° grid box mean TPW, LWP, pressure, SST and the air temperature for different zonal cross sections. The low pressure system is situated around 48° to 51° N on the west coast of the Atlantic. The corresponding frontal systems are related to large LWP and TPW in the central part of the Atlantic. The longitudinal TPW gradient increases away from the center of the pressure system. Regions with large LWP coincide with those of large TPW. The warm front is shown in the north east of the centre of the low. Except for the maxima in TPW the structure along the latitudes correspond well to the temperature field. The air temperature follows roughly the SST. Along one latitude the SST is lower on the west side where the Labrador current at the coast line moves south. The SST increases towards 40°W to the centre of the Gulf current. Here the different latitudinal lines separate. Towards the east side of the Atlantic the temperature at different latitudes are close. The air temperature follows the SST. Near the coast the influence of land can be observed. On the west side of the basain the air temperature is colder than the SST due to off shore cold winds.

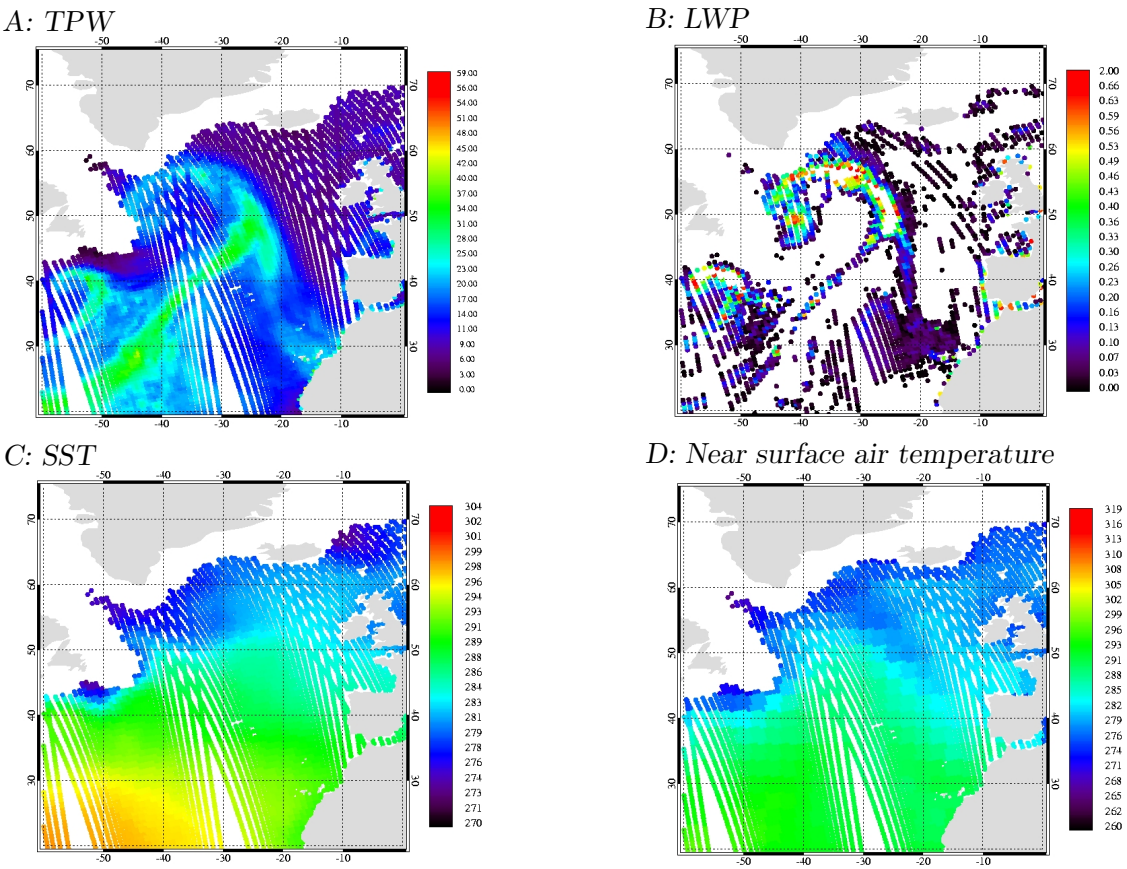

Figure 6.2: *The 28th January 2001 morning overpasses of the NOAA-16 AMSU instrument.* **A** *gives the retrieved TPW in kg/m^2.* **B** *shows the LWP in kg/m^2. Negative values and values larger than 2 kg/m^2 are not included. For the TPW and LWP retrieval surface informations are used. These data are taken from the 2.5° NCEP–NCAR reanalysis.* **C** *shows the SST, and* **D** *the near surface air temperature on AMSU FOV grid.*

The next day, the 0 UTC weather chart shows the position of the low pressure system south east of Greenland. On the back side of the system dry air flows over the Atlantic. More humid air is related to the warm front and the ridge east of the low. See figure 6.4 for the

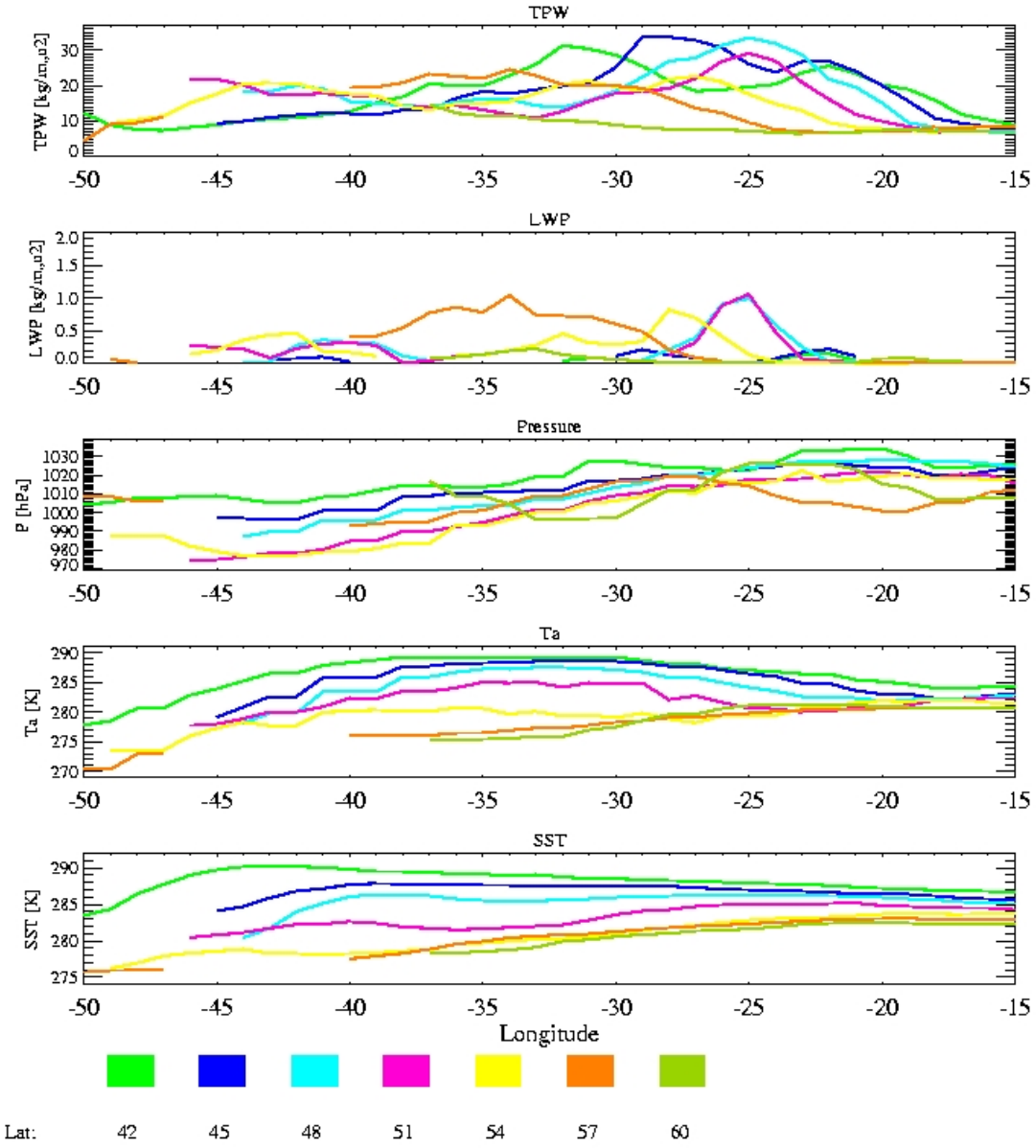

Figure 6.3: *The 1° mean horizontal distribution of TPW, LWP, surface pressure, atmospheric temperature and SST (top to bottom) at different latitudes for the 28th January 2001. The central latitude is colour coded.*

weather chart and figure 6.5 for the TPW, LWP and surface state.

The horizontal distribution of TPW, LWP and the surface quantities are shown in figure 6.6. The whole low pressure system has moved east. The fronts corresponding to the high values in TPW and LWP moved northe east. In the south west a new frontal system appears with its frontal systems present in large TPWs.

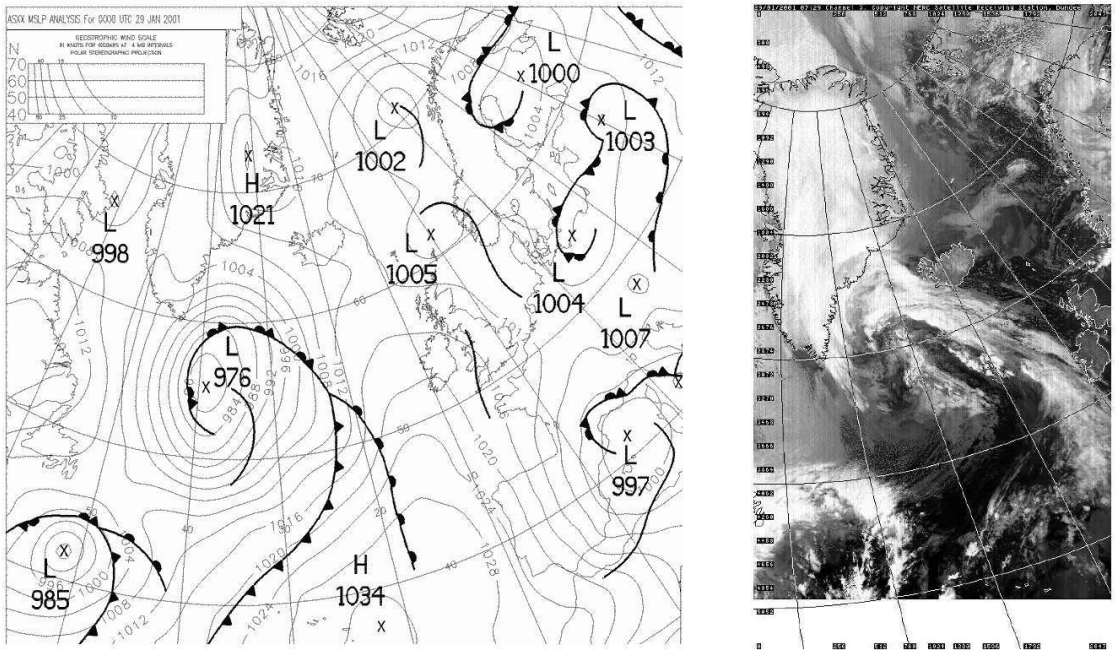

Figure 6.4: *Synoptical situation for the 29th, January 2001. On the left the 0 UTC surface chart of the UK–Met Office is shown. On the right the NOAA AVHRR channel 3 morning overpass is shown.*

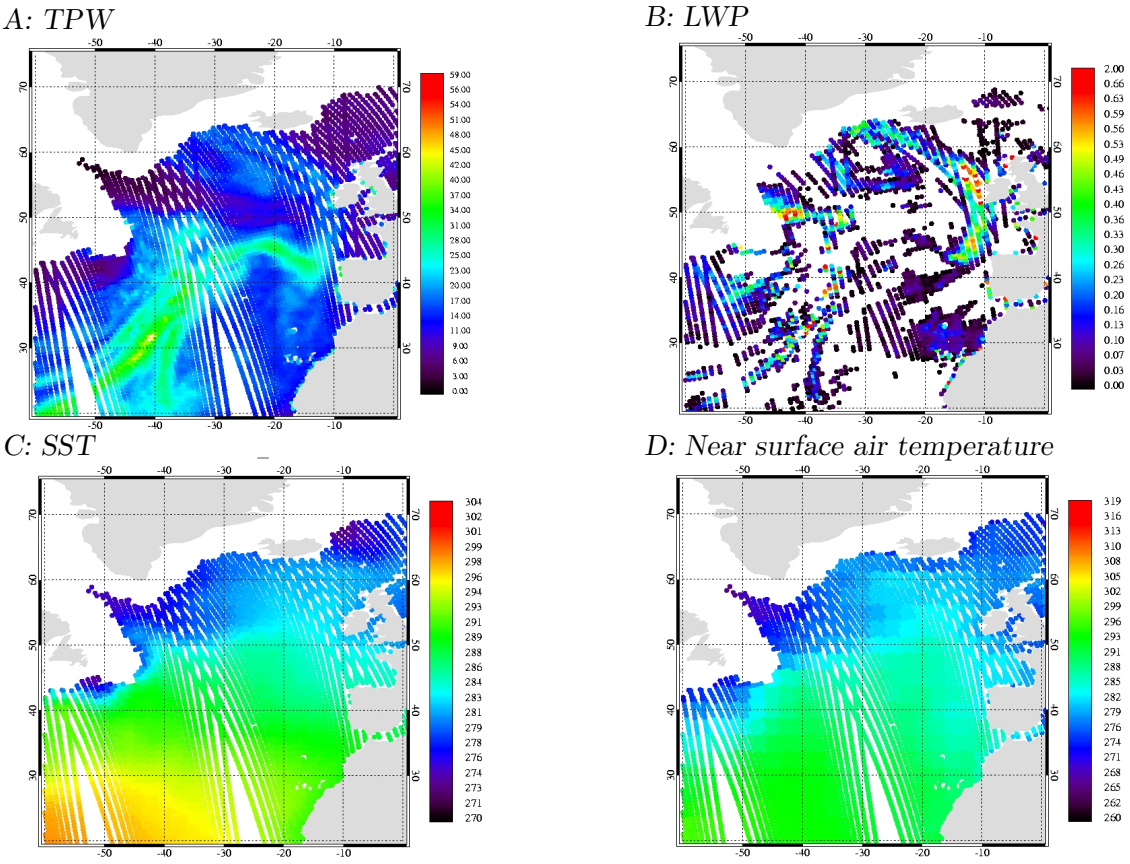

Figure 6.5: *The 29th January 2001 morning overpasses of the NOAA-16 AMSU instrument.* **A** *gives the retrieved TPW in kg/m^2.* **B** *shows the LWP in kg/m^2. Negative values and values larger than 2 kg/m^2 are not included. For the TPW and LWP retrieval surface informations are used. These data are taken from the 2.5° NCEP–NCAR reanalysis.* **C** *shows the SST, and* **D** *the near surface air temperature on AMSU FOV grid.*

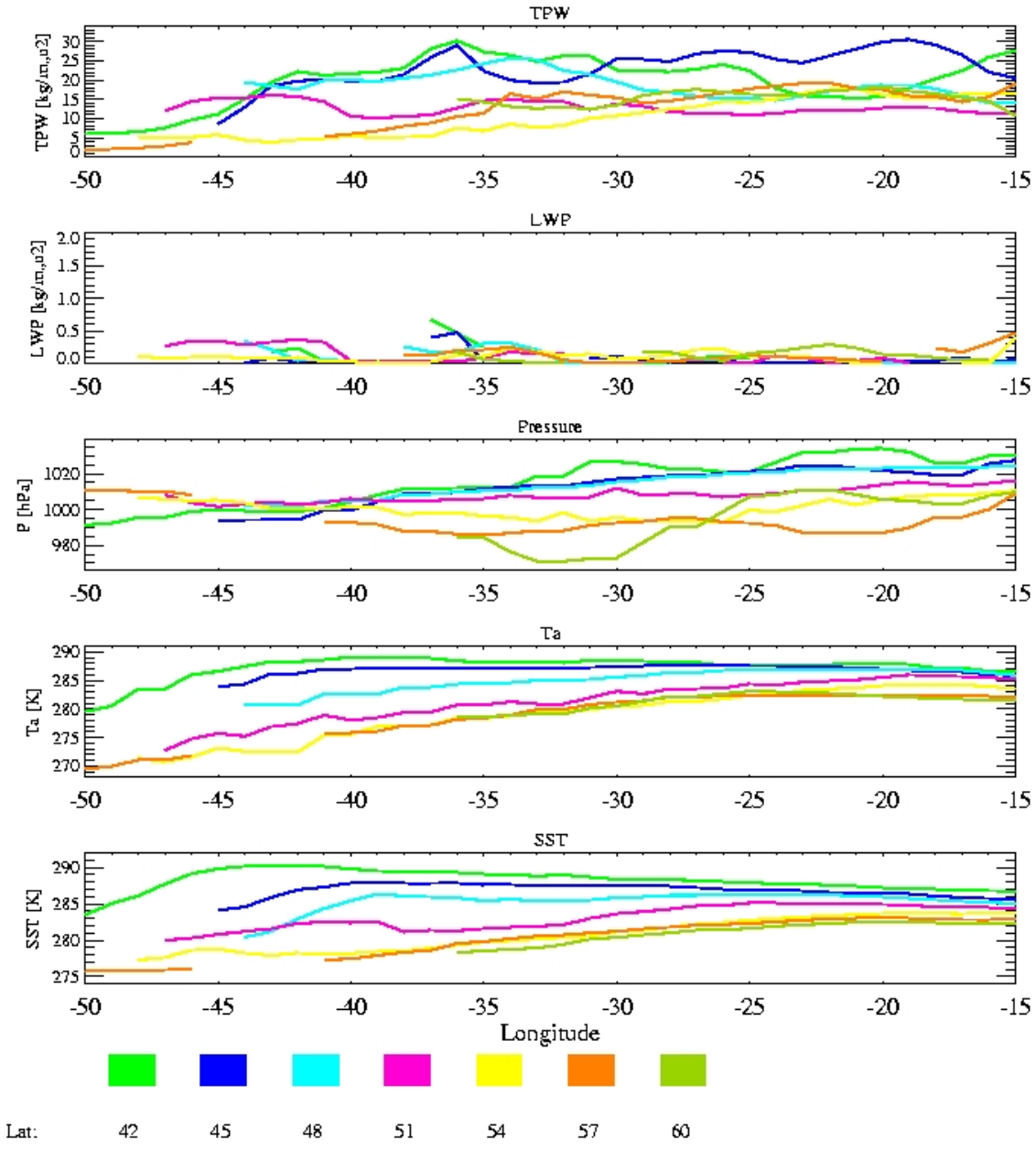

Figure 6.6: *The 1° mean horizontal distribution of TPW, LWP, surface pressure, atmospheric temperature and SST (top to bottom) at different latitudes for the 29th January 2001. The central latitude is colour coded.*

6.2 Second case: 28 – 30 March 2001

The UK-Met Office chart of March 28th 2001 0 UTC (see figure 6.7 left) shows a frontal system spans over the Atlantic along 50° N latitude. Along this line several regional lows are found and a occlusion point can be seen. A trough in 500 hPa spans from Greenland towards the Iberian peninsula. Cold and dry air is related to the trough around Iberia and the Atlantic around the Azores. Over the Atlantic only a few LWP observations are found (see figure 6.8). During the day the trough is separated from the North due to a ridge coming in from the west, see figure 6.10. This ridge is related to warm and humid air containing clouds. In the centre of this band large LWP values are reached (see figure 6.11). A low pressure system is moving to the North Atlantic area from the west. On 30th, March, this low has propagated further north east (figure 6.13). A cloud band stretches from Ireland towards the Carebean. This band is small and separates two dry areas (figure 6.14). West of the Iberian peninsula thin clouds are observed. The cold air of the trough is still present and saturated over the warm ocean surface.

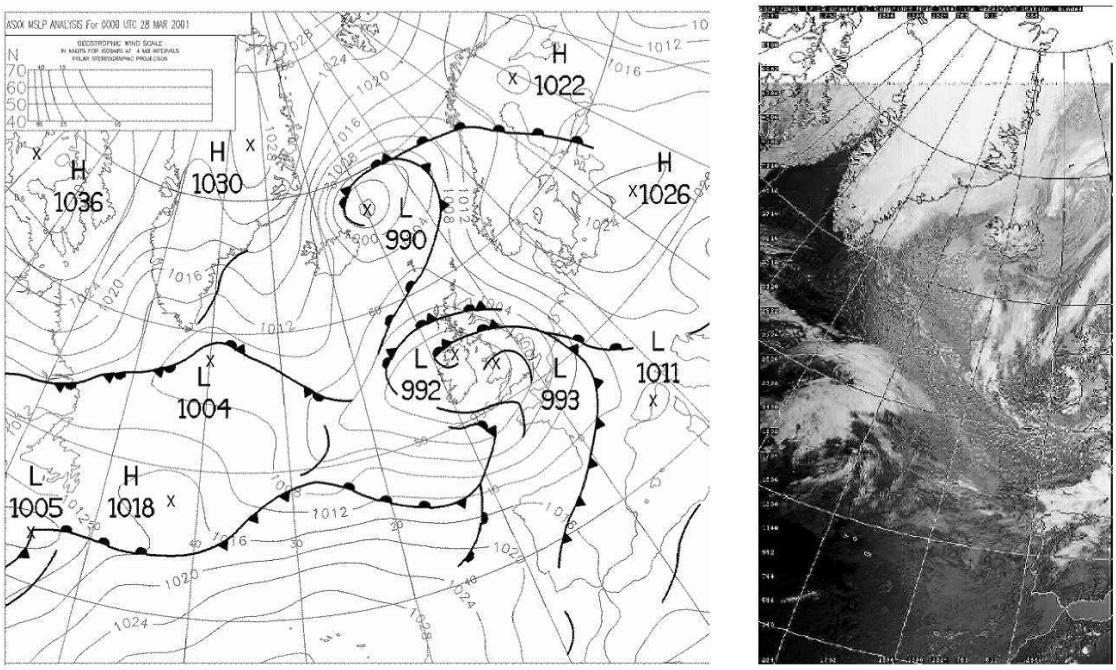

Figure 6.7: *Synoptical situation for the 28th, March 2001. On the left the 0 UTC surface chart of the UK–Metoffice is shown. On the right the NOAA AVHRR channel 3 morning overpass is shown.*

The horizontal distribution of TPW, LWP and the surface parameter are shown in figure 6.9 for the 28th March 2001. South of New Foundland a low pressure system is developing. The humid air east of the pressure minimum is related to the warm front. The moist area is small in longitudinal extend. The TPW decreases towards the east part of the Atlantic. The dry air is connected to the cold air trough over the east edge of the area and the Iberian peninsula. During the day the low pressure system moves east. The warm front represented by the humid air is moving north east. The system is followed by cold dry air originating from the American continent. The frontal system is clearly visible in the TPW and LWP field an in the longitudinal distributions shown in figure 6.12. The TPW follow basicly SST and air temperature. However, the characteristics of the maxima in TPW is related to the occurrence of clouds. Towards the 30th of March 2001 the low pressure system moves further east. In the longitudinal distributions this movement is visible in the shift of the TPW

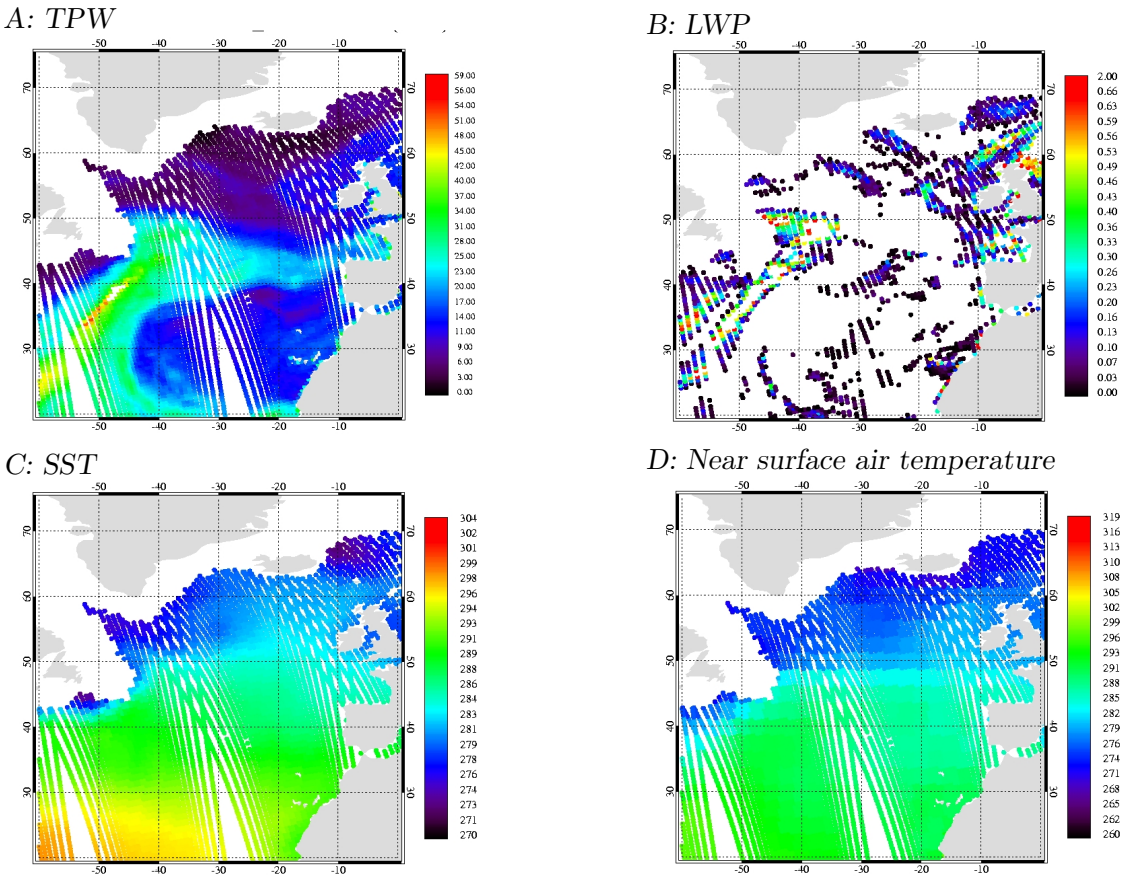

Figure 6.8: *The morning overpasses of the NOAA-16 AMSU instrument.* **A** *gives the retrieved TPW in kg/m^2.* **B** *shows the LWP in kg/m^2. Negative values and values larger than 2 kg/m^2 are not included. For the TPW and LWP retrieval surface informations are used. These data are taken from the 2.5° NCEP–NCAR reanalysis.* **C** *shows the SST, and* **D** *the near surface air temperature on AMSU FOV grid.*

maxima. The distinct LWP maxima is observed in the occlusion area, where the cold front reaches the warm front. Synoptically this is the point with strongest rainfall along the frontal lines (see figure 6.15).

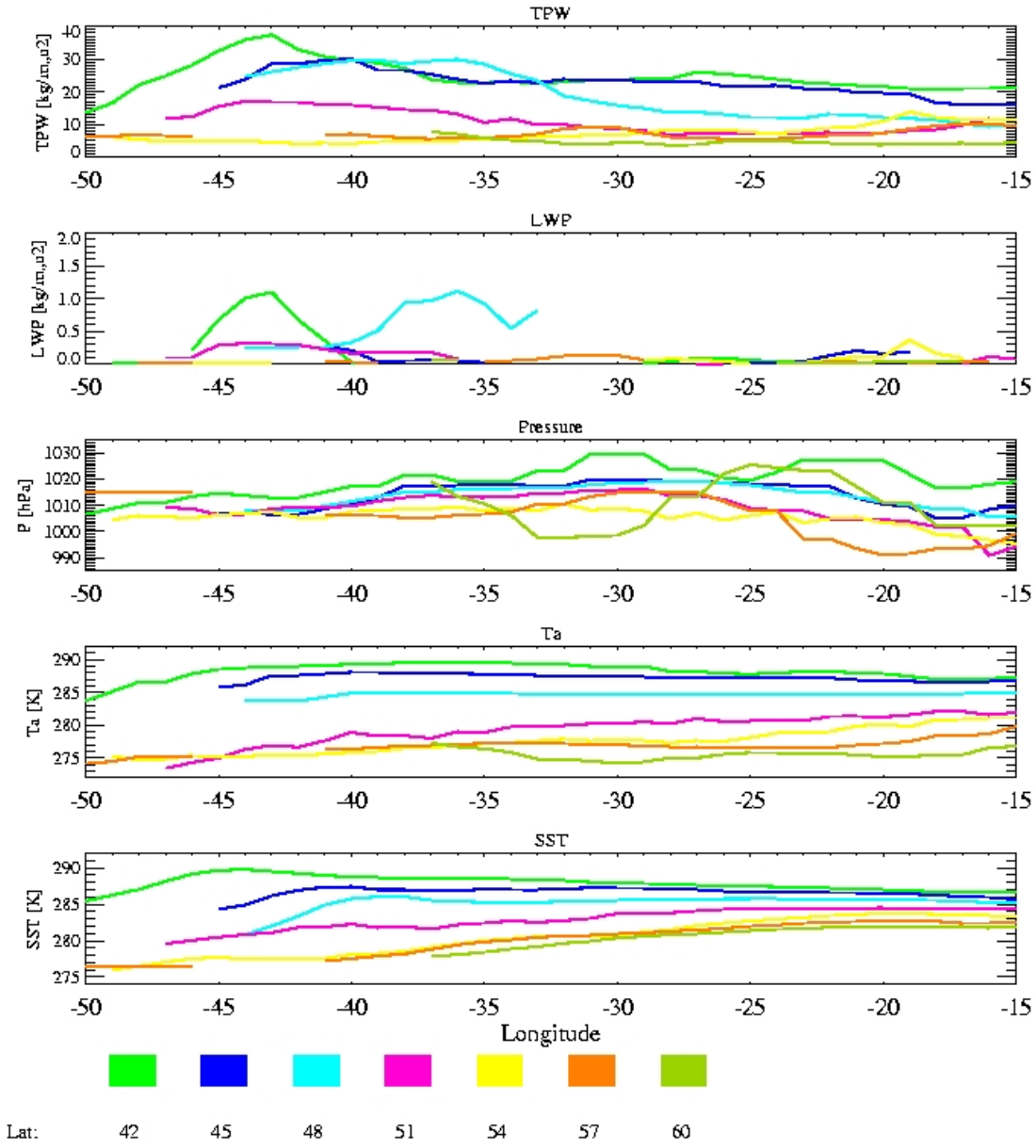

Figure 6.9: *The 1° mean horizontal distribution of TPW, LWP, surface pressure, atmospheric temperature and SST (top to bottom) at different latitudes for the 28th March 2001. The central latitude is colour coded.*

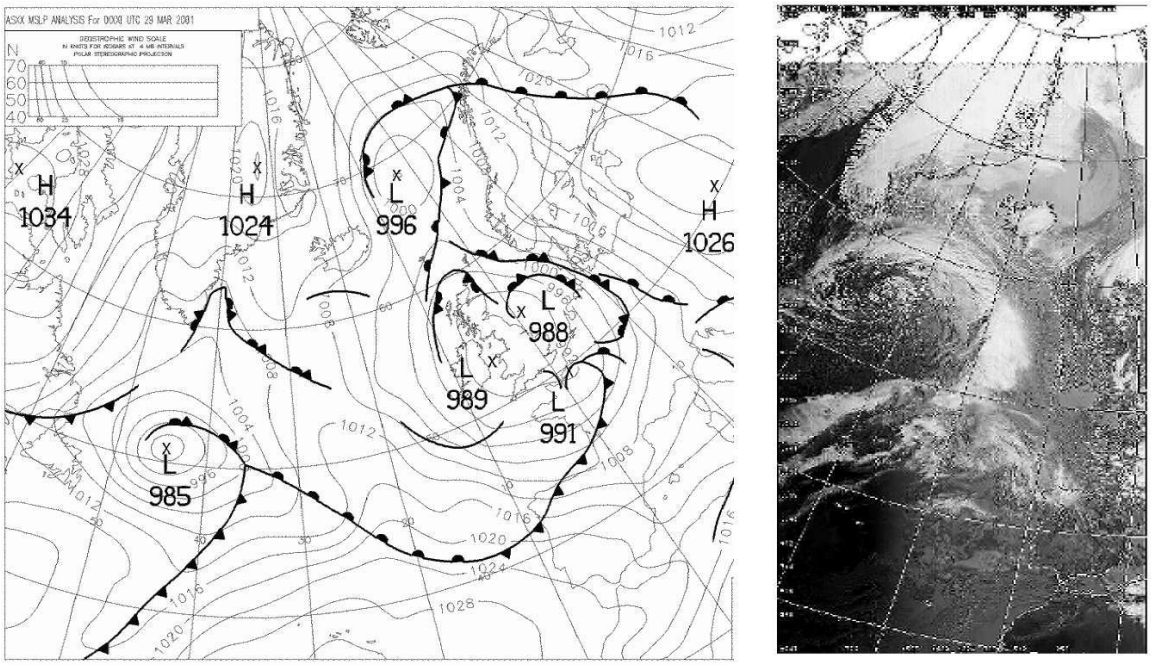

Figure 6.10: *Synoptical situation for the 29th, March 2001. On the left the 0 UTC surface chart of the UK–Metoffice is shown. On the right the NOAA AVHRR channel 3 morning overpass is shown.*

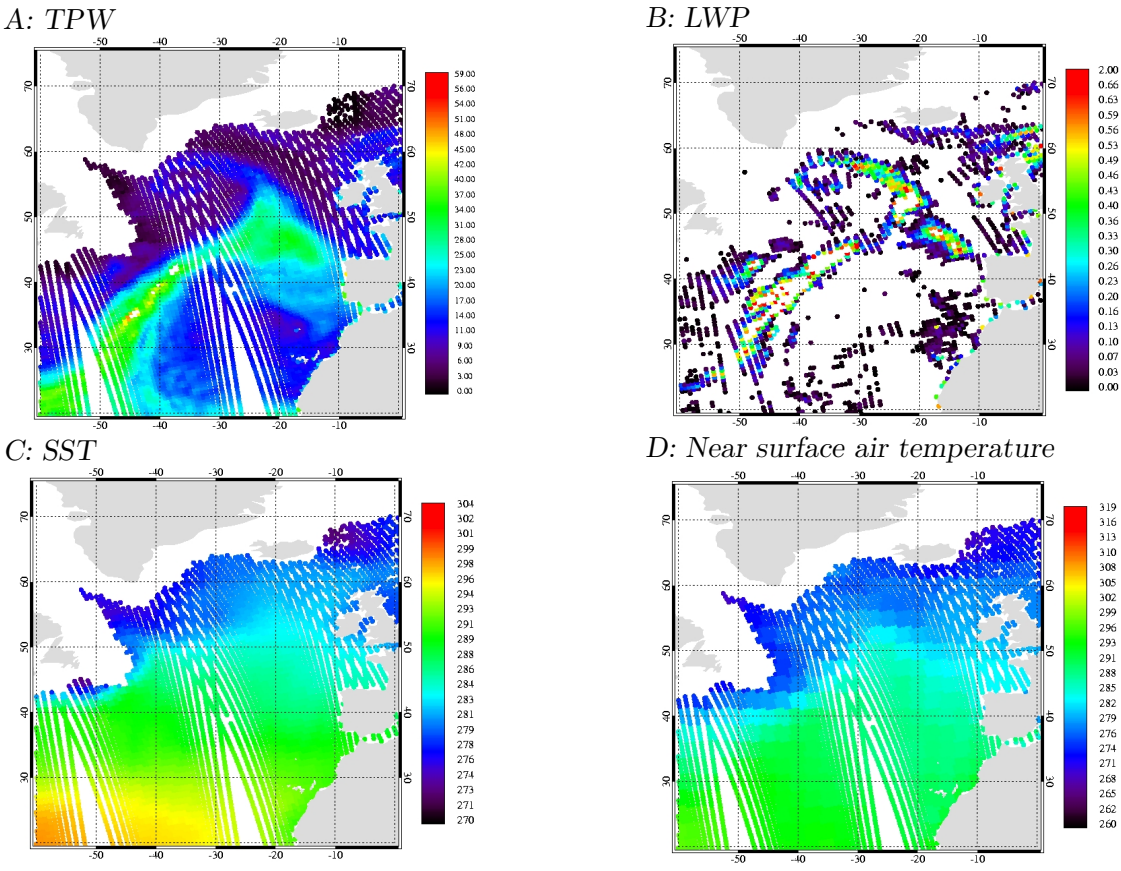

Figure 6.11: *The morning overpasses of the NOAA-16 AMSU instrument.* **A** *gives the retrieved TPW in kg/m*^{2}*.* **B** *shows the LWP in kg/m*^{2}*. Negative values and values larger than 2 kg/m*^{2} *are not included. For the TPW and LWP retrieval surface informations are used. These data are taken from the 2.5° NCEP–NCAR reanalysis.* **C** *shows the SST, and* **D** *the near surface air temperature on AMSU FOV grid.*

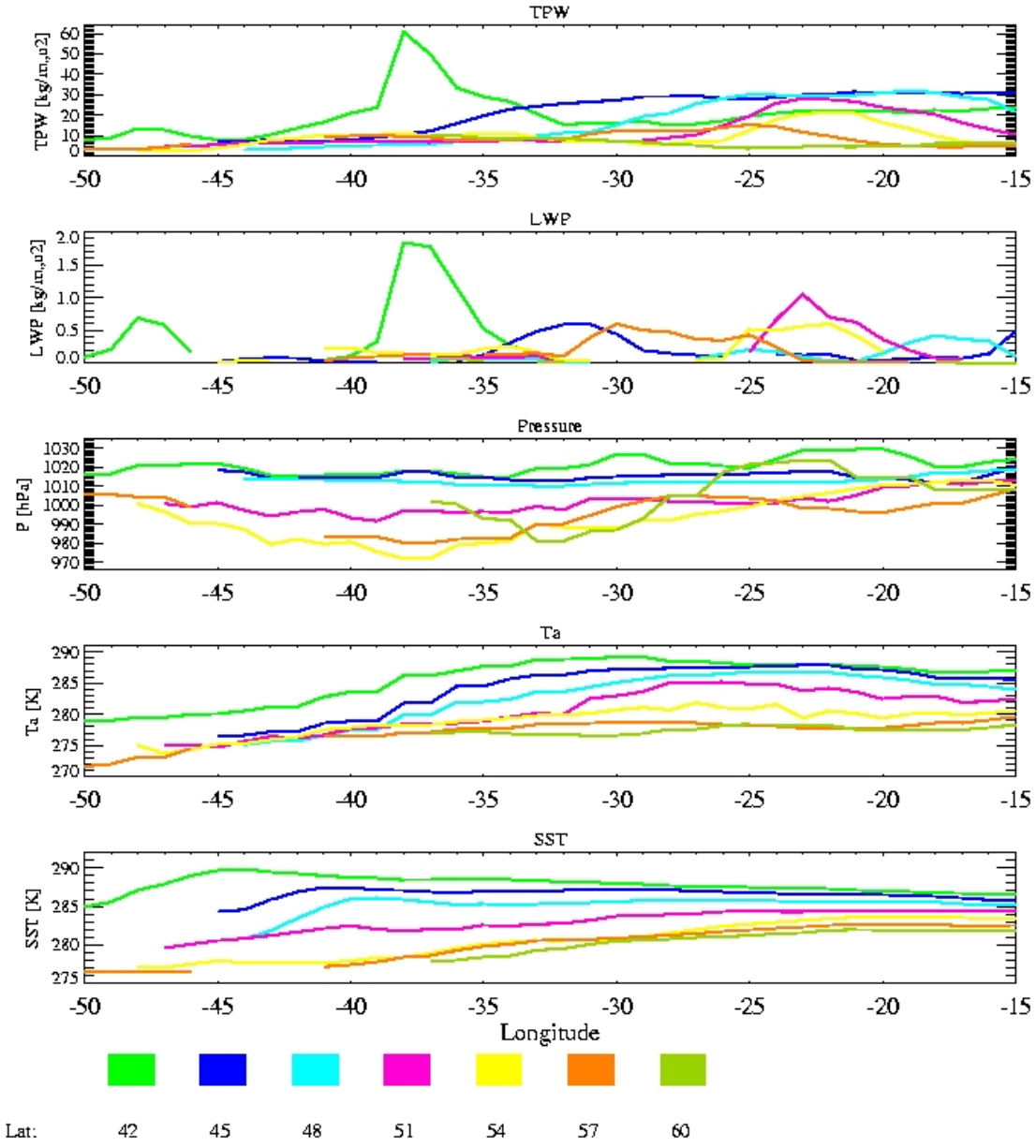

Figure 6.12: *The 1° mean horizontal distribution of TPW, LWP, surface pressure, atmospheric temperature and SST (top to bottom) at different latitudes for the 29th March 2001. The central latitude is colour coded.*

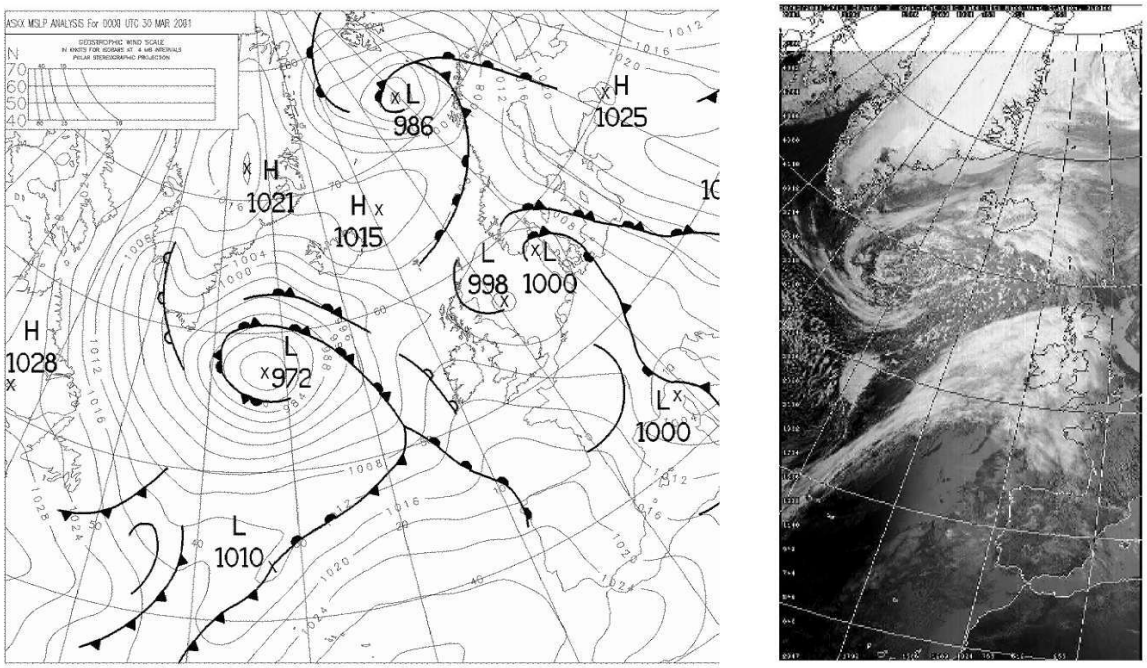

Figure 6.13: *Synoptical situation for the 30th, March 2001. On the left the 0 UTC surface chart of the UK–Metoffice is shown. On the right the NOAA AVHRR channel 3 morning overpass is shown.*

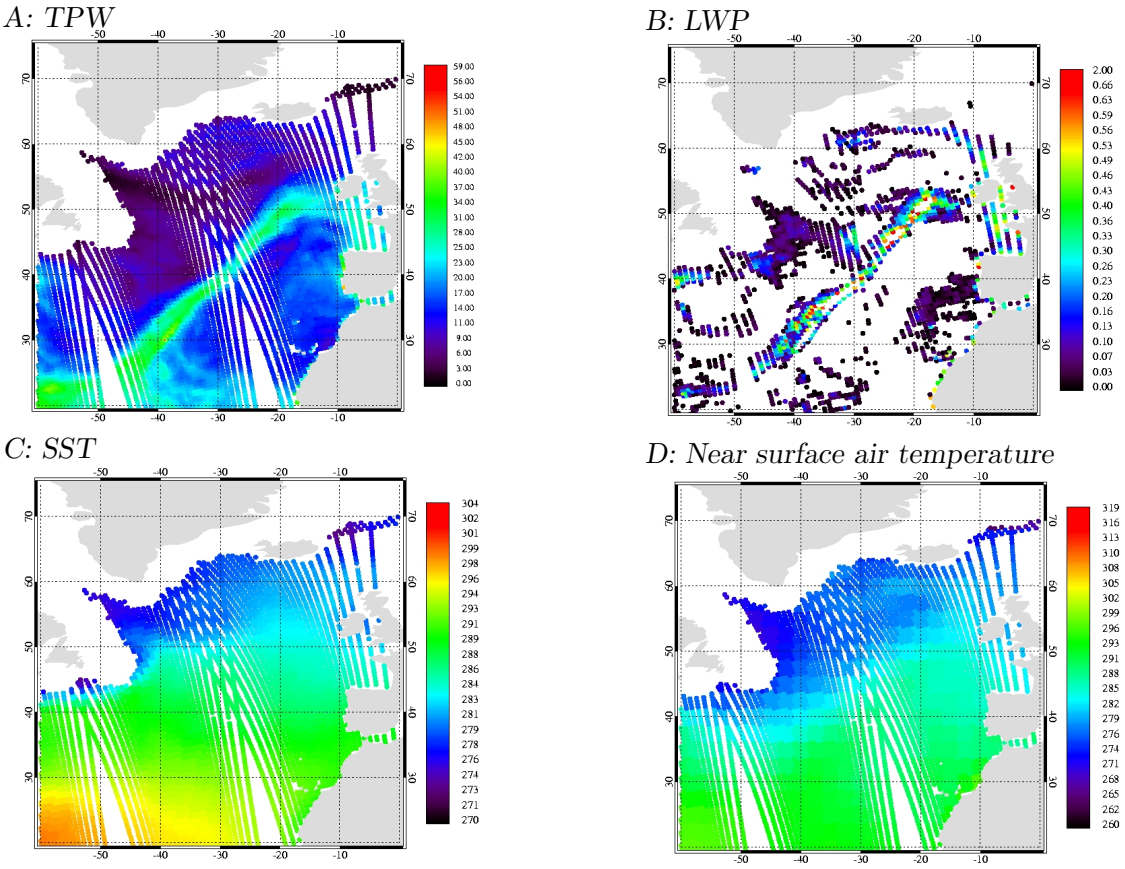

Figure 6.14: *The morning overpasses of the NOAA-16 AMSU instrument.* **A** *gives the retrieved TPW in kg/m*^{2}*.* **B** *shows the LWP in kg/m*^{2}*. Negative values and values larger than 2 kg/m*^{2} *are not included. For the TPW and LWP retrieval surface informations are used. These data are taken from the 2.5° NCEP–NCAR reanalysis.* **C** *shows the SST, and* **D** *the near surface air temperature on AMSU FOV grid.*

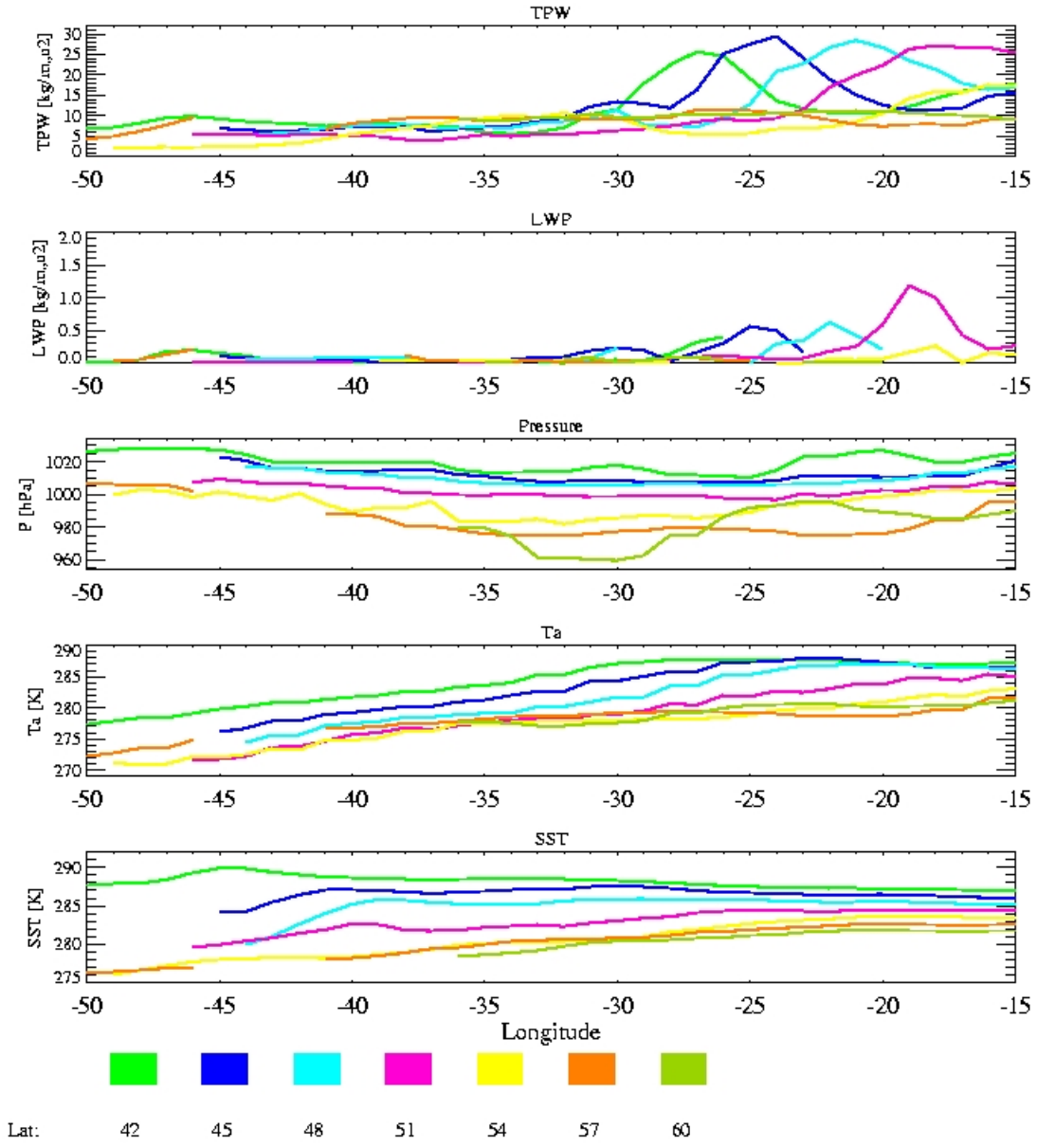

Figure 6.15: *The 1° mean horizontal distribution of TPW, LWP, surface pressure, atmospheric temperature and SST (top to bottom) at different latitudes for the 30th March 2001. The central latitude is colour coded.*

6.3 Concluding Remarks

The TPW is depending on the air temperature. Thus, on first hand we expect the horizontal TPW distribution to follow the air temperature fields. Over the ocean due to evaporation and mixing an increase in the air temperature should follow an increase of absolute humidity and TPW. However, the observed TPW fields show more structure than the temperature fields. Additional structure is found in cloudy areas. Obviously, rising of dry and/or cold air masses as well as water vapour in convective regions locally affects the TPW.

Chapter 7

Spatial TPW as measured from Satellite

Polar orbiting satellites enable global observations of environmental properties. In this study the microwave emission from atmospheric water is measured with AMSU, the advanced microwave sounding unit, onboard the NOAA–16 polar orbiting satellite. The NOAA–16 satellite passes over Europe about noon (12 UTC) in ascending direction and descending orbit at night time (about 2 UTC). The microwave emission is independent of the solar radiation. The diurnal cycle of TPW is neglectable. The ability of the atmosphere to contain water vapour is coupled to the atmospheric temperature which has a diurnal cycle therefore the relative humidity is affected by the time of day but not the absolute humidity. The TPW is defined as the vertical integral of the absolute humidity. Changes in TPW are due to the annual temperature variations and passing of weather regimes like low pressure systems with their different air masses.

For this study the AMSU TPW and LWP algorithm described by Grody et al. (2001) has been applied. For the retrieval the emissions at 23.8 GHz and 31.4 GHz are used. Auxiliary data like sea surface temperature, air temperature and surface wind field are taken from the NCEP/NCAR reanalysis. For microwave retrieval a good knowledge of the emitting surface is important. Therefore most algorithms using this frequencies are operating over the oceans only. Sea ice as emitting surface is also critical in the water vapour and LWP retrieval. Pixels with a sea surface temperature lower than 2 K are not used in this study. Land surfaces in the vicinity of the field of view are increasing the measured radiance. To avoid overestimations of TPW and LWP grid boxes with land inside and boxes with land in the neighbouring boxes are excluded.

The mean LWP shown in this section denotes the mean LWP of non–precipitating clouds. A threshold of 0.5 kg/m^2 is used to eliminate precipitating clouds in the statistical analysis. This value is commonly used. The all–sky TPW is hence except precipitation and precipitating clouds. For field of views with a retrieved LWP of 0. kg/m^2 the pixel is considered

clear–sky. A mean over all pixels in a grid cell is denoted as clear–sky TPW. The spatial size used in this study is a $0.5° \times 0.5°$ latitude $\times$ longitude grid.

7.1 Global TPW Distributions

Figure 7.1 shows the global distribution of all–sky TPW along its seasonal cycle. The tropical regions show largest values. The seasonal drift of the inner tropical convergence zone is clearly visible. Near the continents larger TPW values are connected to warm ocean boundary currents. Lower TPW values are related to the cold ocean currents. The subsidence regions of the Hadley circulation are related to dry atmosphere. These features are present in the clear–sky TPW as well (see figure 7.2). The absolute TPW is lower for clear–sky cases. The monthly mean LWP show some climatological structures, see figure 7.3. The dry subtropic areas are prominent. The ITCZ and the monsoon clouds are found in the mean fields. The mid–latitudes show larger LWP in areas where frontal systems are formed.

To analyse the water vapour in cloudy situations and the difference to the clear–sky case in section 5.3 the ratio of all–sky TPW to clear–sky TPW is defined as measure of the so–called excess water vapour. In figure 7.4 the global distribution of excess water vapour is shown.

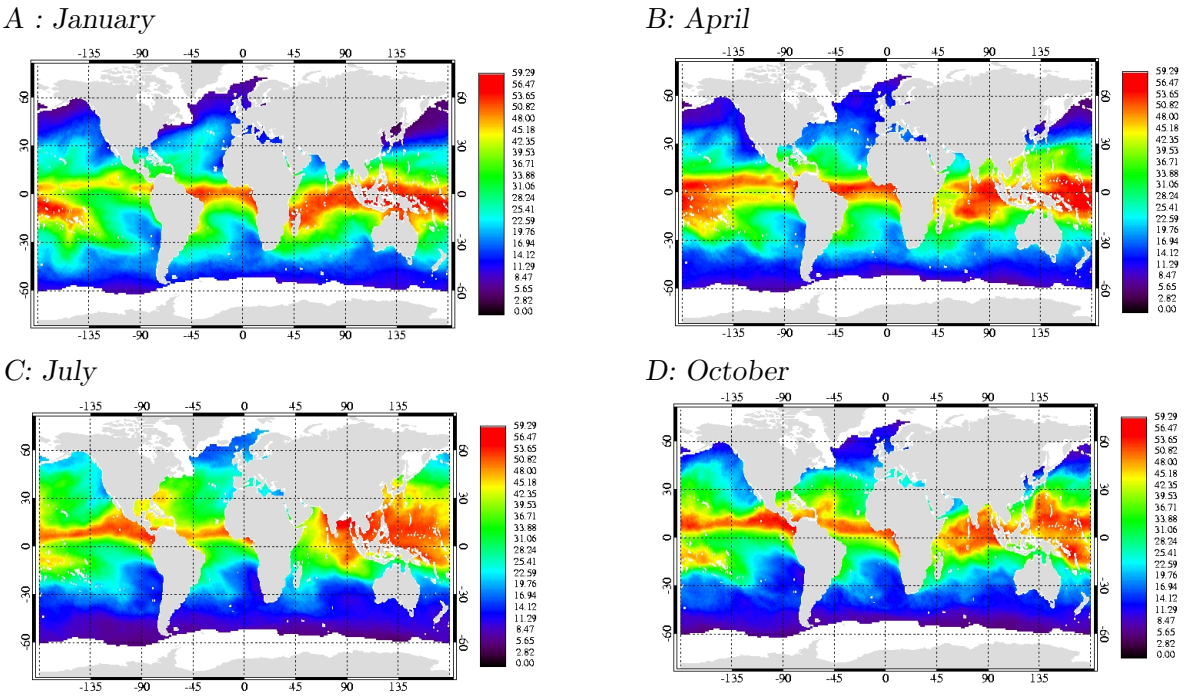

Figure 7.1: *Monthly mean vertical integrated total precipitable water (TPW) in [kg/m^2] derived from AMSU measurements for A January, B April, C July, and D October 2004.*

In the subsidence regions the ratio is smaller than 1 which expresses larger TPW values in the clear–sky case. Here colder air related to changes in the sea surface temperature are related with a drier atmosphere due to changes in the capacity of the atmosphere to hold the water vapour. Mainly this air results from equatorwards winds. Nevertheless, the ratios are slightly smaller than 1, so the difference in TPW is small in these cases. Largest variability and largest ratios are found in the midlatitudes, where the storm tracks are visible in the excess water vapour fields. In January the cold and dry air of the American continent flow over the warm gulf stream and saturates. This is striking in a ratio below 0.85 (15% drier is the all–sky atmosphere compared to the clear–sky). The clear–sky cases are related to a gulf stream parallel flow with warmer but cloud free air. The same feature are found in the all–sky minus clear–sky TPW fields in figure 7.5.

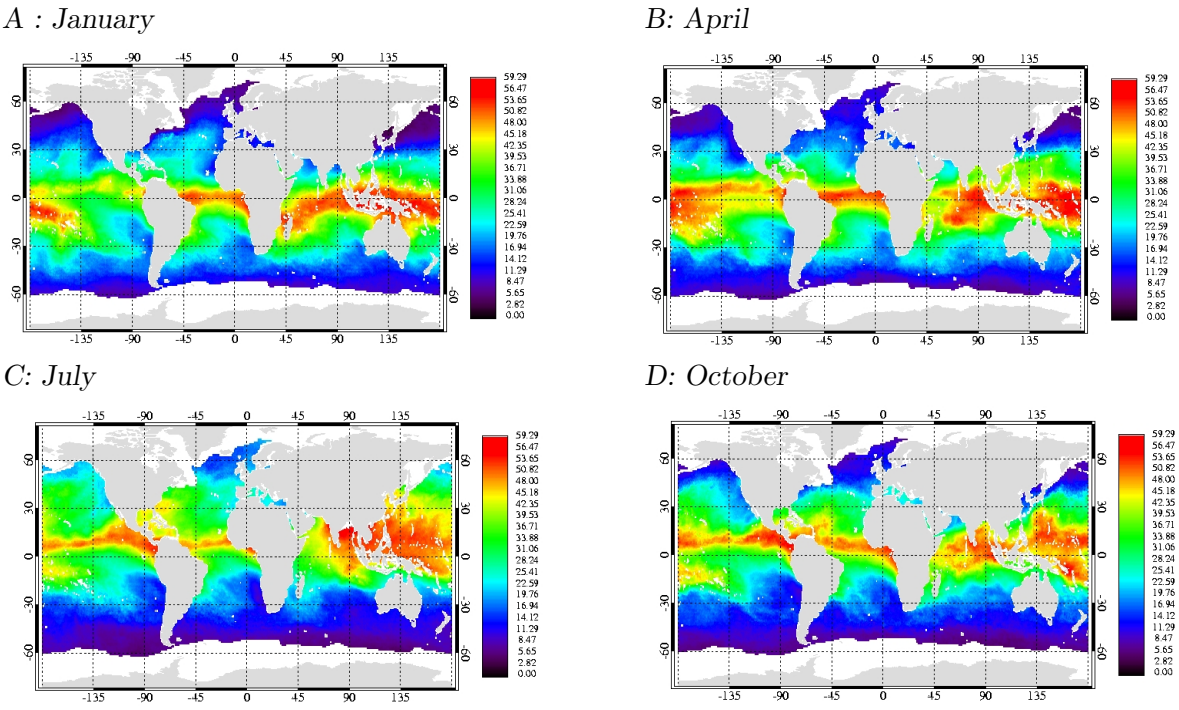

Figure 7.2: *Monthly mean vertical integrated total precipitable water (TPW) in [kg/m^2] for clear–sky situations derived from AMSU measurements for A January, B April, C July, and D October 2004.*

A : January

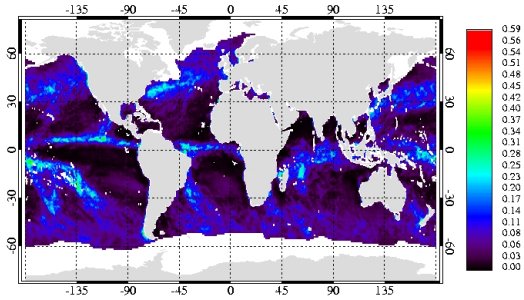

B: April

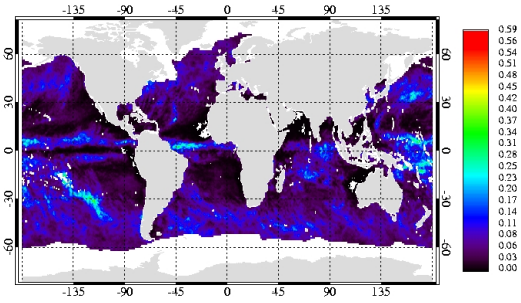

C: July

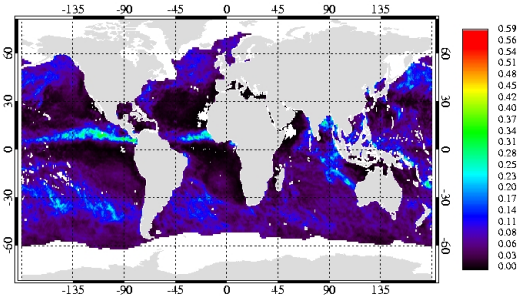

D: October

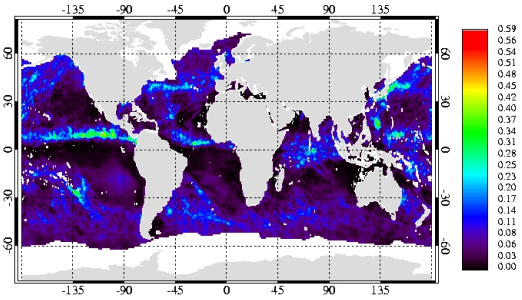

Figure 7.3: *Monthly mean vertical integrated liquid water (LWP) in [kg/m^2] for non–precipitating clouds derived from AMSU measurements for A January, B April, C July, and D October 2004.*

A : January

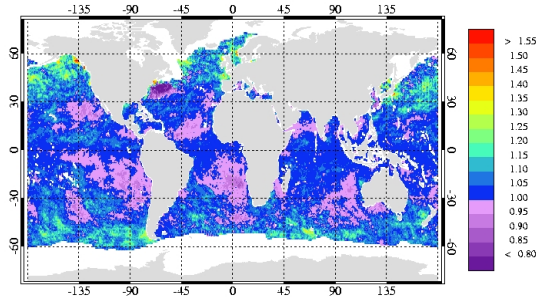

B: April

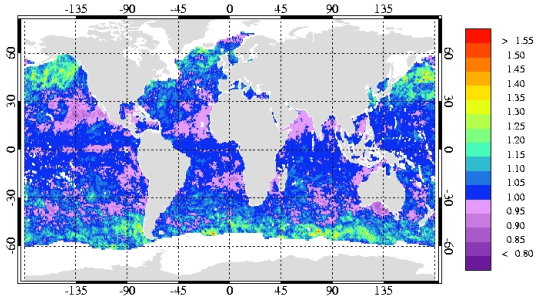

C: July

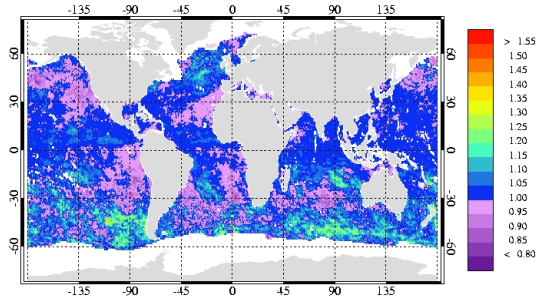

D: October

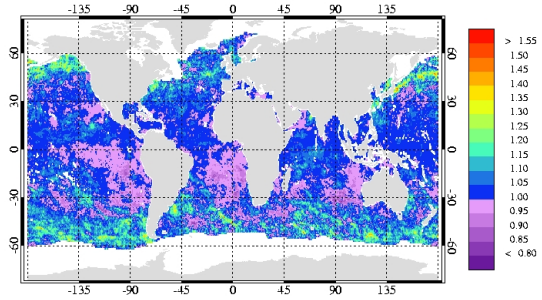

Figure 7.4: *Monthly mean excess water vapour (all–sky TPW divided by clear–sky TPW) for non–precipitating clouds derived from AMSU measurements for A January, B April, C July, and D October 2004.*

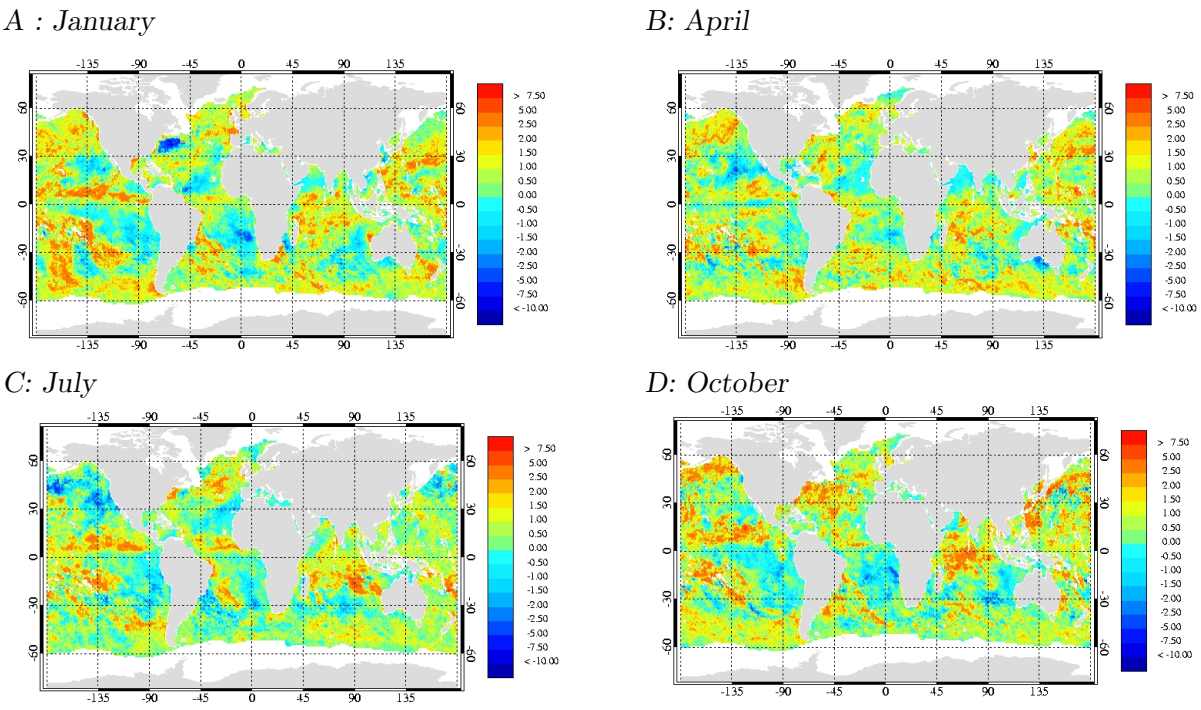

Figure 7.5: *Monthly mean all–sky TPW minus clear–sky TPW In [kg/m^2] for non–precipitating clouds derived from AMSU measurements for A January, B April, C July, and D October 2004.*

7.2 Excess Water Vapour over the North Atlantic

A : January

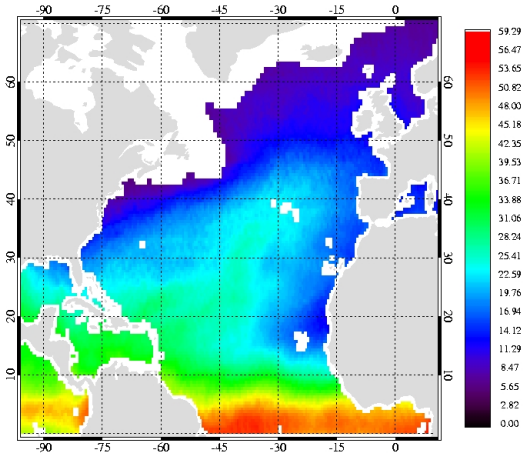

B: April

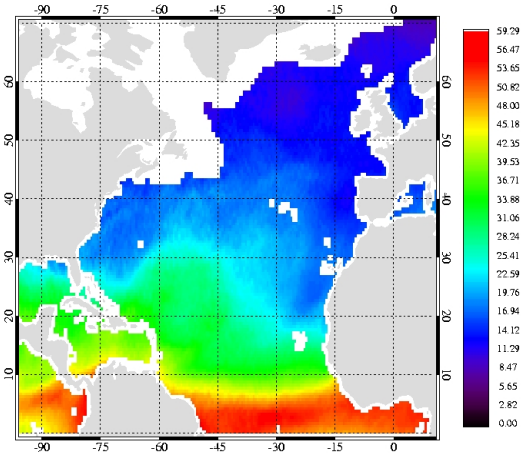

C: July

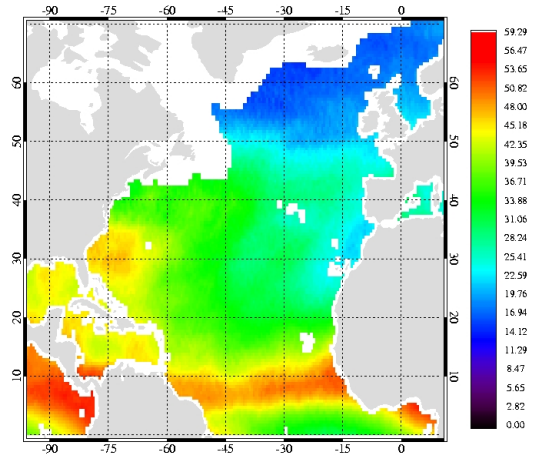

D: October

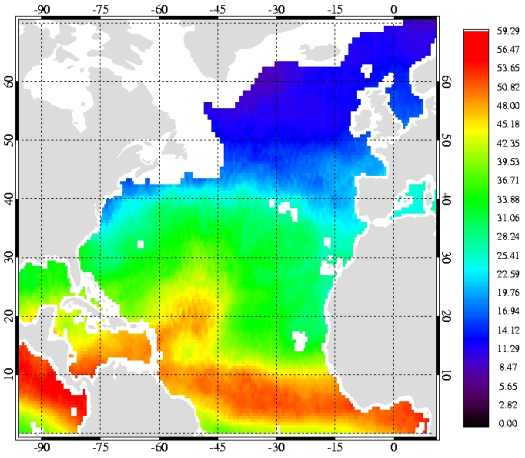

Figure 7.6: *Monthly mean vertical integrated total precipitable water (TPW) in [kg/m^2] derived from AMSU measurements for A January, B April, C July, and D October 2004.*

For a deeper description of the excess water vapour at its dependencies the north Atlantic is investigated. The other ocean basins are described in appendix **??**.
The all–sky TPW is shown in figure 7.6. The seasonal cycle of the TPW is clearly visible. The tropics with the ITCZ moves north during the northern hemispheric summer with maximum northern extend in October. Similar behaviour is shown in the clear–sky TPW in figure 7.7. The cloud liquid water fields (see figure 7.3) show largest values in the ITCZ and in the mid–latitudes, related to the frontal systems.

The excess water vapour is given in figure 7.8. In the mid latitudes the ratio of all–sky to

clear–sky TPW is positive, and the largest values are found in the cyclogenetic regions (e.g. south east of Greenland). The variability in this region is high. Values below 1, which characterises situations where cloudy atmospheres are related to less water vapour than cloud free situations. The dominant cause for this is a change in air mass and thus an expression of the coupling of humidity and air temperature. The cloud free atmosphere is related to warm air, which can contain more water vapour than a colder saturated air mass. This situations are found in the subtropics. In absolute numbers of excess water vapour the values are close to 1. In January a field with values below 0.9 is found close to New Foundland. Here two weather situations are present in winter time. A offshore cold dry air from the North American continent blows over the warm gulf stream and saturates at low absolute humidity levels. In contrast warm air flows along the gulf stream with larger absolute humidity values, but

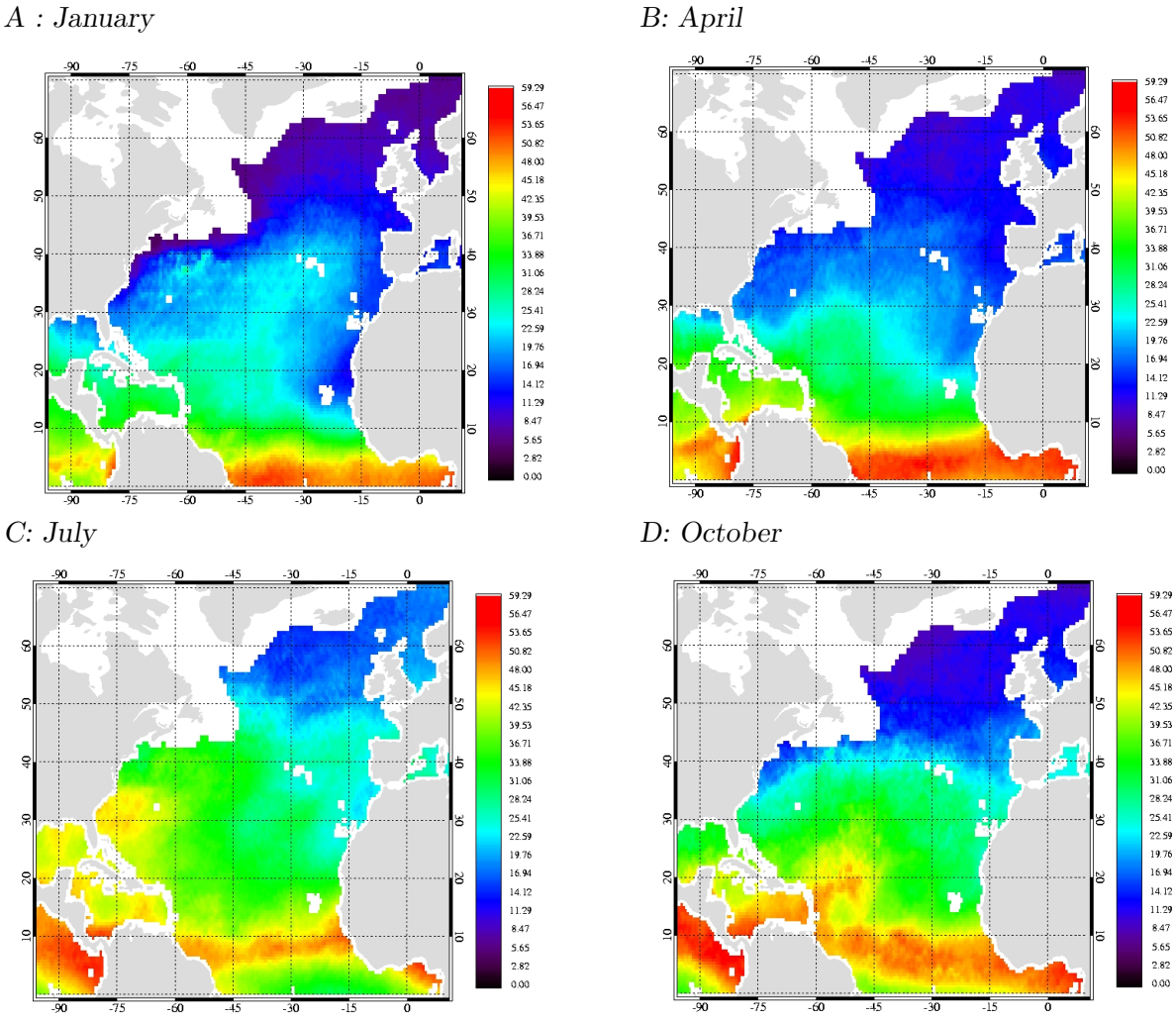

Figure 7.7: *Monthly mean vertical integrated total precipitable water (TPW) in [kg/m^2] for clear–sky situations derived from AMSU measurements for A January, B April, C July, and D October 2004.*

saturation does not occur. In summer the differences in air masses are smaller, therefore the ratios are closer to 1.

In figure 7.9 the relation of clear–sky towards the all–sky TPW is given for one year and in figure 7.10 for four years. The years 2001 to 2005 are used for this study. For the year 2002 the LWP and TPW retrieval gives continously too low values most likely due to calibration errors of the AMSU. In the Tropics this difference compared to the other years is about 20 kg/m^2. In the auxiliary data and the calibration procedure no explanation is found for this behaviour. For this reason the data of 2002 are excluded from this study.

A : January

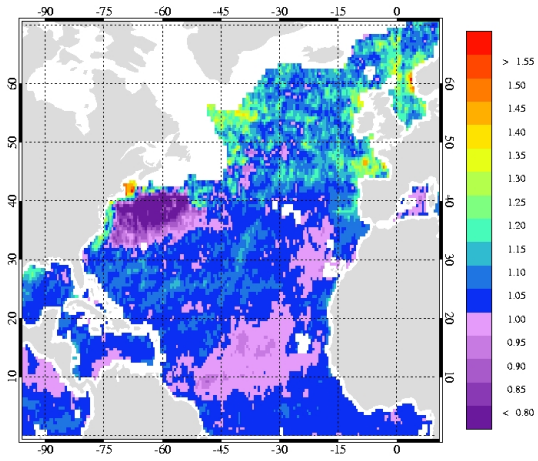

B: April

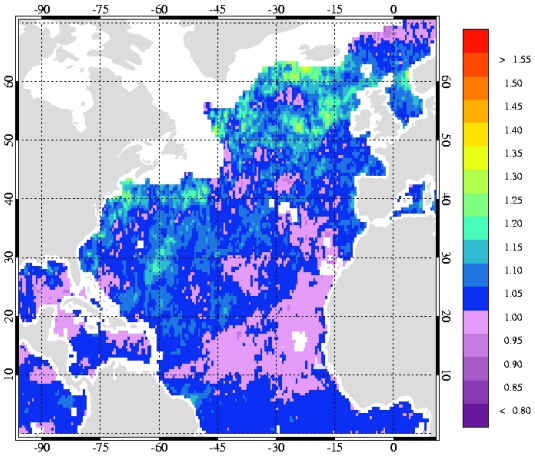

C: July

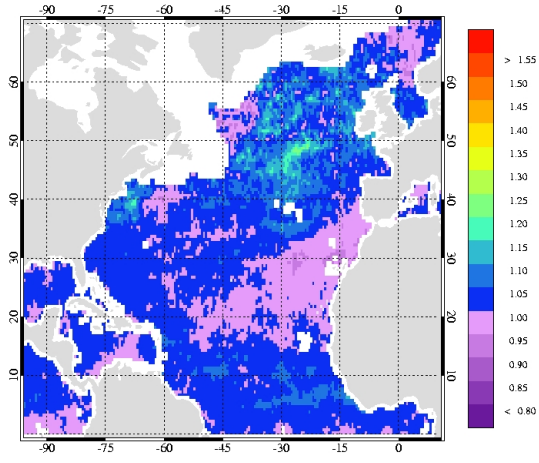

D: October

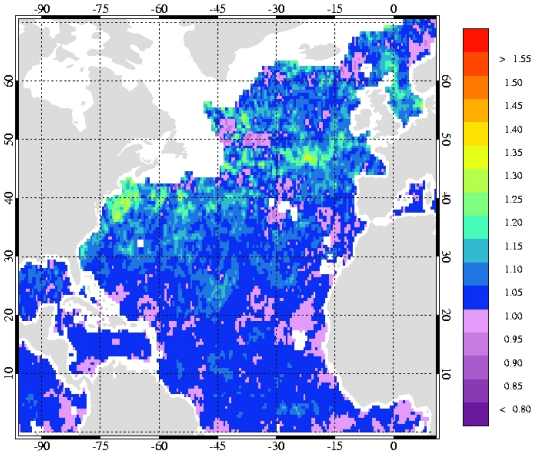

Figure 7.8: *Monthly mean excess water vapour (all–sky TPW divided by the clear–sky TPW) for non–precipitating clouds derived from AMSU measurements for A January, B April, C July, and D October 2004.*

The relation of clear–sky TPW towards the all–sky TPW as shown in figure 7.9 and figure 7.10 shows a small positive bias. The temperature dependence of absolute humidity is clearly visible in the colour coding by latitude. The tropics are found in the large TPW area whereas the mid– to high–latitude mark the lower end. The ratio are stronger scattered for small clear–sky TPW. For larger clear–sky TPW the difference between cloud and cloud–free TPW is small, which might be explained by nearly saturated atmospheres. The frequency distribution of excess water vapour shows for most of the cases the ratio is above 1. Less then 10 % of the data points are smaller than one. The function describing the clear–sky TPW towards the excess water vapour shows an exponential decrease towards larger clear–sky TPW.

In figure 7.11 (*A*) the variation of the retrieved parameterisations of the excess water vapour according to the clear–sky TPW is shown for the year 2004 and in 7.12 (*A*) for the years 2001–2005 (except 2002). For low clear–sky TPW the ratio varies between 1.1 and 1.4 depending on the time of the year. Largest ratios and steepest increase of the fit function are found in summer and autumn. This is explained by the difference in air masses forced through a grid point by low pressure systems. Looking at the four–years mean the characteristics of the functions are similar to that for a single year. A power–law function (see equation 7.1) is used to express the results. In table 7.1 the coefficients for the proposed relation are given. The ratio can also be expressed in terms of kg/m^2. The fit functions shown in the figures 7.11 (*B*) and 7.12 (**B**). For a monthly mean clear–sky TPW of 10 kg/m^2 the underestimation towards an all–sky TPW is about 2 kg/m^2 for the summer month.

A : Excess water vapour depending on Latitude

B: Excess water vapour frequency distribution

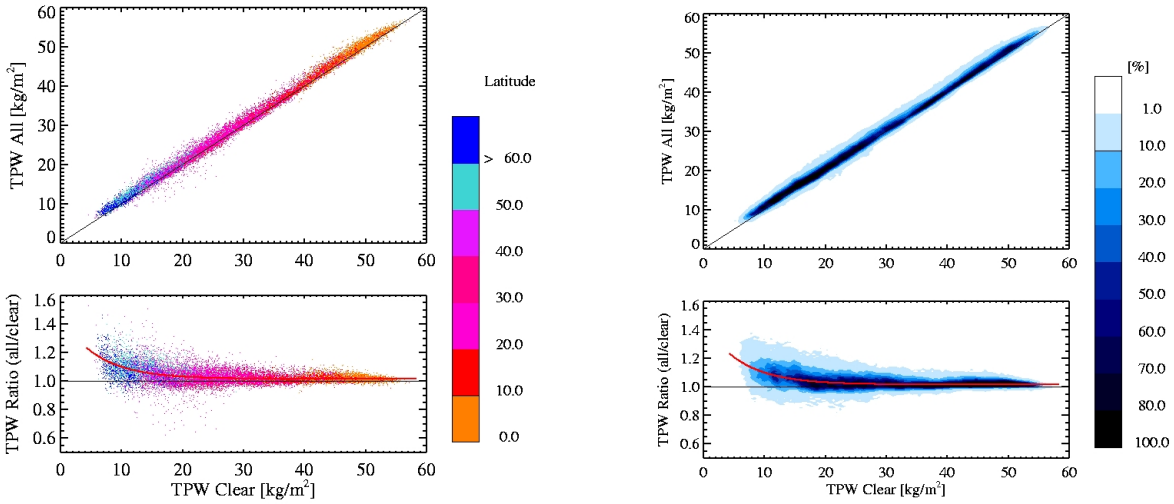

Figure 7.9: *Relation of clear–sky TPW towards the all–sky TPW (upper panel) and towards the ratio of all–sky TPW and clear–sky TPW. The TPW is given in [kg/m^2]. Data are taken from the year 2004. A: Colours give the latitude range. B: Frequency distribution of the data points in figute A.*

$$Y \;=\; a_0\, a_1^X \;+\; a_2 \tag{7.1}$$

The zonal relation of the all to clear TPW ratio is shown in figure 7.13. Both the diagrams for one and for all years show an increase towards high latitudes. In the mid–latitudes several excess water vapour values below 0.8 are observed mainly in winter time. On zonal average the excess water vapour is larger than 1. The maximum underestimation related to clear–sky TPW is about 20% corresponding to an excess water vapour of 1.2.

The frequency distributions of the monthly mean excess water vapour over the North Atlantic (see figure 7.14) and globally (see figure 7.15) show a peak close to 1. The frequency distribution for all years are given in figure 7.16. The mean and median are larger than 1 and are varying throughout the year with largest values in autumn. The mean and median are larger for the global distributions. The statistical parameters are given in table 7.2.

The difference in all–sky to clear–sky TPW is largest in the mid– and high–latitudes. Due to the temperature humidity coupling the excess water vapour therefore is largest when the clear–sky TPW is related to cold dry atmospheres. Here the excess water vapour is about

A : Excess water vapour depending on Latitude

B: Excess water vapour frequency distribution

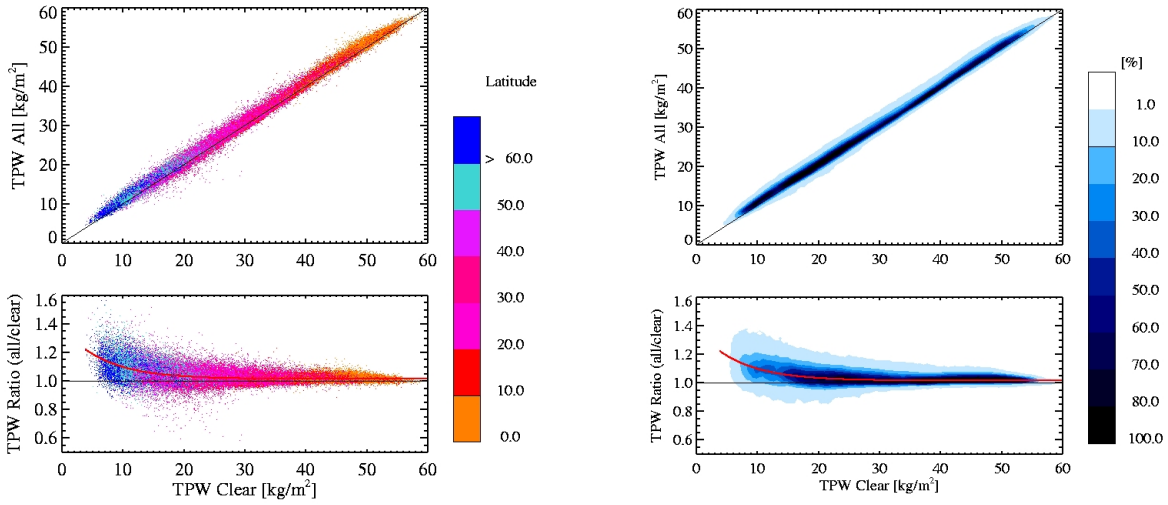

Figure 7.10: *Relation of clear–sky TPW towards the all–sky TPW (upper panel) and towards the ratio of all–sky TPW and clear–sky TPW. The TPW is given in [kg/m^2]. Data are taken from February 2001 to October 2005 (except 2002). A: Colours give the latitude range. B: Frequency distribution of the data points in figute A.*

20%, in absolute numbers about 1–2 kg/m^2. The excess water vapour decreases with increasing clear–sky TPW values but still 1% underestimation occurs for the tropics. The frequency distribution for global excess water vapour gives a mean underestimation in TPW of 2.6%.

7.3 Concluding remarks

The AMSU retrieval of TPW for non–precipitating clouds over four years of data are used to derive monthly mean excess water vapour. For the ocean areas a power–law function describes the relation of the excess water vapour on the clear–sky TPW. Largest all–to–clear TPW ratios are observed in the mid– to high–latitudes. Here the underestimation due to neglecting clouds in TPW climatologies is about 20% (1-2 kg/m^2.). The functional behaviour is established for monthly and seasonal means for individual years. This behaviour does not change significantly when multiyear averages are used. Thus, we conclude that it is feasible to perform an all–sky correction of TPW based on clear–sky measurements.

A: Excess water vapour

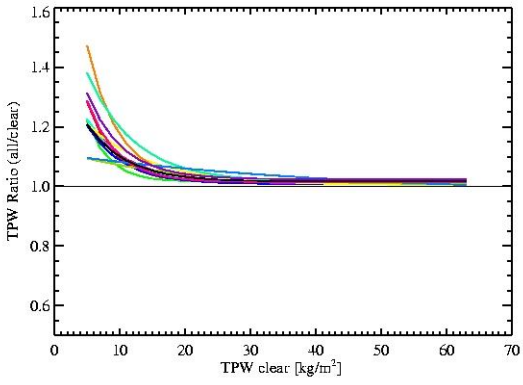

B: underestimation

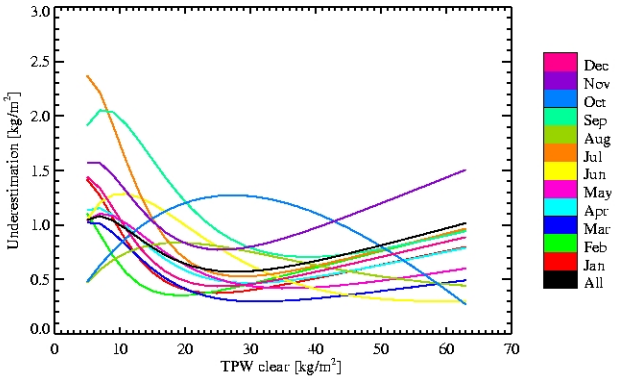

Figure 7.11: *A* Excess water vapour depending on the clear–sky TPW for the year 2004. *B* Clear–sky water vapour bias as derived from the excess water vapour. Colours denote the month. The underestimation is given in relation to the clear–sky water vapour path used in a climatology.

A: Excess water vapour *B: underestimation*

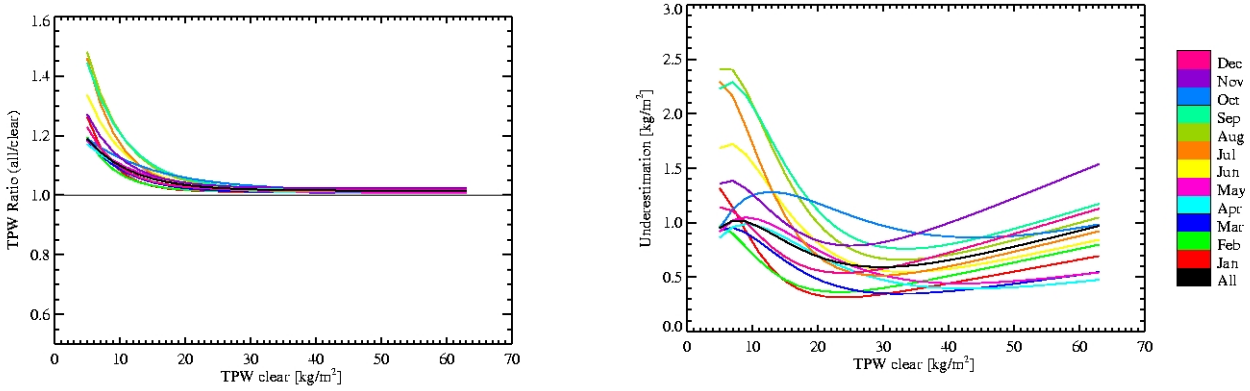

Figure 7.12: *A* Excess water vapour depending on the clear–sky TPW for the years 2001–2005 (except 2002). *B* Clear–sky water vapour bias as derived from the excess water vapour. Colours denote the month. The underestimation is given in relation to the clear–sky water vapour path used in a climatology.

A: 2004 *C: 2001–2005*

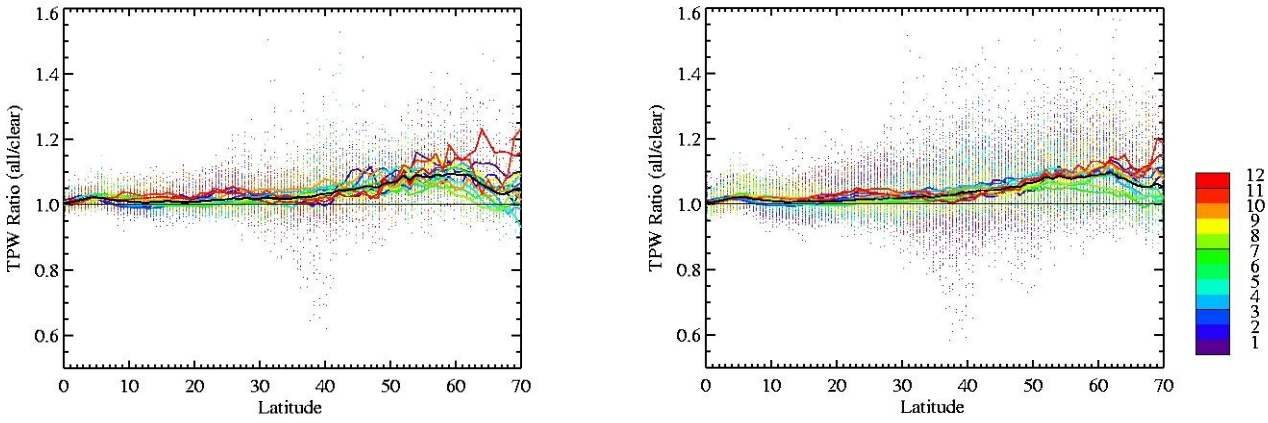

Figure 7.13: *Zonal distribution of the ratio (all–sky TPW by clear–sky TPW). Colours denote the month. A: only 2004 data, and B: data are taken from February 2001 to October 2005 (except 2002).*

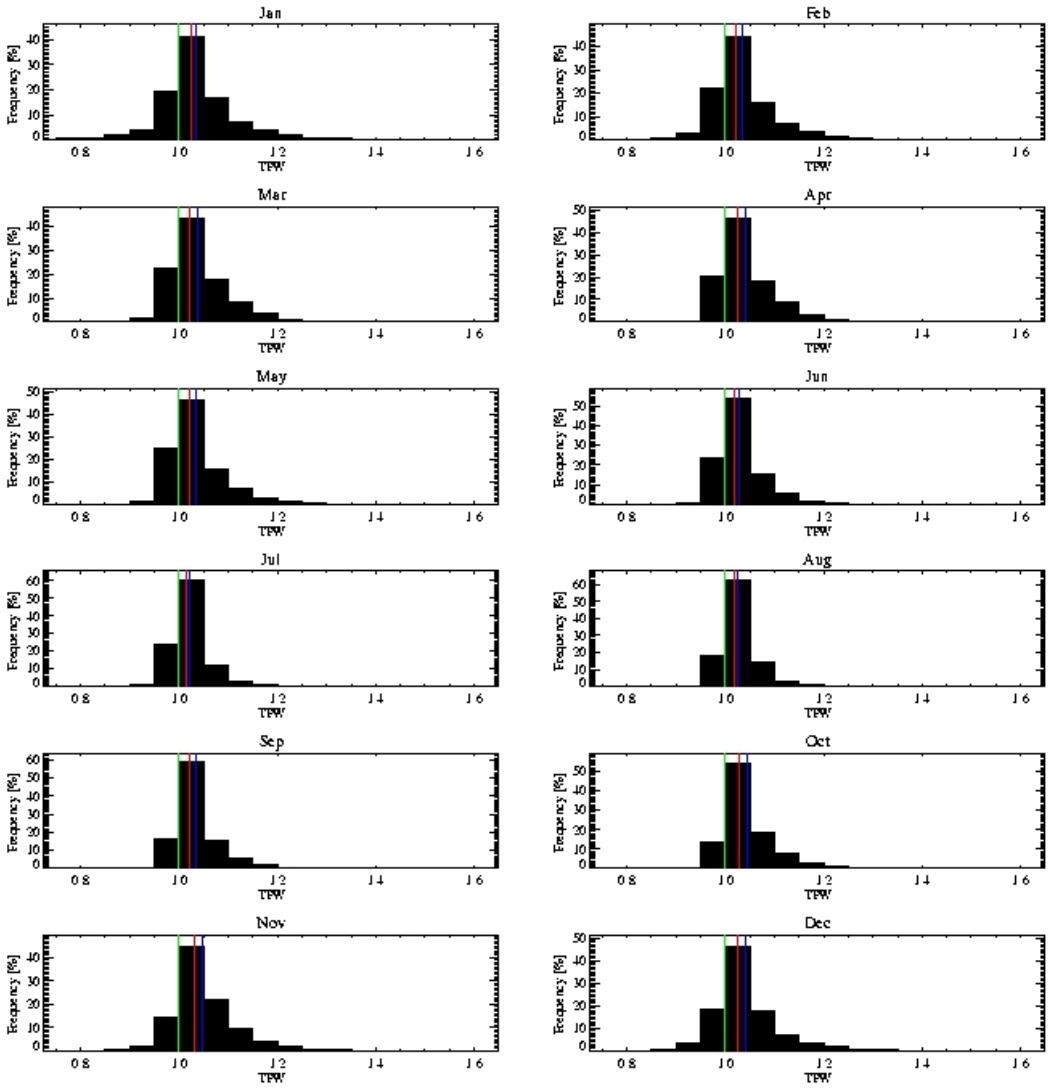

Figure 7.14: *Frequency distribution of the excess water vapour of each month for the North Atlantic for the years 2001-2005 (except 2002). The green line gives the excess water vapour of 1. In red the median and in blue the mean value of the distribution is marked.*

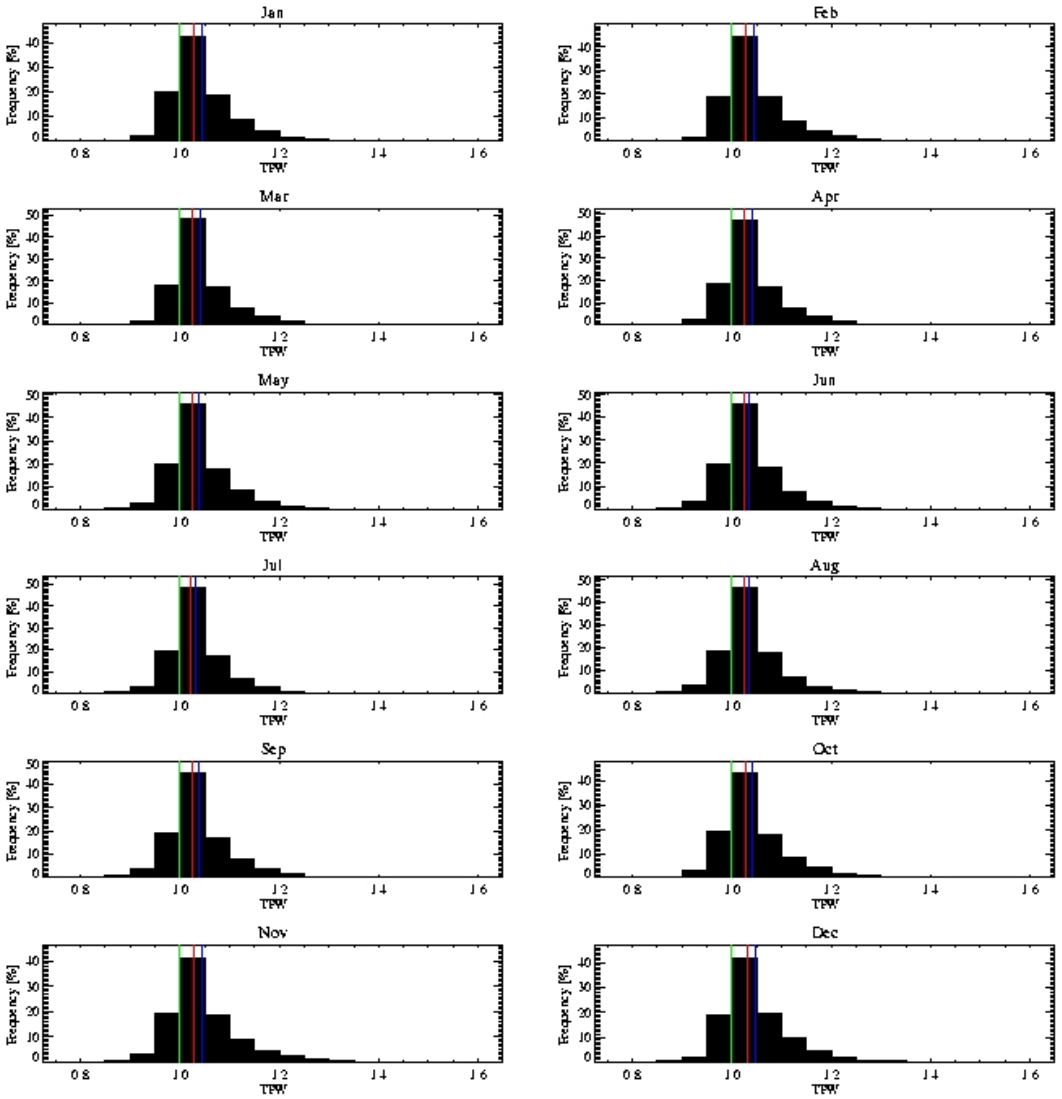

Figure 7.15: *Global frequency distribution of the excess water vapour of each month for the years 2001-2005 (except 2002). The green line gives the excess water vapour of 1. In red the median and in blue the mean value of the distribution is marked.*

A: North Atlantic *B: Global*

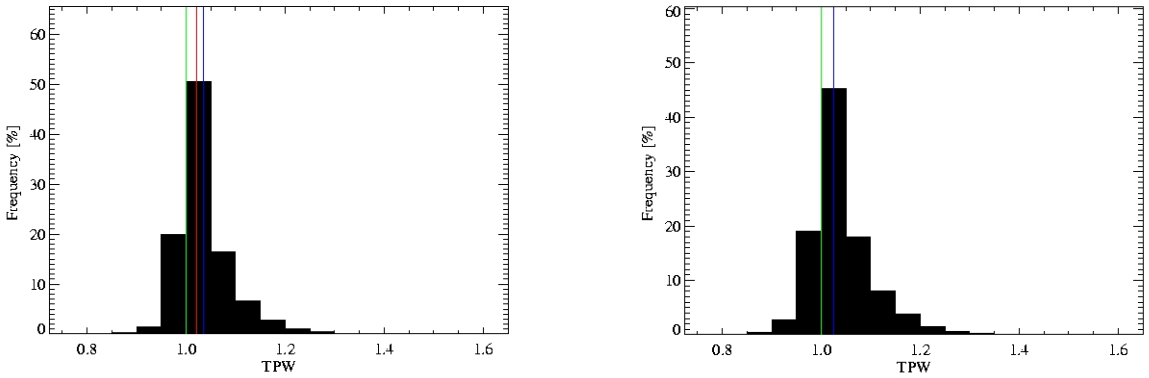

Figure 7.16: *Frequency distribution of the excess water vapour for the North Atlantic (A) and global (B) for the years 2001-2005 (except 2002). The green line gives the excess water vapour of 1. In red the median and in blue the mean value of the distribution is marked.*

Month	A_0	A_1	A_2
North Atlantic			
Jan	0.896	0.776	1.011
Feb	0.564	0.798	1.013
Mar	0.399	0.850	1.009
Apr	0.298	0.888	1.007
May	0.318	0.887	1.008
Jun	0.737	0.848	1.013
Jul	1.249	0.813	1.015
Aug	1.121	0.838	1.017
Sep	0.965	0.849	1.019
Oct	0.277	0.912	1.015
Nov	0.599	0.838	1.024
Dec	0.578	0.817	1.018
All	0.366	0.863	1.015

Table 7.1: *The parameters of the function expressing the ratio vs clear–sky TPW using all years.*

Year	N	N (1)	mean	median	Standart Dev.
North Atlantic					
Year	686087	1017	1.035	1.022	0.0575
Jan	59658	313	1.036	1.024	0.0831
Feb	59660	127	1.036	1.021	0.0678
Mar	59659	61	1.039	1.023	0.0599
Apr	59660	78	1.040	1.024	0.0548
May	59660	205	1.034	1.020	0.0551
Jun	59660	44	1.029	1.018	0.0442
Jul	59660	12	1.021	1.014	0.0345
Aug	59660	34	1.026	1.018	0.0358
Sep	59660	4	1.036	1.023	0.0478
Oct	59660	12	1.044	1.029	0.0549
Nov	44745	72	1.047	1.033	0.0663
Dec	44745	55	1.040	1.025	0.0669
Global					
Year	9435516	6371	1.026	1.026	0.0626
Jan	820477	1611	1.044	1.028	0.0686
Feb	820480	317	1.044	1.029	0.0628
Mar	820479	148	1.041	1.026	0.0604
Apr	820480	196	1.041	1.026	0.0617
May	820480	467	1.039	1.026	0.0596
Jun	820480	381	1.036	1.024	0.0599
Jul	820480	1063	1.032	1.022	0.0552
Aug	820480	1349	1.036	1.024	0.0612
Sep	820480	163	1.038	1.024	0.0648
Oct	820480	189	1.041	1.027	0.0646
Nov	615360	295	1.045	1.029	0.0697
Dec	615360	192	1.047	1.031	0.0659

Table 7.2: *Statistical parameters discribing the frequency distributions of the excess water vapour.*

Chapter 8

Summary and conclusions

In this report the relation of the water vapour in clear and all–sky situations is investigated using radiosonde humidity profiles and satellite based TPW. Previous work shows a lower TPW in clear cases compared to cloudy cases. The goal of this study is to examine wether there is a systematic difference between both situations and wether it can be expressed in terms of climatological ratios of all– to clear–sky TPW.
From radiosonde humidity profiles with colocated cloud observations it is proven that the vertically integrated absolute humidity is increasing with cloud cover. Compared to clear–sky TPW there is about 10–20% more water in cloudy atmospheres.

The examination of Lindenberg TPW in both clear– and all–sky situations shows a strong coupling of the monthly mean clear– to the all–sky values. The ratio of all– to clear–sky TPW, denoted as excess water vapour, is large in cases of small mean TPW, which occurs during winter time only. Exploring the causes for the variability in excess water vapour for several stations is beyond the scope of this study. The stations have different numbers of observations of clear and cloudy cases. For low cloud cover the excess water vapour is not effected. Furthermore, small uncertainties in the definition of clear–sky situations are not effecting the retrieved excess water vapour. These results where based on cloud detection by the synoptical observations. However, for broken cloudiness the radiosonde not necessarily passes a cloud during the ascent. Therefore a threshold in the minimum dewpoint difference in the profile is used as an additional cloud detection criteria. With this the different stations have the same data amount and a sufficient number of cases for the calculation of monthly mean TPW. For clear–sky TPWs larger than 10 kg/m^2 the excess water vapour is nearly constant between 1.1 to 1.3. Towards lower clear–sky TPW the increase differs from station to station. Maximum excess water vapour values of 1.5 are found for clear–sky TPW of 5 kg/m^2. These clear–sky TPW situations are rare and the regression is based on few data only.
For the European region a function for the dependency of clear– to all–sky TPW is obtained. The relation depends on the season and on surface pressure. In high pressure situations the relation of excess water vapour is not pronounced.
The results have been discussed in terms of statistical sampling errors. Mean TPW values

are strongly depending on the number of cases included. The significance of these results is strongly depending on the number of input data. Specific weather situations bias the mean, especially for clear–sky TPW.

Regarding mid–latitude low pressure systems it is shown that the TPW fields depend strongly on the SST and air temperature fields. However, the structures found in the TPW field are not only explainable by the temperature variability. Cloud fields related to frontal systems are clearly visible in the daily TPW fields. On monthly means the TPW pattern resemble more those of the temperature field.

The monthly mean excess water vapour over the oceans is examined with AMSU measurements. For non–precipitating clouds a functional relation of the excess water vapour depending on the clear–sky TPW similar to the surface based analysis is found. For the different oceans only small variations occur. The excess water vapour is about 1% in the tropics and increases polewards. The influence of clouds on the TPW is largest in the mid–to high latitudes. Here the underestimation due to neglecting clouds in TPW climatologies is about 20% (1-2 kg/m^2). The functional behaviour is established for monthly and seasonal means for individual years. This behaviour does not change significantly when multiyear averages are used. Thus, we conclude that it is feasible to perform an all–sky correction of TPW based on clear–sky measurements.

We recall that the present study is limited to non–precipitating clouds with LWP lower than 0.5 kg/m^2. Thus, taking all clouds into account may lead to different relations between clear– and cloudy–sky TPW. This is indicated by slight difference between satellite and radiosonde excess water vapour.

Bibliography

Arabey, E., 1975: Radiosonde data as means for revealing cloud layers. *Meteor. Gidrol.*, **6**, 32–37.

Bates, J. and D. Jackson, 2001: Trends in upper–tropospheric humidity. *Geophysical Research Letters*, **28**(9), 1695–1698.

Bühler, S., A. von Engeln, E. Brocard, V. John, T. Kuhn, and P. Erikson, 2004c: The impact of humidity and temperature variations on clear–sky outgoing longwave radiation. *Journal of Geophysical Research*. Submited.

Crewell, S., M. Drusch, v. Meijgaard, and v. Lammeren, 2002: Cloud observations and modeling within the european baltex cloud liquid water network. *Boreal Environment Research*, **7**, 235–245.

Elachi, C., 1987: *Introduction to the Physics and Techniques of Remote Sensing*. Wiley Series in Remote Sensing.

English, S., 1999: Estimation of temperature and humidity profile information from microwave radiances over different surface types. *Journal of Applied Meteorology*, **38**, 1526–1541.

Gaffen, D. and W. Elliot, 1993: Column water vapour content in clear and cloudy skies. *Journal of Climate*, **6**, 2278–2286.

Grody, N., J. Zhao, R. Ferraro, F. Weng, and R. Boers, 2001: Determination of precipitable water and cloud liquid water over oceans from the NOAA-15 advanced microwave sounding unit. *Journal of Geophysical Research*, **106**(D3), 2943–2953.

Hauschildt, H. and A. Macke, 2004: Precipitable water in cloudy atmospheres from combined solar, thermal and microwave measurements. literature study on existing tpw measurements in cloudy area. Technical report, CMSAF, DWD.

Kidder, S. and T. Vonder Haar, 1995: *Satellite Meteoroloy*. Academic Press.

Lanzante, J. and G. Gahrs, 2000: The "clear–sky bias" of TOVS upper-tropospheric humidity. *Journal of Climate*, **13**, 4034–4041.

Löhnert, U. and S. Crewell, 2003: Accuracy of cloud liquid water path from ground-based microwave radiometry - 1. dependency on cloud model statistics. *Radio Science*, **38**(3).

Marsden, D. and F. Valero, 2004: Observation of water vapor greenhouse absorption over the gulf of mexico using aircraft and satellite data. *Journal of Atmosperic Science*, **61**, 745 – 753.

Naud, C., J. Muller, and E. Clothiaux, 2003: Comparison between active sensor and radiosonde cloud bondaries over the ARM southern great plains site. *Journal of Geophysical Research*, **108**(D4).

Pruppacher, H. and J. Klett, 1997: *Microphysics of Clouds and Precipitation*. Reidel Publishing Company.

Revercomb, H., D. Turner, D. Tobin, R. Knuteson, W. Feltz, J. Barnard, J. Bösenberg, S. Clough, D. Cook, R. Ferrare, J. Goldsmith, S. Gutman, R. Halthore, B. Lesht, J. Liljegren, H. Linne, J. Michalsky, V. Morris, W. Porch, S. Richardson, B. Schmid, M. Splitt, T. Van Hove, E. Westwater, and D. Whiteman, 2003: The ARM program's water vapor intensive observation periods. *Bulletin American Meteorological Society*, **84**(2), 217 – 237.

Ruprecht, E., 1996: Atmospheric water vapor and cloud water: an overview. *Adv. Space Res.*, **18**(7).

Soden, B. and J. Lanzante, 1996: An assessment of satellite and radiosonde cimatologies of upper–tropospheric water vapor. *Journal of Climate*, **9**, 1235–1250.

Stephens, G. and S. Tjemkes, 1993: Water vapor and its role in the earth's greenhouse. *Aust. J. Phys.*, **46**.

Trenberth, K., J. Christy, and J. Olson, 1987: Global atmosheric mass, surface pressure, and water vapor variations. *Journal of Geophysical Research*, **92**(D12), 14,815–14,826.

Turner, D., B. Lesht, S. Clough, J. Liljegren, H. Revercomb, and D. Tobin, 2003: Dry bias and variability in vaisala rs80-h radiosondes: The ARM experience. *Journal of Atmospheric and Oceanic Technology*, **20**, 117–132.

Wahl, S., A. Macke, and J. Schulz, 2003: Precipitable water in cloudy areas. *VS-Plan 7.7*, p. 26.

Wang, J. and W. Rossow, 1995: Determination of cloud vertical structure from upper–air observations. *Journal of Applied Meteorology*, **34**, 2243 – 2258.

Wang, J., W. Rossow, T. Uttal, and M. Rozendaal, 1999: Variability of cloud vertical structure during astex observed from a combination of rawinsonde, radar, ceilometer, and satellite. *Monthly Weather Review*, **127**, 2484 – 2502.

Westwater, E., 1997: Remote sensing of tropospheric temperature and water vapor by integrated observing systems. *Bulletin American Meteorological Society*, **78**(9), 1991 – 2006.

Appendix A

Cloud — clear statistics from radiosonde measurements

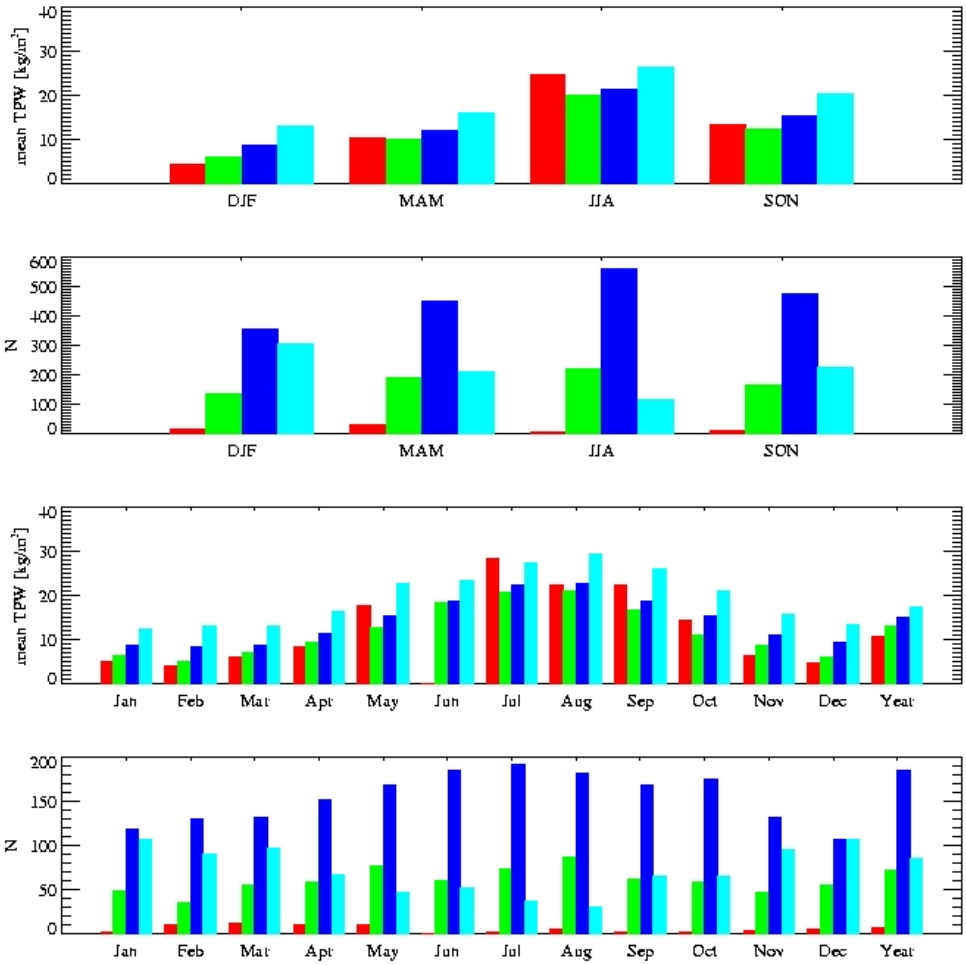

Figure A.1: *10 years of data from Schleswig sorted by the observed cloud cover: clear–sky in red, scattered cloudiness (1-4 octas) in green, broken cloudiness (5-7 octas) in blue, and overcast in cyan. From Top to bottom: Seasonal mean TPW in the cloud classes, number of cases per cloud class per season, monthly mean TPW per cloud classes and the number of cases per class. The last block in the monthly dispartment gives yearly mean (for the number of cases is given by the ordinate number times 10).*

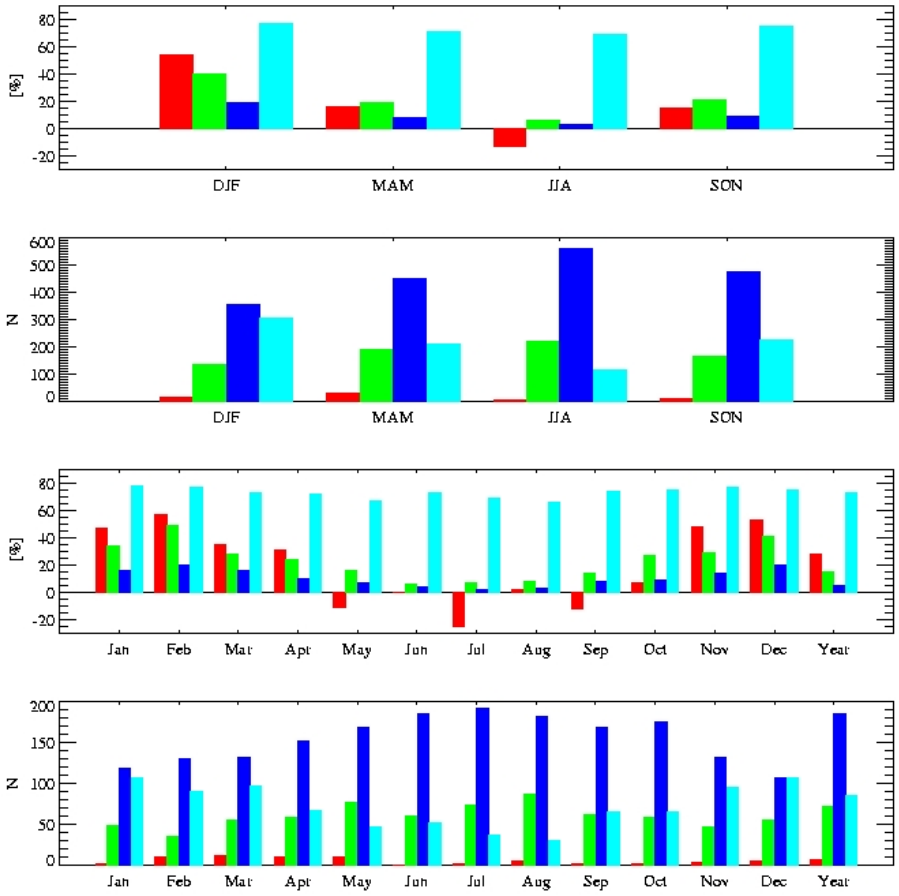

Figure A.2: *The bias estimators and the probability according to Gaffen and Elliot (1993): the b_0 in red, b_4 in green, b_7 in blue, and the probability in cyan. From Top to bottom: Seasonal bias estimators, number of cases per cloud class (see figure A.1) per season, monthly bias estimators and the number of cases per class. The last block in the monthly dispartment gives yearly mean (for the number of cases is given by the ordinate number times 10).*

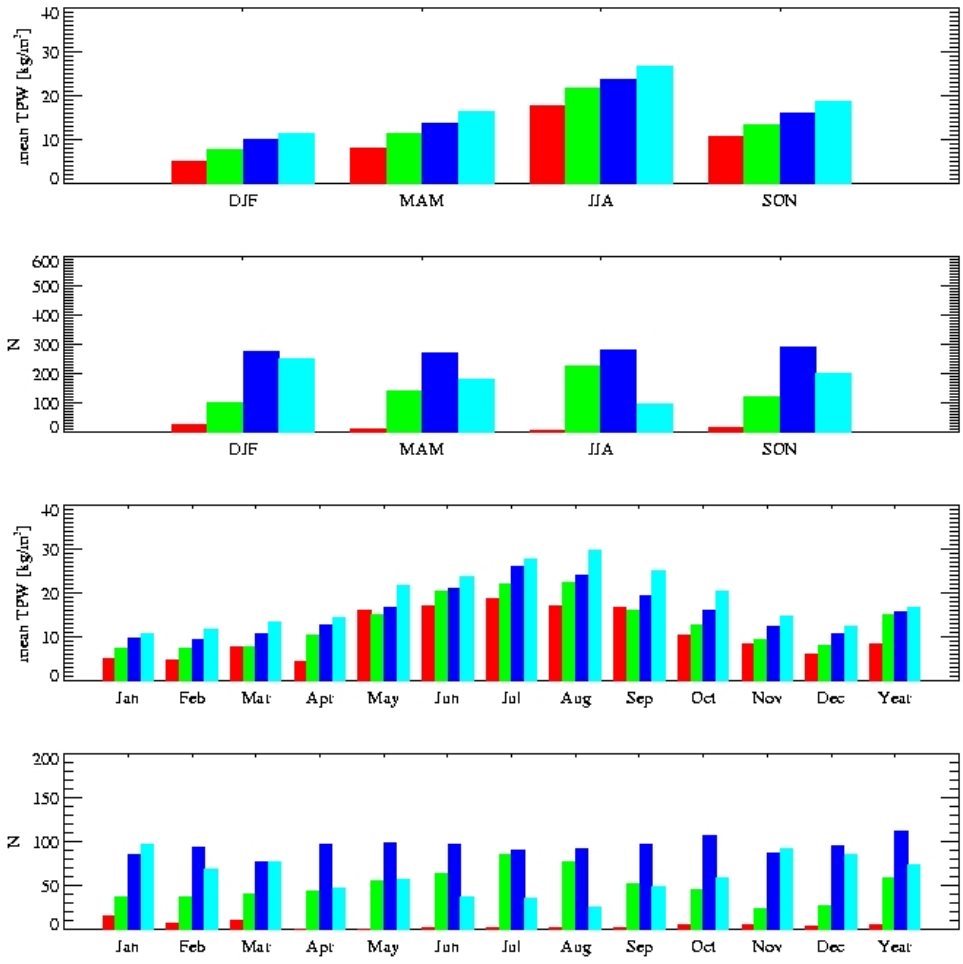

Figure A.3: *10 years of data from Stuttgart sorted by the observed cloud cover: clear–sky in red, scattered cloudiness (1-4 octas) in green, broken cloudiness (5-7 octas) in blue, and overcast in cyan. From Top to bottom: Seasonal mean TPW in the cloud classes, number of cases per cloud class per season, monthly mean TPW per cloud classes and the number of cases per class. The last block in the monthly dispartment gives yearly mean (for the number of cases is given by the ordinate number times 10).*

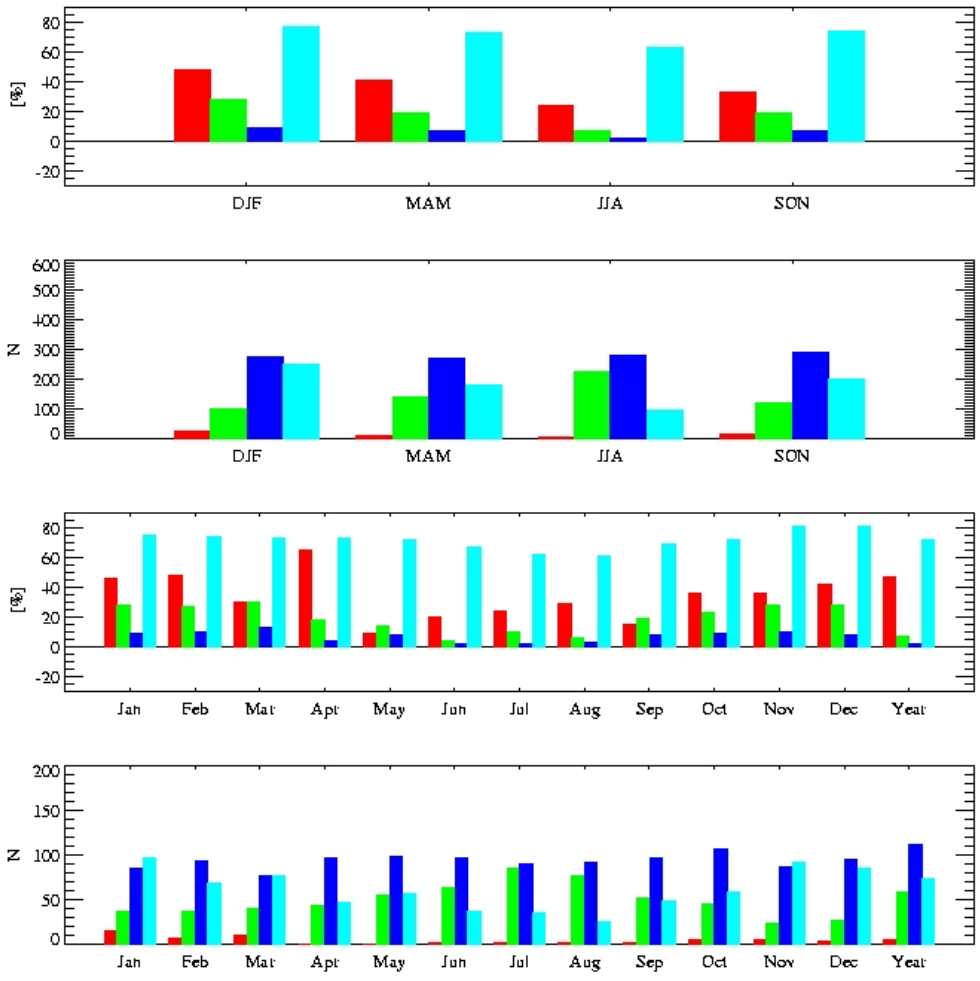

Figure A.4: *The bias estimators and the probability according to Gaffen and Elliot (1993): the b_0 in red, b_4 in green, b_7 in blue, and the probability in cyan. From Top to bottom: Seasonal bias estimators, number of cases per cloud class (see figure A.3) per season, monthly bias estimators and the number of cases per class. The last block in the monthly dispartment gives yearly mean (for the number of cases is given by the ordinate number times 10).*

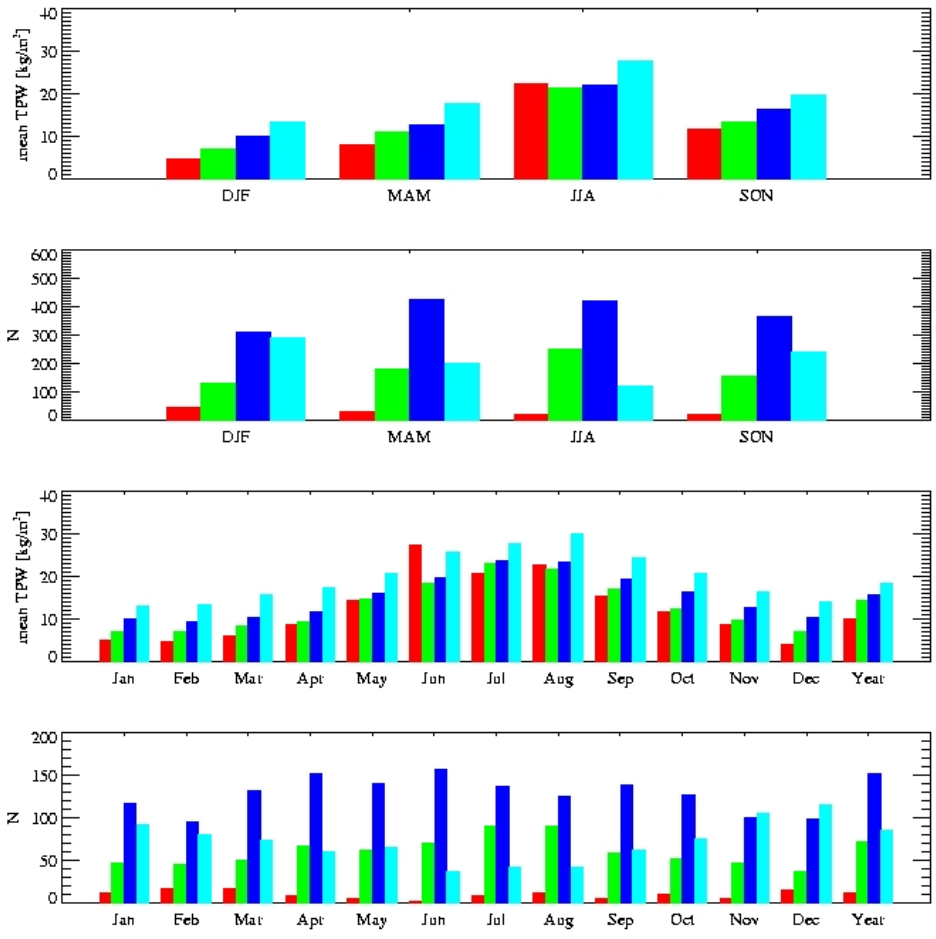

Figure A.5: *10 years of data from Essen sorted by the observed cloud cover: clear–sky in red, scattered cloudiness (1-4 octas) in green, broken cloudiness (5-7 octas) in blue, and overcast in cyan. From Top to bottom: Seasonal mean TPW in the cloud classes, number of cases per cloud class per season, monthly mean TPW per cloud classes and the number of cases per class. The last block in the monthly dispartment gives yearly mean (for the number of cases is given by the ordinate number times 10).*

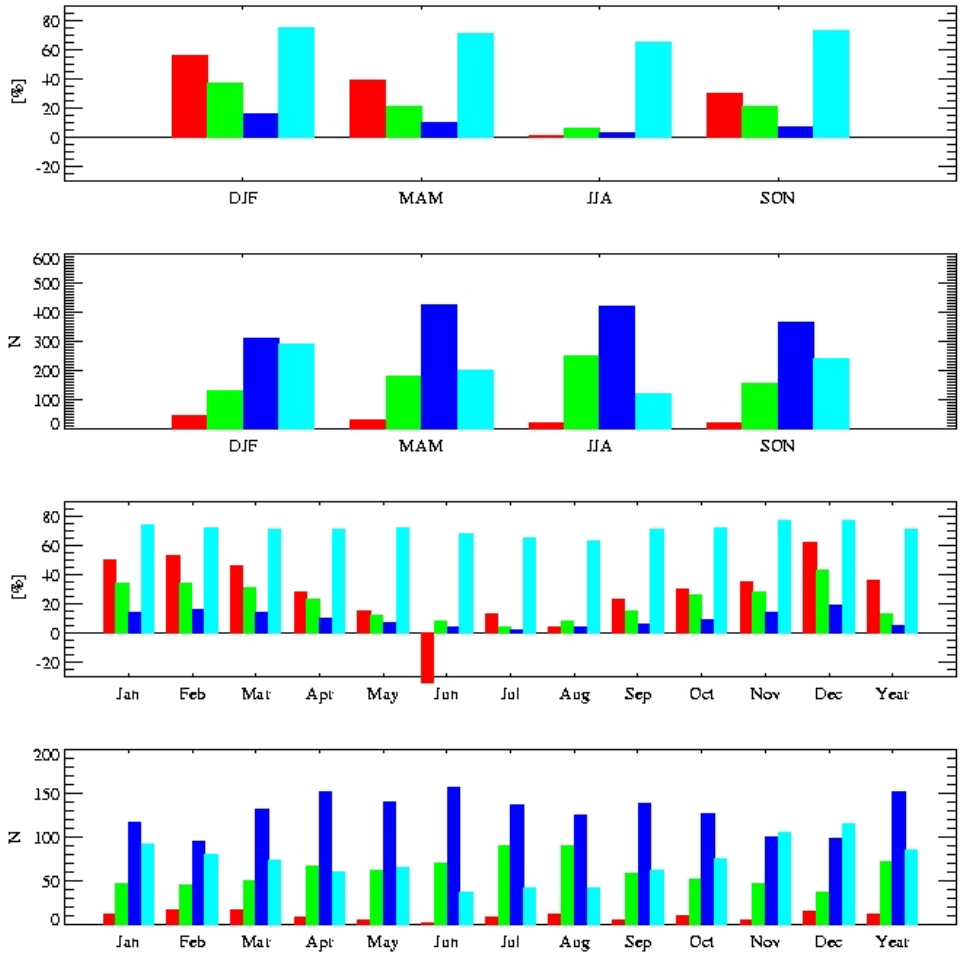

Figure A.6: *The bias estimators and the probability according to Gaffen and Elliot (1993): the b_0 in red, b_4 in green, b_7 in blue, and the probability in cyan. From Top to bottom: Seasonal bias estimators, number of cases per cloud class (see figure A.5) per season, monthly bias estimators and the number of cases per class. The last block in the monthly dispartment gives yearly mean (for the number of cases is given by the ordinate number times 10).*

	DJF		MAM		JJA		SON		Year	
	TPW	**N**	**TPW**	**N**	**TPW**	**N**	**TPW**	**N**	**TPW**	**N**
Lindenberg										
CLR	4.95	67	9.04	45	18.09	24	12.94	42	9.64	178
SCT	6.89	104	12.26	180	22.78	212	14.32	157	15.31	653
BKN	9.15	308	13.20	413	23.24	520	16.60	422	16.45	1663
OVC	11.58	373	15.94	261	28.06	156	19.17	262	17.00	1052
ALL	9.61	852	13.60	899	23.82	912	16.79	883	16.06	3546
Schleswig										
CLR	4.45	19	10.56	32	24.67	8	13.63	10	10.96	69
SCT	6.03	139	10.11	192	20.22	222	12.63	169	13.02	722
BKN	8.93	356	12.24	454	21.47	561	15.41	477	15.22	1848
OVC	13.03	305	16.31	211	26.31	119	20.31	226	17.58	861
ALL	9.86	819	12.69	889	21.82	910	16.11	882	15.26	3500
Essen										
CLR	4.67	45	8.15	32	22.40	23	11.74	21	10.19	121
SCT	7.27	130	11.08	180	21.34	252	13.48	159	14.51	721
BKN	10.04	312	12.90	426	22.28	420	16.63	368	15.79	1526
OVC	13.62	290	17.87	201	27.92	123	19.80	243	18.42	857
ALL	10.60	777	13.52	839	22.84	818	16.84	791	15.99	3225
Stuttgart										
CLR	5.25	28	8.07	13	17.64	6	10.87	15	8.40	62
SCT	7.70	101	11.50	141	21.88	227	13.53	122	15.26	591
BKN	10.05	276	13.71	274	23.65	280	16.21	292	15.94	1122
OVC	11.61	253	16.36	182	26.85	98	18.92	201	16.82	734
ALL	10.09	658	13.87	610	23.45	611	16.43	630	15.85	2509

Table A.1: Seasonal and annual mean TPW in kg/m^2 in the cloud classes (CLR = clear, SCT = scattered (1-4 octas), BKN = broken (5-7 octas), OVC = overcast) and without regards to cloudiness (ALL) for the four German stations. N gives the number of observations comprising the mean.

	DJF	MAM	JJA	SON
Lindenberg				
CLR/OVC	0.43	0.57	0.64	0.67
SCT/OVC	0.60	0.77	0.81	0.75
BKN/OVC	0.79	0.83	0.83	0.87
B0	0.48	0.33	0.24	0.23
B4	0.36	0.15	0.06	0.16
B7	0.16	0.07	0.04	0.06
P	0.76	0.71	0.68	0.73
Essen				
CLR/OVC	0.34	0.46	0.80	0.59
SCT/OVC	0.53	0.62	0.76	0.68
BKN/OVC	0.74	0.72	0.80	0.84
B0	0.56	0.40	0.02	0.30
B4	0.38	0.21	0.06	0.21
B7	0.17	0.10	0.04	0.08
P	0.75	0.72	0.66	0.74

	DJF	MAM	JJA	SON
Schleswig				
CLR/OVC	0.34	0.65	0.94*	0.67
SCT/OVC	0.46	0.62	0.77	0.62
BKN/OVC	0.68	0.75	0.82	0.76
B0	0.55	0.17	-0.13*	0.15
B4	0.41	0.20	0.07	0.21
B7	0.19	0.09	0.03	0.09
P	0.77	0.71	0.70	0.76
Stuttgart				
CLR/OVC	0.45	0.49	0.66*	0.57
SCT/OVC	0.66	0.70	0.81	0.72
BKN/OVC	0.87	0.84	0.88	0.86
B0	0.48	0.42	0.25*	0.34
B4	0.29	0.19	0.07	0.19
B7	0.09	0.08	0.03	0.07
P	0.77	0.73	0.64	0.74

Table A.2: Seasonal ratios of the mean TPW in a cloud class (CLR = clear, SCT = scattered (1-4 octas), BKN = broken (5-7 octas)) towards the overcast mean TPW (OVC) for each station. The bias indices (dimensionless), and the probability of a sounding passing through a cloud as defined in the equations 5.2 to 5.5 are given. A dash is given when no clear–sky observations are done, ratios and indices based on less then 10 observations are marked (*).

Appendix B

Spatial TPW as measured from Satellite

B.1 South Atlantic

A : Excess water vapour depending on Latitude

B: Excess water vapour frequency distribution

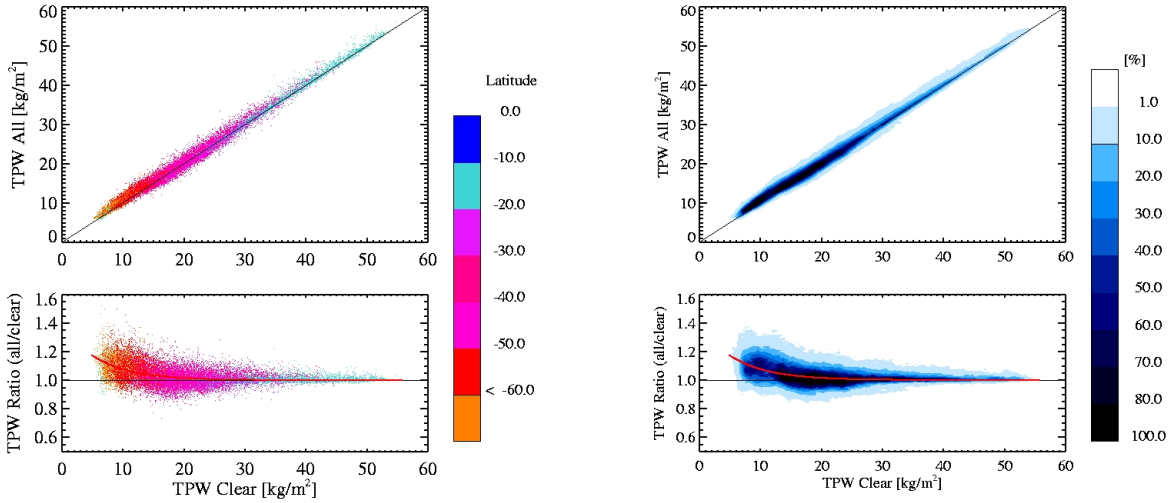

Figure B.1: *South Atlantic: Relation of clear–sky TPW towards the all–sky TPW (upper panel) and towards the ratio of all–sky TPW and clear–sky TPW. The TPW is given in [kg/m^2]. Data are taken from the year 2004. A: Colours give the latitude range. B: Frequency distribution of the data points in figute A.*

A : Excess water vapour depending on Latitude

B: Excess water vapour frequency distribution

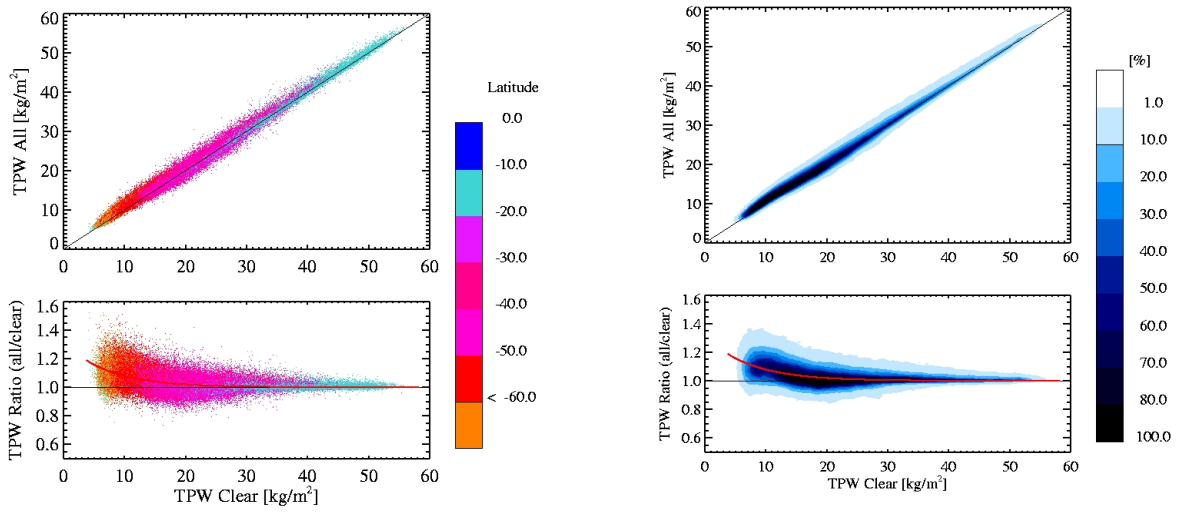

Figure B.2: *South Atlantic: Relation of clear–sky TPW towards the all–sky TPW (upper panel) and towards the ratio of all–sky TPW and clear–sky TPW. The TPW is given in [kg/m^2]. Data are taken from February 2001 to October 2005 (except 2002). A: Colours give the latitude range. B: Frequency distribution of the data points in figute A.*

A: Excess water vapour

B: underestimation

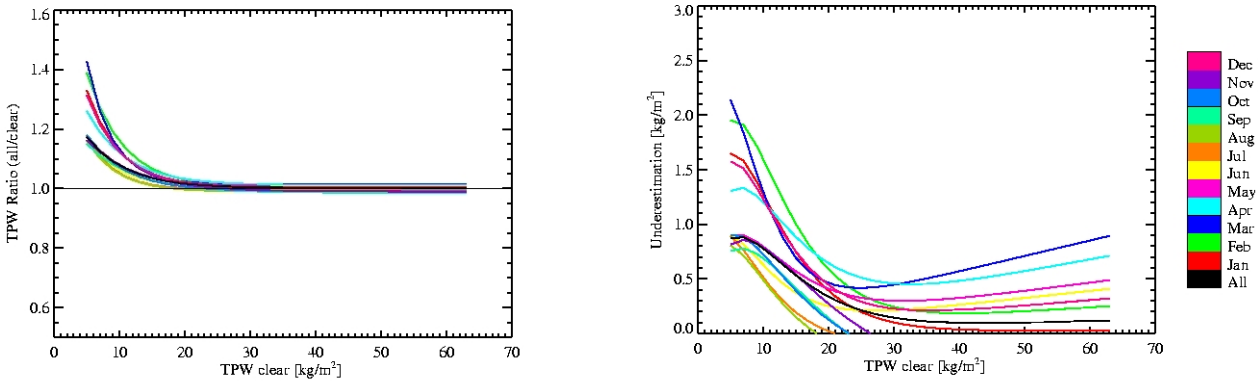

Figure B.3: South Atlantic: *A* Excess water vapour depending on the clear–sky TPW for the year 2004. *B* Clear–sky water vapour bias as derived from the excess water vapour. Colours denote the month. The underestimation is given in relation to the clear–sky water vapour path used in a climatology.

A: Excess water vapour *B: underestimation*

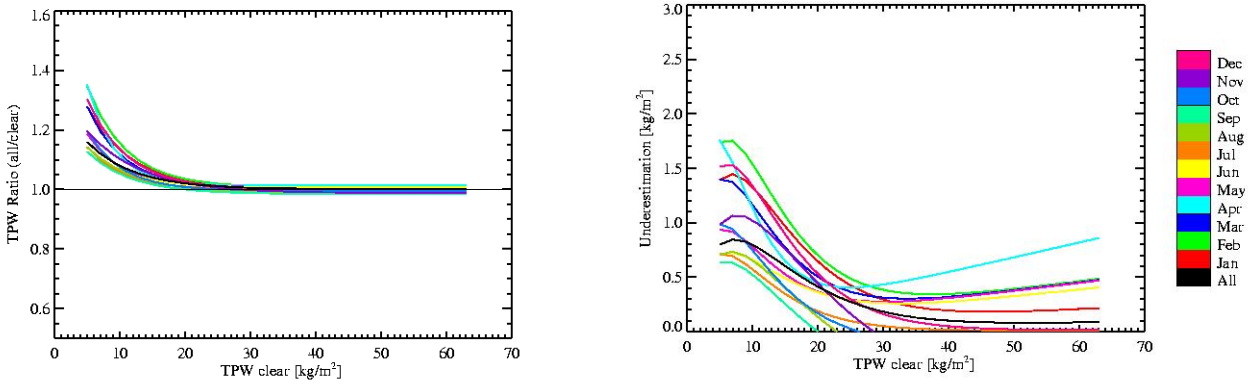

Figure B.4: South Atlantic: *A* Excess water vapour depending on the clear–sky TPW for the years 2001–2005 (except 2002). *B* Clear–sky water vapour bias as derived from the excess water vapour. Colours denote the month. The underestimation is given in relation to the clear–sky water vapour path used in a climatology.

A: 2004 *C: 2001–2005*

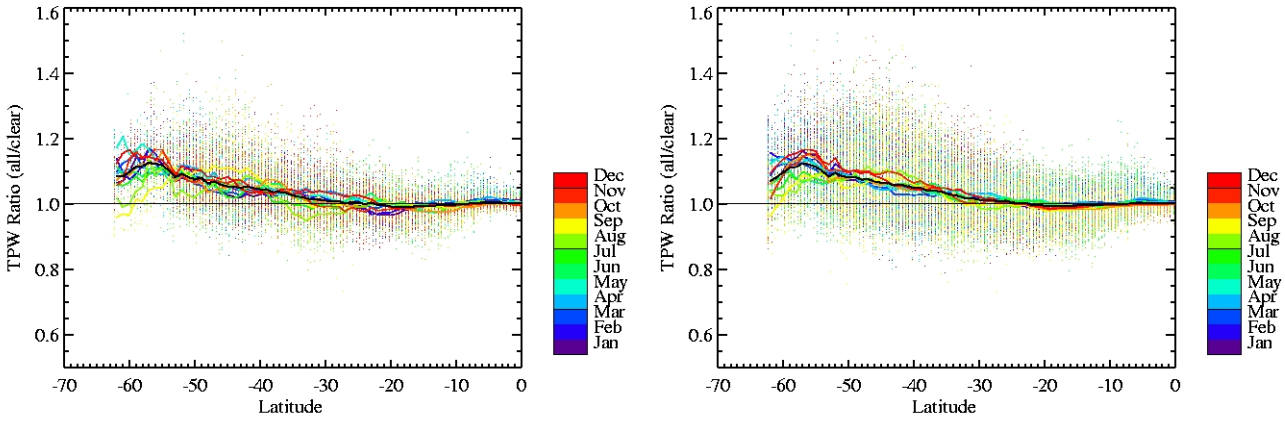

Figure B.5: *South Atlantic: Zonal distribution of the ratio (all–sky TPW by clear–sky TPW). Colours denote the month. A: only 2004 data, and B: data are taken from February 2001 to October 2005 (except 2002).*

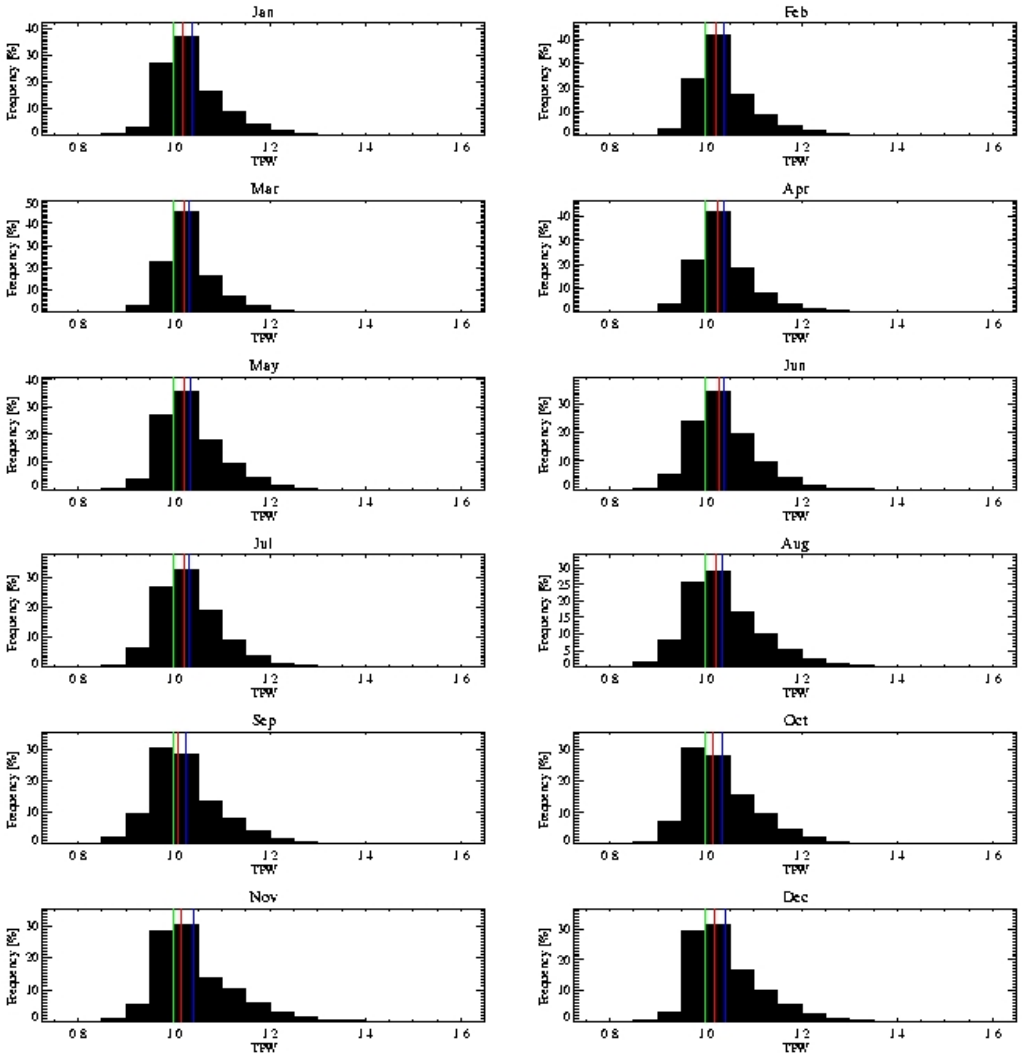

Figure B.6: *Frequency distribution of the excess water vapour of each month for the South Atlantic for the years 2001-2005 (except 2002). The green line gives the excess water vapour of 1. In red the median and in blue the mean value of the distribution is marked.*

A: South Atlantic

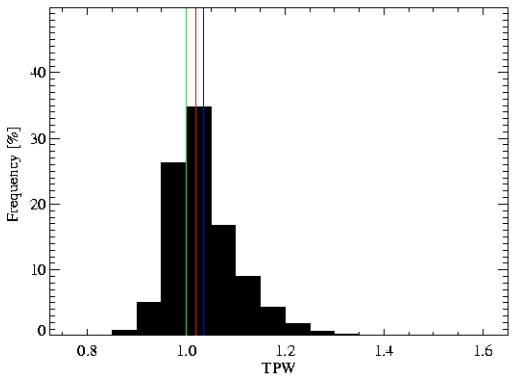

B: Global

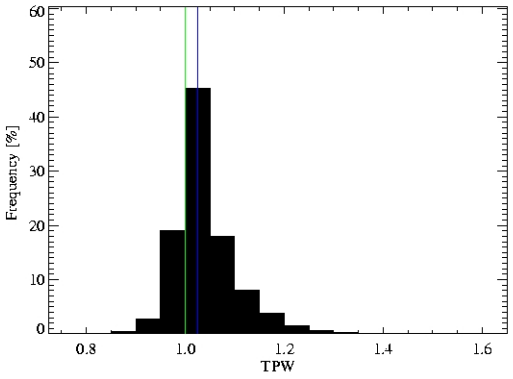

Figure B.7: *Frequency distribution of the excess water vapour for the South Atlantic (A) and global (B) for the years 2001-2005 (except 2002). The green line gives the excess water vapour of 1. In red the median and in blue the mean value of the distribution is marked.*

Month	A_0	A_1	A_2
South Atlantic			
Jan	0.582	0.869	1.003
Feb	0.787	0.861	1.008
Mar	0.676	0.845	1.007
Apr	1.146	0.833	1.014
May	0.458	0.784	1.008
Jun	0.306	0.829	1.006
Jul	0.354	0.849	1.000
Aug	0.303	0.833	0.986
Sep	0.298	0.875	0.985
Oct	0.514	0.863	0.996
Nov	0.380	0.829	0.987
Dec	0.684	0.887	1.002
All	0.319	0.850	1.001

Table B.1: *South Atlantic: The parameters of the function expressing the ratio vs clear–sky TPW using all years.*

B.2 Pacific

A : Excess water vapour depending on Latitude

B: Excess water vapour frequency distribution

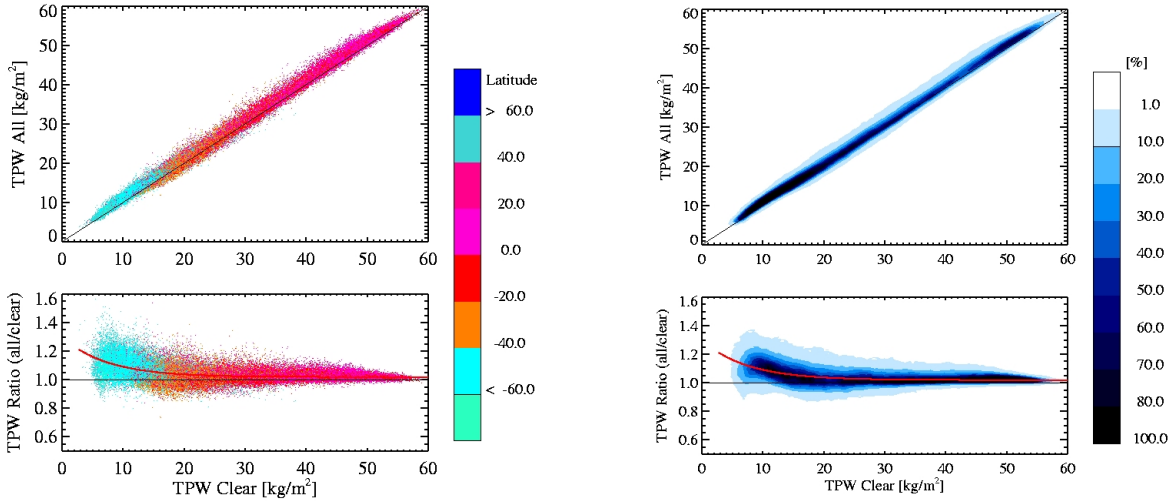

Figure B.8: *Pacific: Relation of clear–sky TPW towards the all–sky TPW (upper panel) and towards the ratio of all–sky TPW and clear–sky TPW. The TPW is given in [kg/m^2]. Data are taken from the year 2004. A: Colours give the latitude range. B: Frequency distribution of the data points in figute A.*

Month	A_0	A_1	A_2
North Atlantic			
Jan	0.262	0.909	1.014
Feb	0.239	0.912	1.016
Mar	0.287	0.886	1.018
Apr	0.599	0.833	1.019
May	0.631	0.805	1.022
Jun	0.492	0.800	1.019
Jul	0.260	0.848	1.015
Aug	0.143	0.870	1.022
Sep	0.280	0.857	1.022
Oct	0.316	0.866	1.021
Nov	0.411	0.856	1.020
Dec	0.309	0.891	1.018
All	0.270	0.878	1.019

Table B.2: *Pacific: The parameters of the function expressing the ratio vs clear–sky TPW using all years.*

A : Excess water vapour depending on Latitude

B: Excess water vapour frequency distribution

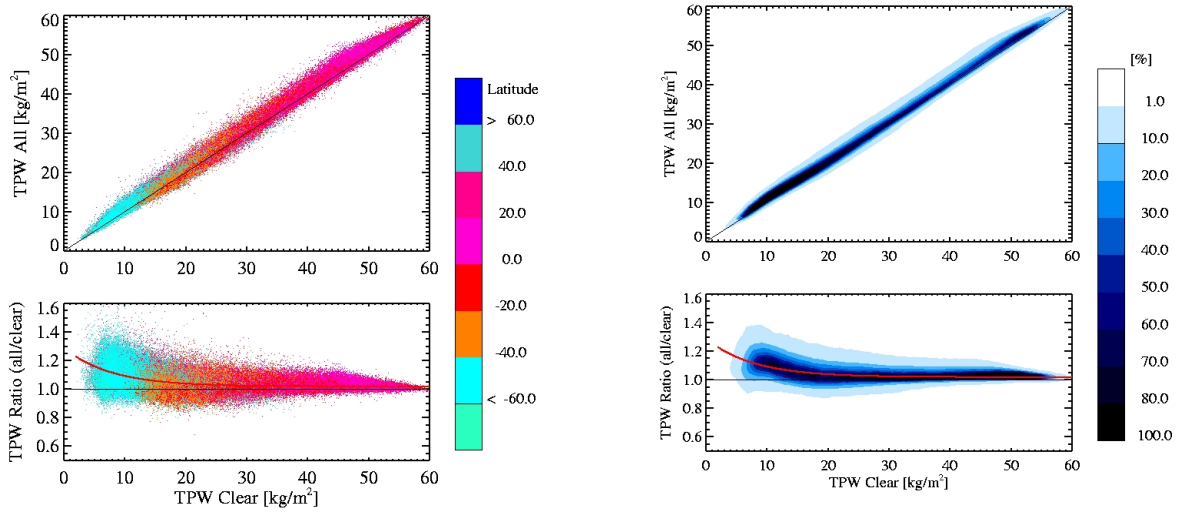

Figure B.9: *Pacific: Relation of clear–sky TPW towards the all–sky TPW (upper panel) and towards the ratio of all–sky TPW and clear–sky TPW. The TPW is given in [kg/m^2]. Data are taken from February 2001 to October 2005 (except 2002). A: Colours give the latitude range. B: Frequency distribution of the data points in figute A.*

A: Excess water vapour

B: underestimation

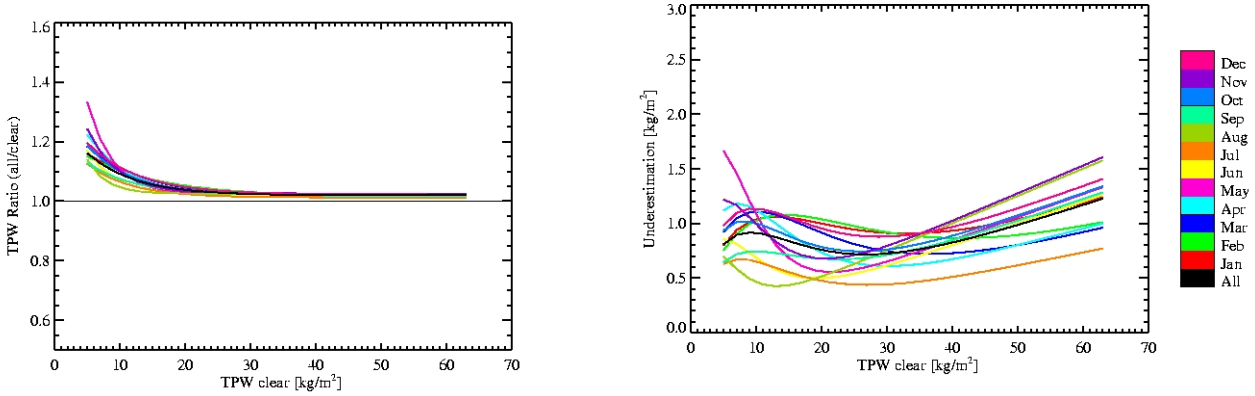

Figure B.10: Pacific: *A* Excess water vapour depending on the clear–sky TPW for the year 2004. *B* Clear–sky water vapour bias as derived from the excess water vapour. Colours denote the month. The underestimation is given in relation to the clear–sky water vapour path used in a climatology.

A: Excess water vapour *B: underestimation*

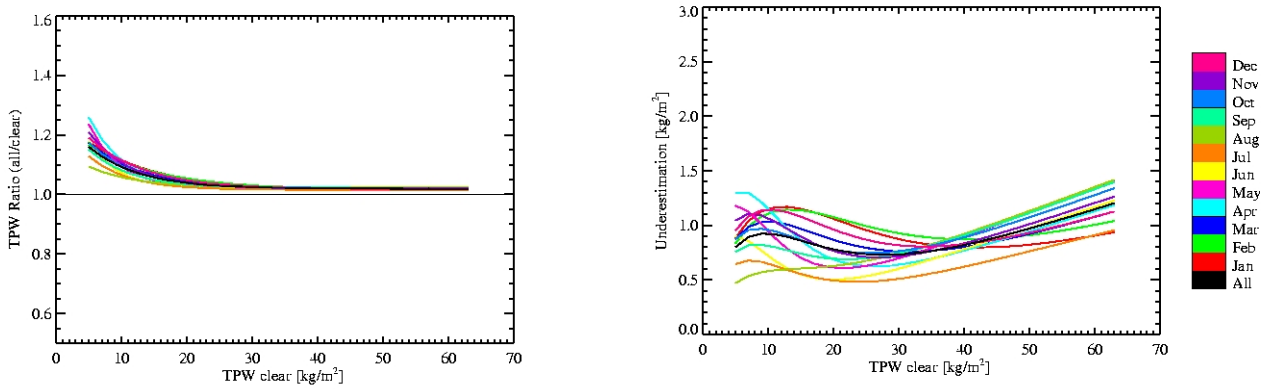

Figure B.11: Pacific: *A* Excess water vapour depending on the clear–sky TPW for the years 2001–2005 (except 2002). *B* Clear–sky water vapour bias as derived from the excess water vapour. Colours denote the month. The underestimation is given in relation to the clear–sky water vapour path used in a climatology.

A: 2004 *C: 2001–2005*

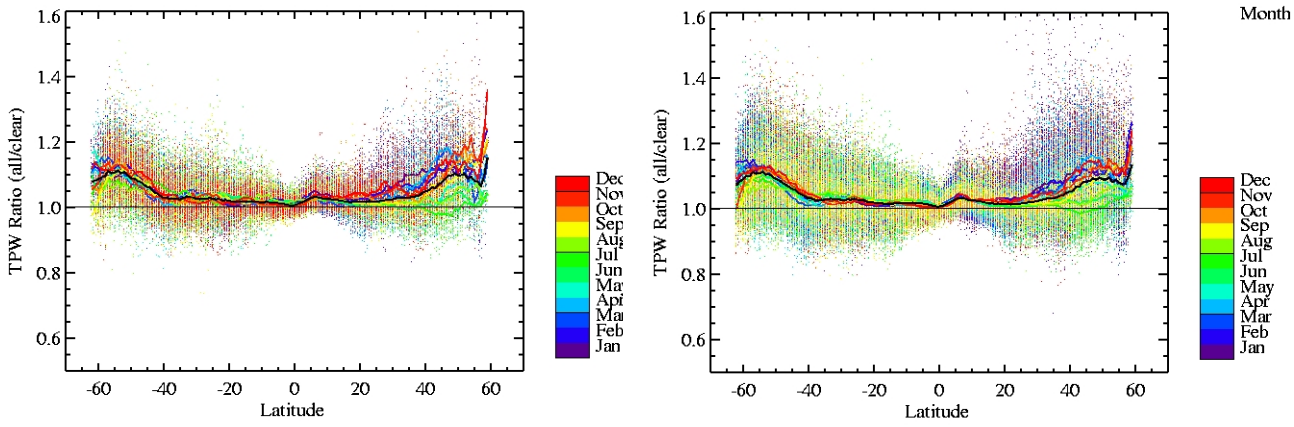

Figure B.12: *Pacific: Zonal distribution of the ratio (all–sky TPW by clear–sky TPW). Colours denote the month. A: only 2004 data, and B: data are taken from February 2001 to October 2005 (except 2002).*

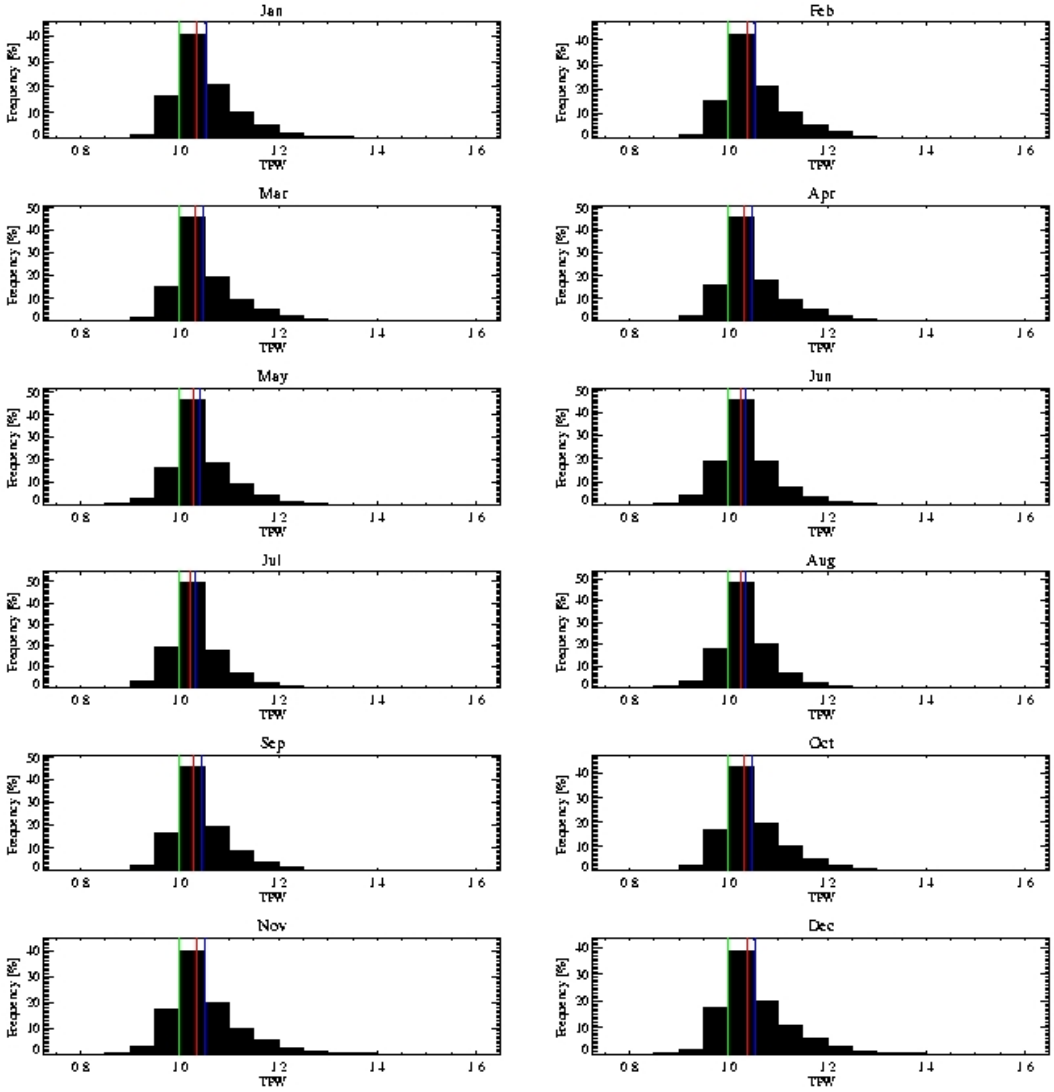

Figure B.13: *Frequency distribution of the excess water vapour of each month for the Pacific for the years 2001-2005 (except 2002). The green line gives the excess water vapour of 1. In red the median and in blue the mean value of the distribution is marked.*

A:Pacific

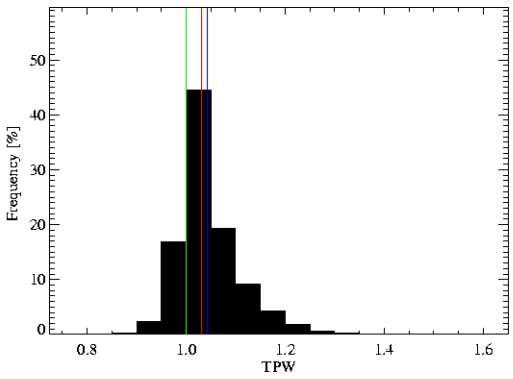

B: Global

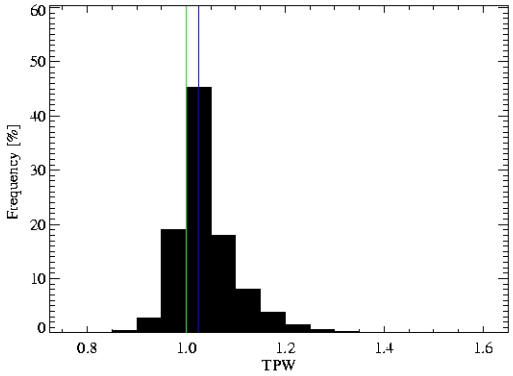

Figure B.14: *Frequency distribution of the excess water vapour for the Pacific (A) and global (B) for the years 2001-2005 (except 2002). The green line gives the excess water vapour of 1. In red the median and in blue the mean value of the distribution is marked.*

B.3 Indic

A : Excess water vapour depending on Latitude

B: Excess water vapour frequency distribution

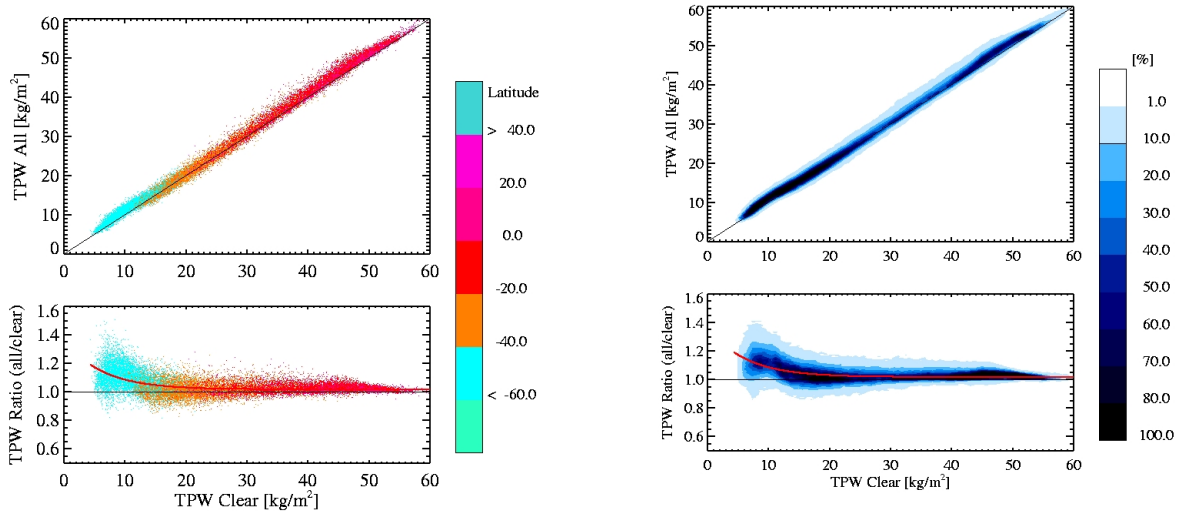

Figure B.15: *Indic: Relation of clear–sky TPW towards the all–sky TPW (upper panel) and towards the ratio of all–sky TPW and clear–sky TPW. The TPW is given in [kg/m^2]. Data are taken from the year 2004. A: Colours give the latitude range. B: Frequency distribution of the data points in figute A.*

Month	A_0	A_1	A_2
North Atlantic			
Jan	0.942	0.810	1.017
Feb	1.112	0.802	1.018
Mar	0.909	0.822	1.017
Apr	0.736	0.813	1.016
May	0.897	0.778	1.020
Jun	0.656	0.773	1.018
Jul	0.313	0.818	1.015
Aug	0.301	0.841	1.012
Sep	0.320	0.839	1.016
Oct	0.499	0.771	1.019
Nov	0.636	0.794	1.022
Dec	0.658	0.820	1.024
All	0.365	0.845	1.017

Table B.3: *Indic: The parameters of the function expressing the ratio vs clear–sky TPW using all years.*

A : Excess water vapour depending on Latitude

B: Excess water vapour frequency distribution

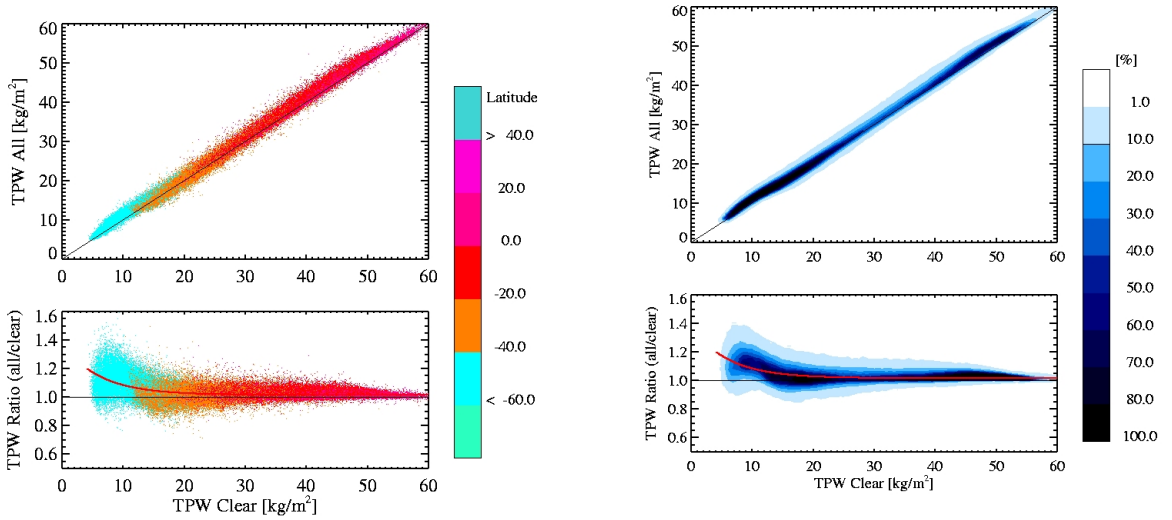

Figure B.16: *Indic: Relation of clear–sky TPW towards the all–sky TPW (upper panel) and towards the ratio of all–sky TPW and clear–sky TPW. The TPW is given in [kg/m^2]. Data are taken from February 2001 to October 2005 (except 2002). A: Colours give the latitude range. B: Frequency distribution of the data points in figute A.*

A: Excess water vapour

B: underestimation

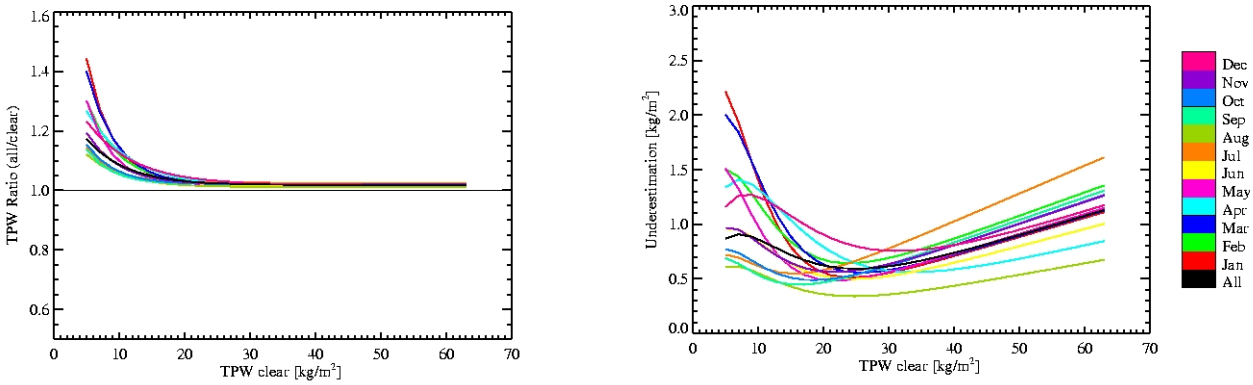

Figure B.17: Indic: *A* Excess water vapour depending on the clear–sky TPW for the year 2004. *B* Clear–sky water vapour bias as derived from the excess water vapour. Colours denote the month. The underestimation is given in relation to the clear–sky water vapour path used in a climatology.

A: Excess water vapour

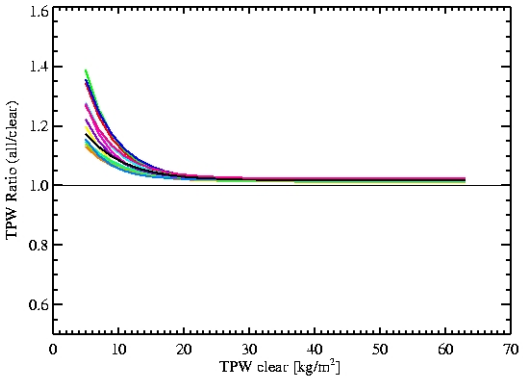

B: underestimation

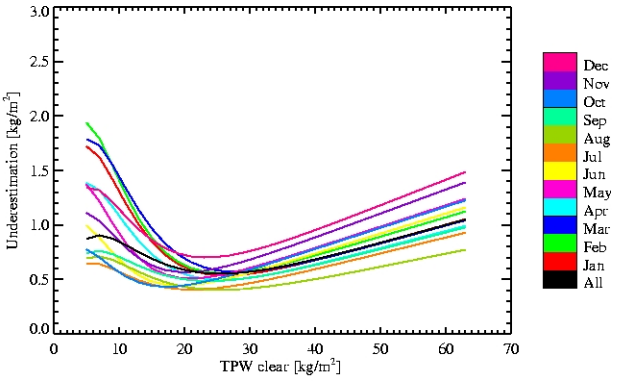

Figure B.18: Indic: *A* Excess water vapour depending on the clear–sky TPW for the years 2001–2005 (except 2002). *B* Clear–sky water vapour bias as derived from the excess water vapour. Colours denote the month. The underestimation is given in relation to the clear–sky water vapour path used in a climatology.

A: 2004

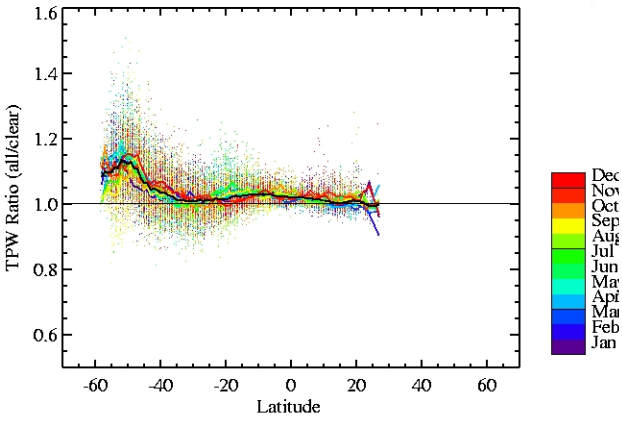

C: 2001–2005

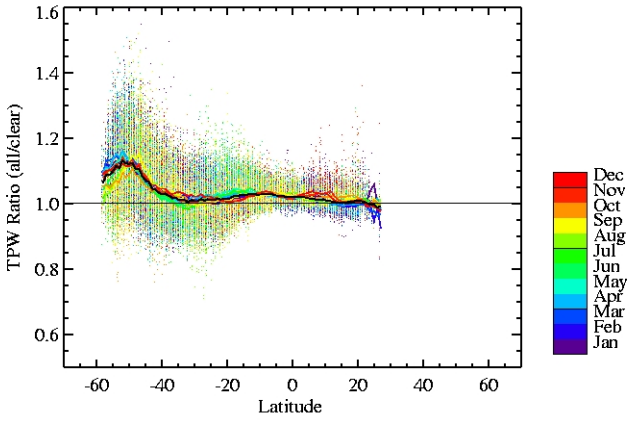

Figure B.19: *Indic: Zonal distribution of the ratio (all–sky TPW by clear–sky TPW). Colours denote the month. A: only 2004 data, and B: data are taken from February 2001 to October 2005 (except 2002).*

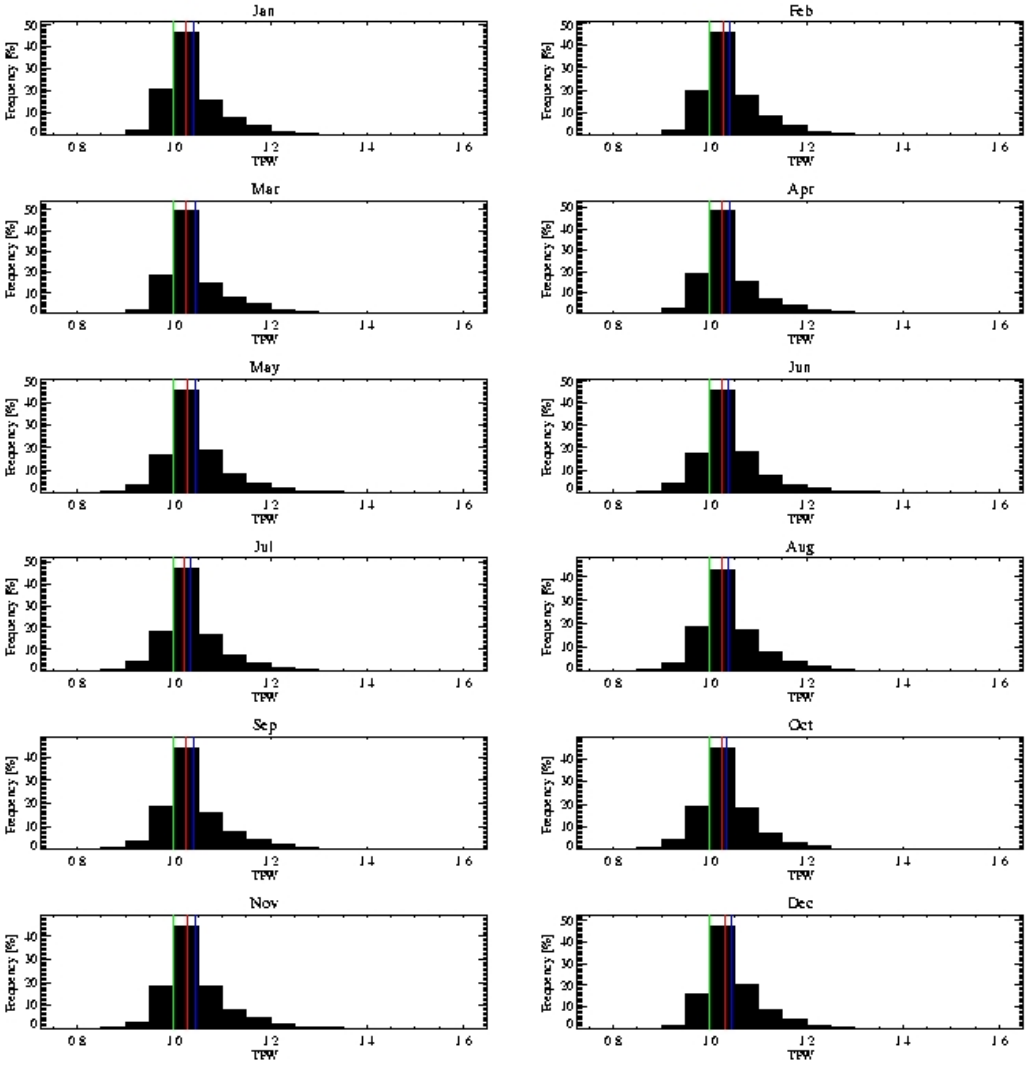

Figure B.20: *Frequency distribution of the excess water vapour of each month for the Indic for the years 2001-2005 (except 2002). The green line gives the excess water vapour of 1. In red the median and in blue the mean value of the distribution is marked.*

A: Indic

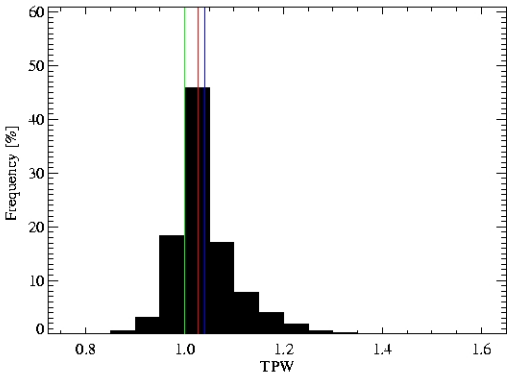

B: Global

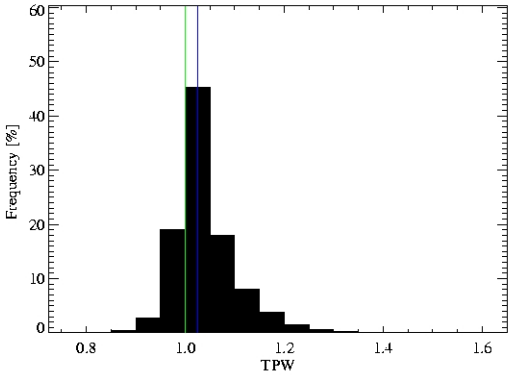

Figure B.21: *Frequency distribution of the excess water vapour for the Indic (A) and global (B) for the years 2001-2005 (except 2002). The green line gives the excess water vapour of 1. In red the median and in blue the mean value of the distribution is marked.*

B.4 Antarctic circumpolar ocean

A : Excess water vapour depending on Latitude

B: Excess water vapour frequency distribution

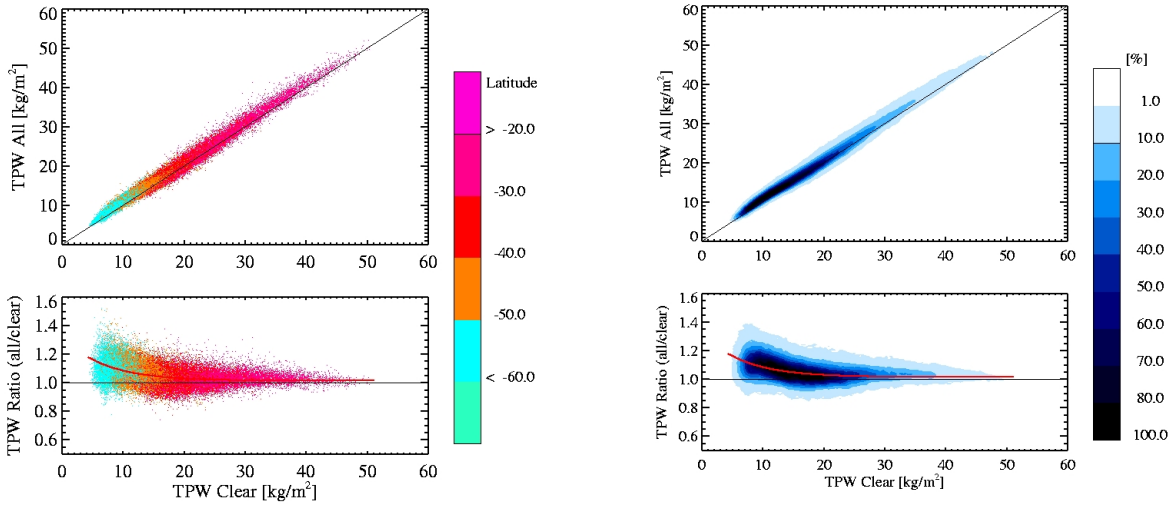

Figure B.22: *Antarctic circumpolar ocean: Relation of clear–sky TPW towards the all–sky TPW (upper panel) and towards the ratio of all–sky TPW and clear–sky TPW. The TPW is given in [kg/m^2]. Data are taken from the year 2004. A: Colours give the latitude range. B: Frequency distribution of the data points in figute A.*

Month	A_0	A_1	A_2
North Atlantic			
Jan	0.633	0.845	1.018
Feb	0.700	0.846	1.018
Mar	0.727	0.834	1.016
Apr	0.772	0.813	1.016
May	0.625	0.807	1.016
Jun	0.404	0.830	1.011
Jul	0.253	0.873	0.998
Aug	0.202	0.883	1.006
Sep	0.274	0.883	0.994
Oct	0.325	0.858	1.008
Nov	0.396	0.869	1.006
Dec	0.444	0.868	1.016
All	0.293	0.871	1.013

Table B.4: *Antarctic circumpolar ocean: The parameters of the function expressing the ratio vs clear–sky TPW using all years.*

A : Excess water vapour depending on Latitude

B: Excess water vapour frequency distribution

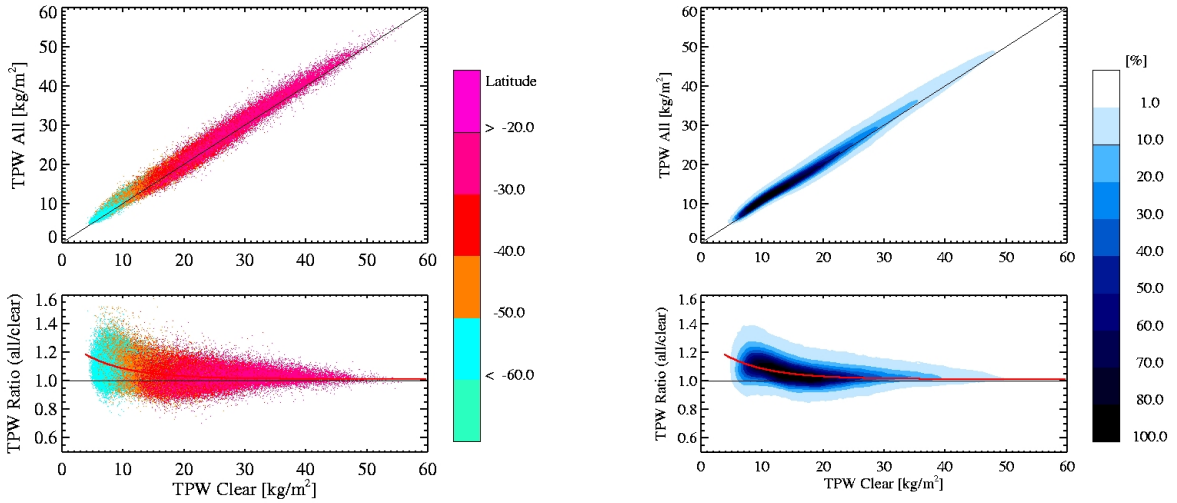

Figure B.23: *Antarctic circumpolar ocean: Relation of clear–sky TPW towards the all–sky TPW (upper panel) and towards the ratio of all–sky TPW and clear–sky TPW. The TPW is given in [kg/m^2]. Data are taken from February 2001 to October 2005 (except 2002). A: Colours give the latitude range. B: Frequency distribution of the data points in figute A.*

A: Excess water vapour

B: underestimation

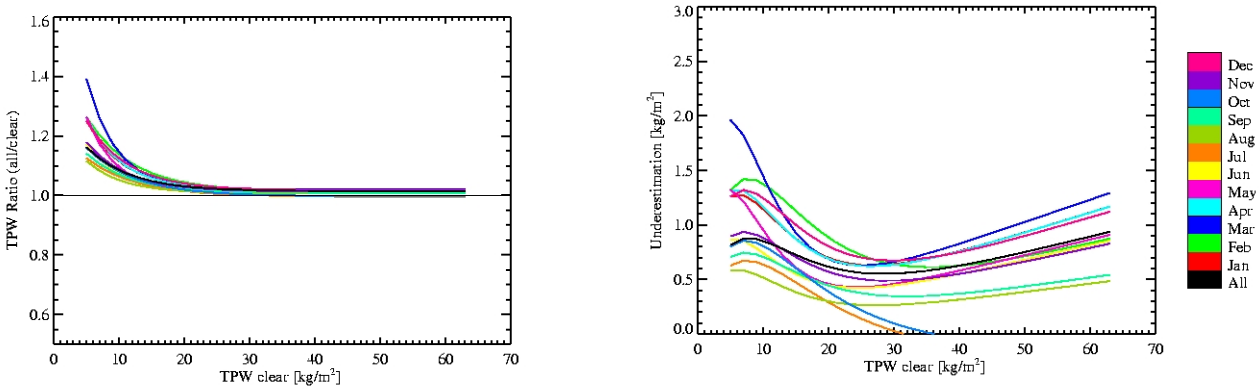

Figure B.24: Antarctic circumpolar ocean: *A* Excess water vapour depending on the clear–sky TPW for the year 2004. *B* Clear–sky water vapour bias as derived from the excess water vapour. Colours denote the month. The underestimation is given in relation to the clear–sky water vapour path used in a climatology.

A: Excess water vapour *B: underestimation*

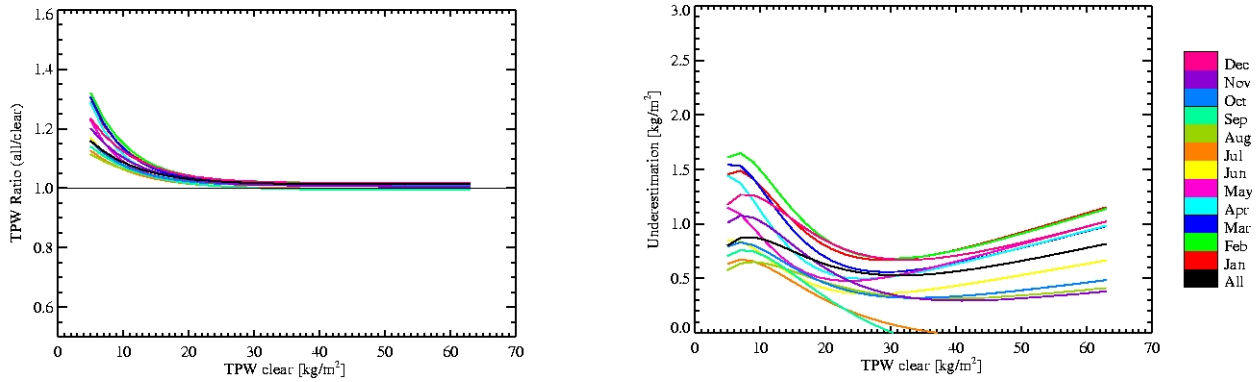

Figure B.25: Antarctic circumpolar ocean: *A* Excess water vapour depending on the clear–sky TPW for the years 2001–2005 (except 2002). *B* Clear–sky water vapour bias as derived from the excess water vapour. Colours denote the month. The underestimation is given in relation to the clear–sky water vapour path used in a climatology.

A: 2004 *C: 2001–2005*

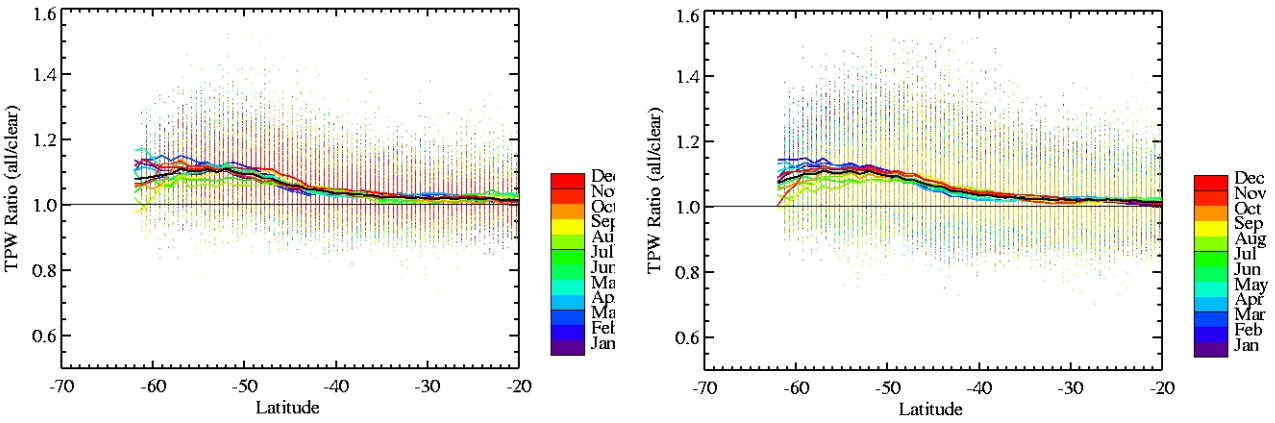

Figure B.26: *Antarctic circumpolar ocean: Zonal distribution of the ratio (all–sky TPW by clear–sky TPW). Colours denote the month. A: only 2004 data, and B: data are taken from February 2001 to October 2005 (except 2002).*

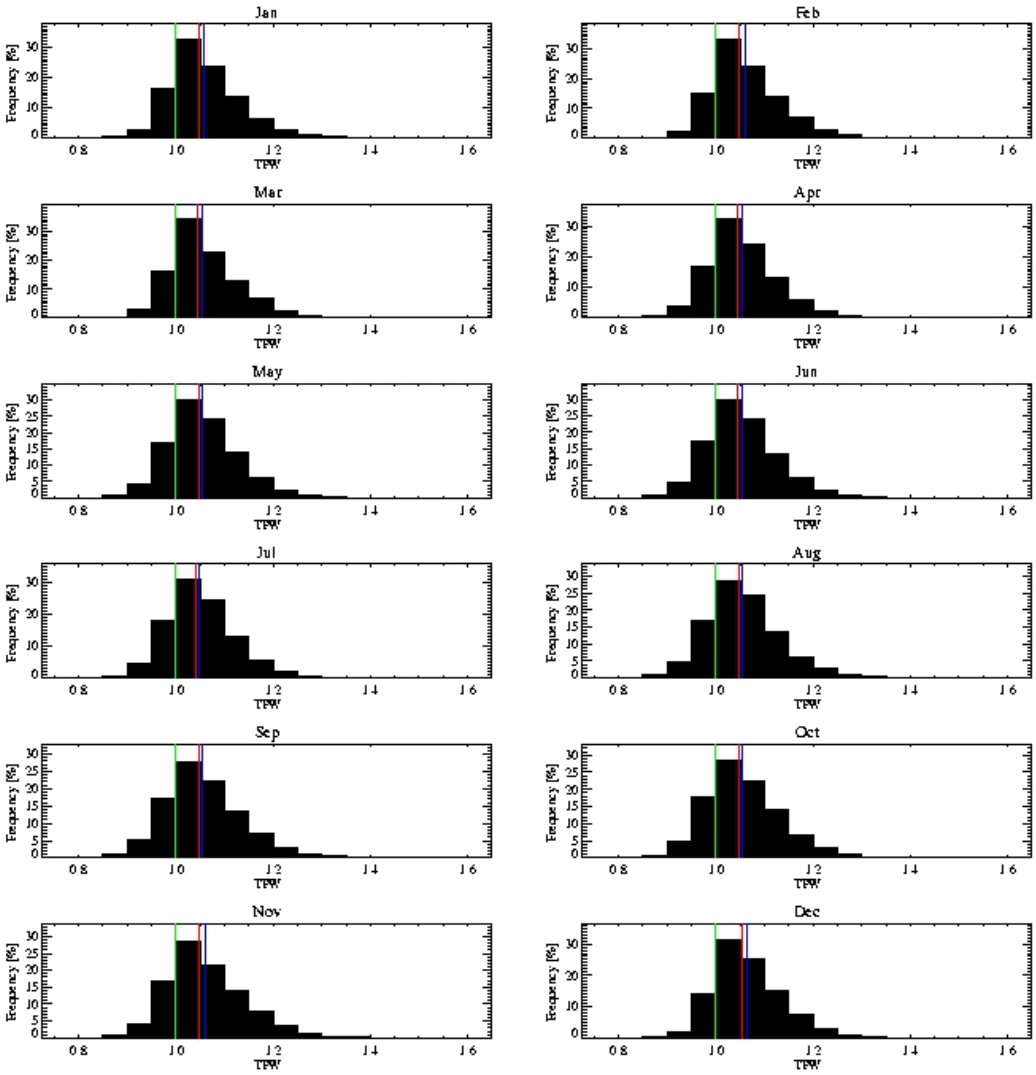

Figure B.27: *Frequency distribution of the excess water vapour of each month for the Antarctic circumpolar ocean for the years 2001-2005 (except 2002). The green line gives the excess water vapour of 1. In red the median and in blue the mean value of the distribution is marked.*

A: Antarctic circumpolar ocean

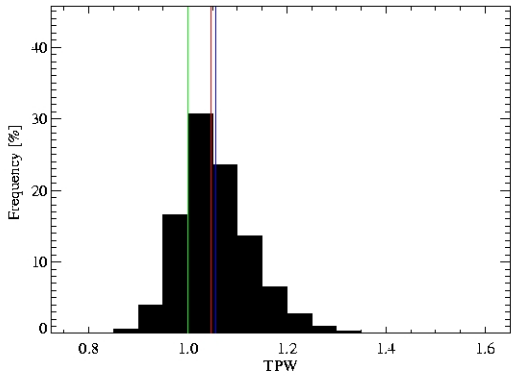

B: Global

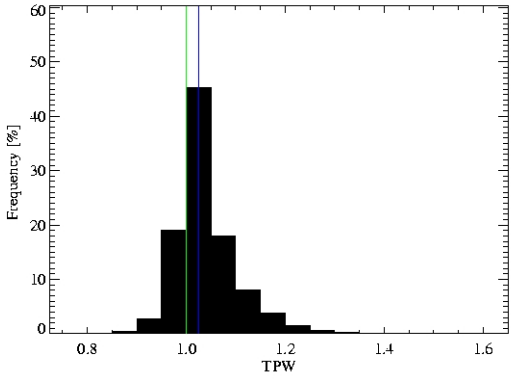

Figure B.28: *Frequency distribution of the excess water vapour for the Antarctic circumpolar ocean(A) and global (B) for the years 2001-2005 (except 2002). The green line gives the excess water vapour of 1. In red the median and in blue the mean value of the distribution is marked.*